Osteology of the Late Triassic Bipedal Archosaur *Poposaurus gracilis* (Archosauria: Pseudosuchia) from Western North America

EMMA R. SCHACHNER,[1*] RANDALL B. IRMIS,[2,3] ADAM K. HUTTENLOCKER,[4] KENT SANDERS,[5] ROBERT L. CIERI,[6] AND STERLING J. NESBITT[7]

[1]Department of Cell Biology and Anatomy, School of Medicine, Louisiana State University Health Sciences Center, New Orleans, Louisiana
[2]Natural History Museum of Utah, University of Utah, Salt Lake City, Utah
[3]Department of Geology and Geophysics, University of Utah, Salt Lake City, Utah
[4]Department of Integrative Anatomical Sciences, Keck School of Medicine, University of Southern California, Los Angeles, California
[5]Department of Diagnostic Imaging, North Canyon Medical Center, Gooding, Idaho
[6]Department of Biology, University of Utah, Salt Lake City, Utah
[7]Department of Geosciences, Virginia Tech, Blacksburg, Virginia

ABSTRACT

Poposaurus gracilis is a bipedal pseudosuchian archosaur that has been poorly understood since the discovery of the holotype fragmentary partial postcranial skeleton in 1915. *Poposaurus*. *gracilis* is a member of Poposauroidea, an unusually morphologically divergent clade of pseudosuchians containing taxa that are bipedal, quadrupedal, toothed, edentulous, and some individuals with elongated thoracic neural spines (i.e., sails). In 2003, a well preserved, fully articulated, and nearly complete postcranial skeleton of *P. gracilis* was discovered with some fragmentary cranial elements from the Upper Triassic Chinle Formation of Grand Staircase-Escalante National Monument of southern Utah, USA. The aim of this work is to describe the osteology of this specimen in detail and compare *P. gracilis* to other closely related pseudosuchian archosaurs. The open neurocentral sutures throughout the majority of the vertebral column, the small size of this individual, and the presence of seven evenly spaced cyclic growth marks in the histologically sectioned femur indicate that this specimen was a skeletally immature juvenile, or subadult when it died. The pes of *P. gracilis* contains multiple skeletal adaptations and osteological correlates for soft tissue structures that support a hypothesis of digitigrady for this taxon. When coupled with the numerous postcranial characters associated with cursoriality, and the many anatomical traits convergent with theropod dinosaurs, this animal likely occupied a similar ecological niche with contemporaneous theropods during the Late Triassic Period. Anat Rec, 00:000–000, 2019. © 2019 American Association for Anatomy

*Correspondence to: Emma Schachner, Department of Cell Biology and Anatomy, School of Medicine, Louisiana State University Health Sciences Center, New Orleans, LA 70112.

E-mail: eschachner@gmail.com

Received 17 November 2018; Revised 10 October 2019; Accepted 14 October 2019.

DOI: 10.1002/ar.24298
Published online 00 Month 2019 in Wiley Online Library (wileyonlinelibrary.com).

Key words: Poposauroidea; cursoriality; Suchia; bipedality; Paracrocodylomorpha

The Late Triassic Epoch comprises a key interval during which pseudosuchian archosaurs possessed high diversity and morphological disparity, coming to dominate many terrestrial ecosystems in terms of diversity and size until the end of the Triassic Period (e.g., Brusatte et al., 2008; Brusatte et al., 2010; Nesbitt, 2011; Benton et al., 2014). One lineage, the Poposauroidea (Fig. 1A), originated from this group during the Early Triassic, and successfully evolved and diversified to fill a range of ecological roles and morphospaces right up until the end of the Triassic Period (Butler et al., 2011; Nesbitt et al., 2011). These animals display a variety of body forms including the bipedal and edentulous shuvosaurids (e.g., *Effigia okeeffeae* and *Shuvosaurus inexpectatus*) (Long and Murry, 1995; Nesbitt and Norell, 2006), a bizarre sail-backed and edentulous taxon (*Lotosaurus adentus*, Zhang, 1975), the possibly aquatic *Qianosuchus mixtus* (Li et al., 2006), the theropod-mimic *Poposaurus gracilis* (Mehl, 1915), and the early sail-backed carnivorous quadrupeds, for example, *Arizonasaurus babbitti* (Nesbitt, 2005) and *Xilousuchus sapingensis* (Nesbitt et al., 2011).

Within Poposauroidea, *P. gracilis*, a bipedal, toothed form, has a striking resemblance to contemporary theropod dinosaurs (Fig. 1B,C). When initially discovered, *P. gracilis* was hypothesized to be related to theropod dinosaurs, based on similarities in the vertebral column and other convergent postcranial characters (Mehl, 1915). The holotype (FMNH UR 357) of this species comprises several vertebral elements, a left ilium, the right femur, the proximal part of the left femur, and a distal part of the ischium; all of which showed considerable signs of taphonomic distortion. Since this discovery, a handful of specimens preserving similar elements have been discovered across the Upper Triassic basins of western North America (Long and Murry, 1995; Weinbaum and Hungerbühler, 2007; Nesbitt,

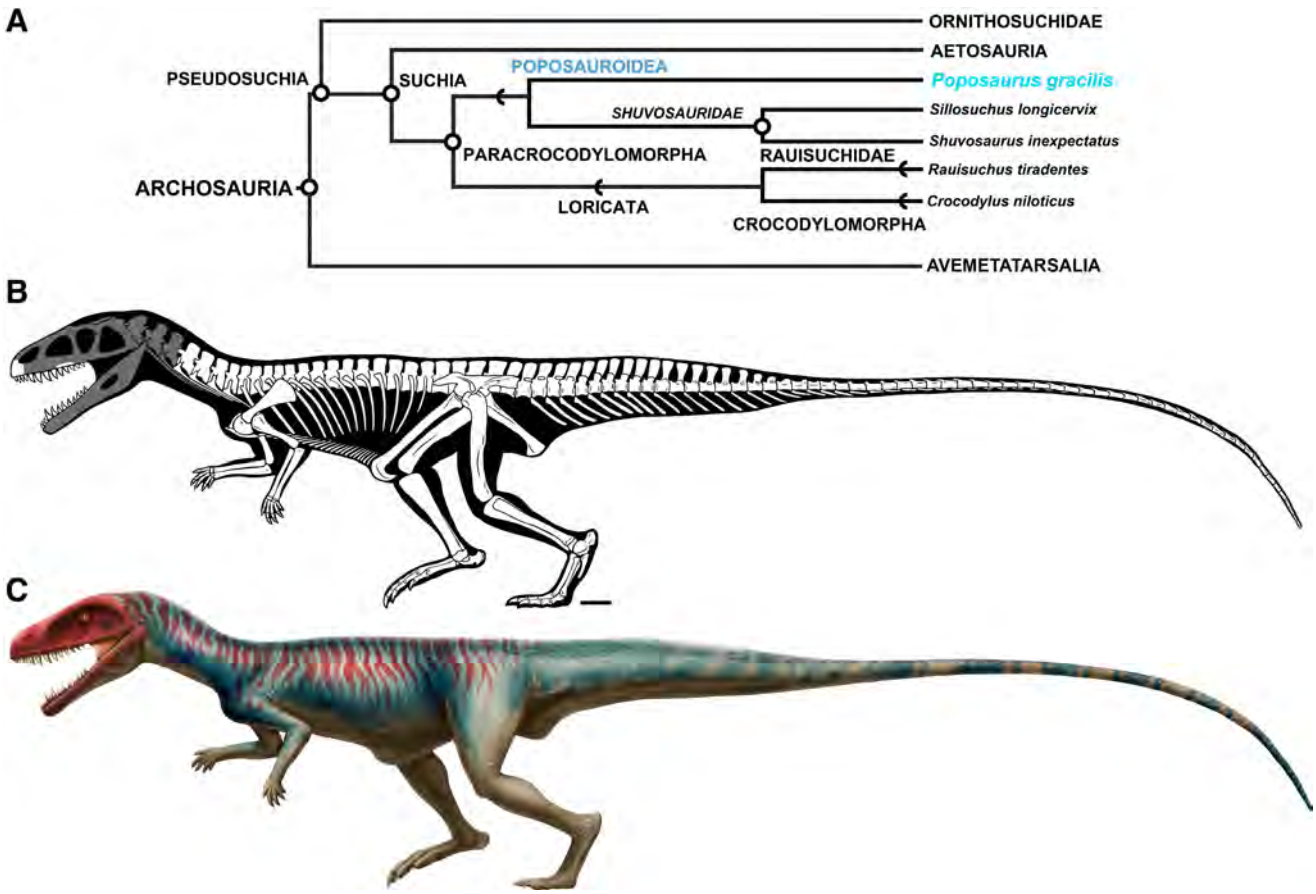

Fig. 1. (**A**) Simplified phylogeny for Archosauria, modified from Nesbitt et al. (2011). (**B**) Skeleton reconstruction of *Poposaurus gracilis* in left lateral view with bones present in the YPM 57100 specimen in white, and the bones of the skeleton that were not recovered in gray. Scale bar = 10 cm. (**C**) Life restoration of *P. gracilis* (illustration by C. Layton).

2011). Moreover, the unusual postcranial morphology of *P. gracilis*, and the lack of cranial material present in most of the known specimens save one (Parker and Nesbitt, 2013), has rendered our understanding of the animal and the evolution of Poposauroidea largely incomplete.

A nearly complete, well-preserved, articulated postcranial skeleton assigned to *P. gracilis* (Fig. 2) with a few cranial elements was discovered in 2003 by a field team from Yale University from the Upper Triassic Chinle Formation of Grand Staircase-Escalante National Monument of southern Utah, USA. (Benoit and Yarborough Fitzgerald, 2004). Gauthier et al. (2011) provided a brief descriptive, phylogenetic, and functional analysis of this specimen. Subsequently, Nesbitt et al. (2011) incorporated anatomical data from the specimen in a large early archosaur phylogenetic analysis, and Schachner et al. (2011b) generated

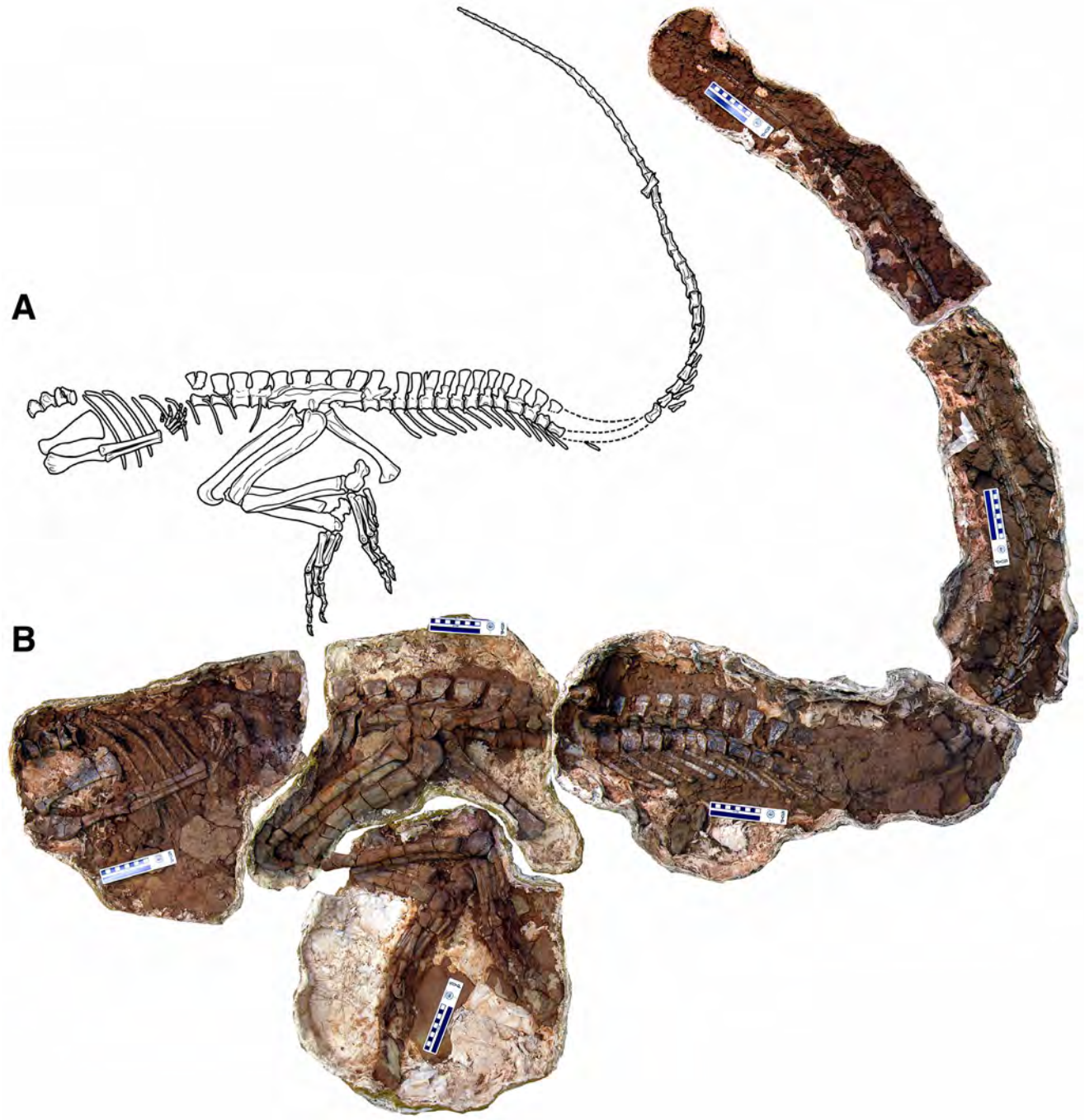

Fig. 2. Overview of bones preserved in *P. gracilis* (YPM 57100). Diagrammatic outline (**A**) and composite photograph (**B**) of the skeleton in its original field jackets. Scale bars = 10 cm.

a reconstruction of the hindlimb musculotendinous system using phylogenetic bracketing and osteological correlates for muscle attachment sites preserved in the pelvis and hindlimb elements. Bates and Schachner (2012) generated a simplified biomechanical model of the hindlimb muscles based upon the YPM 57100 specimen in order to test hypotheses on the evolutionary and functional patterns in archosaur gait and posture, and Farlow et al. (2014) utilized the pedal morphology to inform inference of archosaur trackmakers. However, the osteology of this specimen has not been described in detail, thus the aim of this work is to remedy this situation and compare this taxon to other archosaurs.

Institutional Abbreviations

FMNH UR, Field Museum of Natural History, Chicago, Illinois, USA; PEFO, Petrified Forest National Park, Arizona, USA; PVSJ, Instituto y Museo de Ciencias Naturales, Universidad Nacional de San Juan, Argentina; TMM, Texas Vertebrate Paleontology Collections, Jackson School Museum of Earth History, The University of Texas at Austin, USA; TTU-P, Paleontology Collections, Museum of Texas Tech University, Lubbock, Texas, USA; YPM, Yale Peabody Museum of Natural History, Yale University, New Haven, Connecticut, USA.

METHODS

Imaging and Illustrations

Individual bones were photographed with a Nikon D300 and a Nikon AF-S Micro NIKKOR 60 mm Micro lens. Illustrations were done by hand with Staedler Mars Lumograph pencils (4B-4H) and Sakura of America Pigma MICRON archival ink pens (005-01) on Strathmore Bristol vellum, cleaned up and edited into figures in Adobe Photoshop CS6. Three-dimensional (3D) digital models of the left hindlimb and pes were acquired for a separate project (Bates and Schachner, 2012), and the models of the ankle and pes were used and manipulated for this analysis. These models were generated from individual scans of each disarticulated bone or bone "cluster" depending upon the extent of preparation. These scans were completed with a Polhemus FastSCAN Cobra laser scanner (www.polhemus.com), which produced a high-resolution point cloud, which was then processed in Geomagic Studio 12 (www.geomagic.com). The alignment of each anatomical element was completed in both Geomagic and in Autodesk Maya (http://www.autodesk.com/products/maya/). For more details on mesh production and 3D model production see the Supplemental Information of Bates and Schachner (2012); for more information on the separation of the individual pedal elements that were fossilized as a single unit see Farlow et al. (2014).

Components of the axial skeleton were scanned at the University of Utah Medical Center with a 164 slice dual energy Siemens SOMATOM Definition computed tomography (CT) unit at a slice thickness of 0.6 mm (kVp 140, mAs 500) with data reconstructed in 40 and 60 bone sharp algorithm kernels. The CT DICOMs are available via the open-access data curation website www.datadryad.org.

Bone Histology Sampling and Preparation

Histologic sections of the left femur were prepared in order to investigate the individual's ontogenetic status and patterns of postnatal growth. Prior to thin sectioning, the entire femur was measured, photographed and CT-scanned, and molded and cast to preserve aspects of its gross structure. All of these data are stored in the Yale Peabody Paleontology collections. Sectioning methods were modified from standard techniques applied to fossil bone (Chinsamy and Raath, 1992; Wilson, 1994). These steps included (1) removal of mid-diaphyseal block (which was also cast in addition to the whole bone); (2) embedding of the extracted block in a cold-curing resin under vacuum; (3) cutting of 1 mm wafers from the embedded block on a low-speed Buehler Isomet precision saw with diamond blade; (4) dehydration and mounting of individual wafers onto petrographic slides with 2-ton epoxy (Devcon); (5) grinding and polishing of resulting thick-sections on a Buehler Metaserv grinder-polisher to approximately 90 μm; and (6) digital photography and image analysis. The thin sections were photographed at 50× and 20× on a Nikon Eclipse polarizing microscope with a digital image capture system, and the 20× image series was stitched into a composite high-resolution digital histology slide for study. The slide was imaged using normal transmitted light and cross-polarized light with quarter-wave retardation plate to examine mineral fiber orientations, interosteonal matrix texture, and growth marks. High-resolution images of the sections are available via www.datadryad.org.

SYSTEMATIC PALEONTOLOGY

Archosauria Cope, 1869, *sensu* Gauthier, 1986
Pseudosuchia Zittel, 1887, *sensu* Gauthier and Padian, 1985
Poposauroidea Nopsca, 1923, *sensu* Nesbitt, 2011
Poposaurus gracilis Mehl, 1915

Holotype

FMNH UR 357, dorsal and caudal vertebrae, partial pelvis, and partial femora (Mehl, 1915; Colbert, 1961).

Revised Diagnosis

Poposaurus gracilis can be distinguished by the following unique combination of character states (autapomorphies marked with asterisks): Distinct mediolaterally compressed premaxilla with five premaxillary teeth; caudodorsally projecting ascending process of the maxilla low (20 degrees from the horizontal) (PEFO 34865); mediolaterally compressed and finely serrated (20 serrations/5 mm) maxillary teeth (PEFO 34865); posterior cervical centra with slight or absent ridge on the ventral surface; parapophysis split into two articular surfaces in the posterior cervical vertebrae; hyposphene-hypantrum articulations in the trunk vertebrae; four or five sacral vertebrae; ~56 caudal vertebrae; coracoid with prominent postglenoid process; humerus with a short deltopectoral crest; five fingered manus with metacarpal V the smallest; dorsoventrally compressed unguals present on digits I–III; ilium with a tapering anterior process that extends anteriorly of the pubic peduncle, distinct

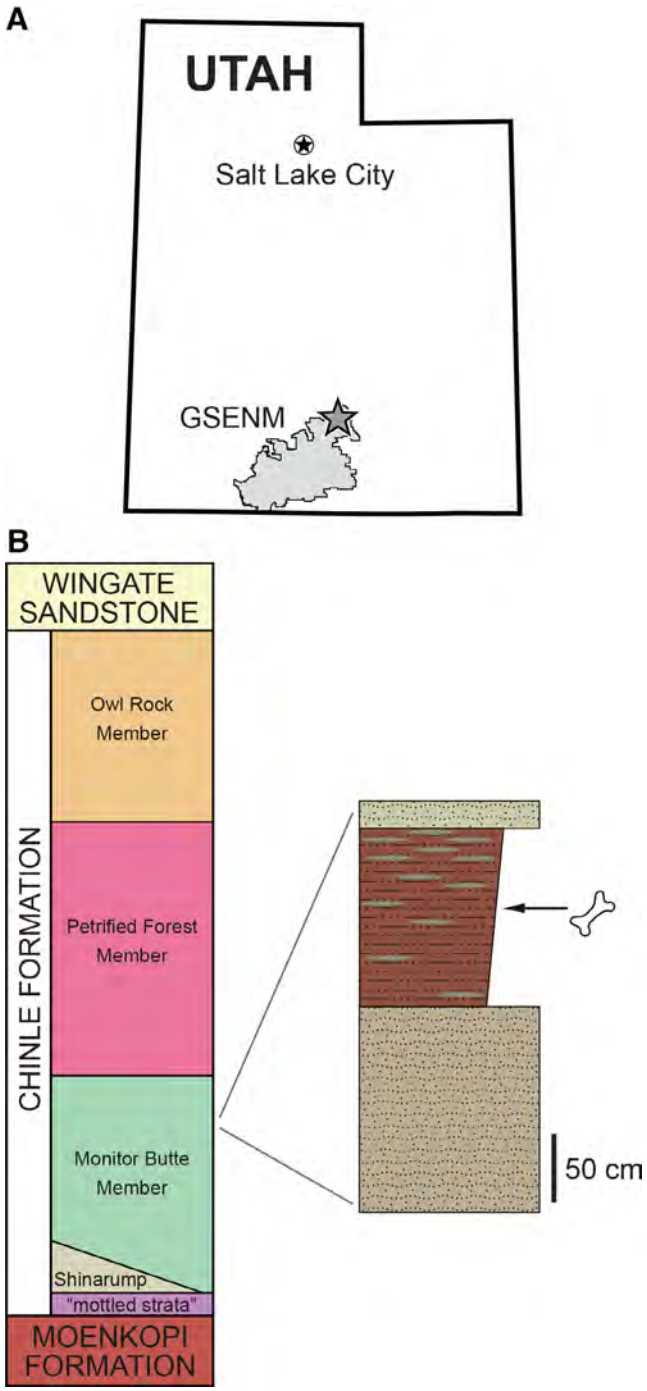

Fig. 3. (**A**) Map of Utah showing location of Grand Staircase-Escalante National Monument (GSENM) with a star indicating the discovery site of YPM 57100. (**B**) Chinle Formation lithostratigraphy in the Circle Cliffs area (GSENM) (following Stewart et al., 1972; Martz et al., 2017), with a detailed stratigraphic section showing the fossiliferous level.

ridge on the dorsolateral portion of the postacetabular blade of the ilium*; ventral margin of the acetabulum concave in lateral view; pubis with a posteriorly hooked expansion (=boot) that is rounded in lateral view and tapered*; deep pit on the proximal surface of the ischium that receives a concave ischial process of the ilium*; ischium with a ventral expansion at the distal end; calcaneum with a deep groove on the caudal surface of the calcaneal tuber; metatarsal III longest; phalanges absent on digit V; pedal unguals dorsoventrally compressed.

Referred Specimen

YPM 57100, fragmentary premaxillae, teeth, and an articulated postcranial skeleton (see Gauthier et al., 2011 for justification of the referral). See Weinbaum and Hungerbühler (2007) and Parker and Nesbitt (2013) for other referred specimens.

Locality and Horizon

Circle Cliffs, Grand Staircase-Escalante National Monument, Garfield County, Utah, USA. The site, which also contained the nearly complete articulated skeleton of a small crocodylomorph, is within the upper Monitor Butte Member of the Upper Triassic Chinle Formation. The Monitor Butte Member in this area is ~50–60 m thick (Stewart et al., 1972), and the site is ~40 m above the base of the unit. This stratigraphic interval is likely early-middle Norian (~227–215 Ma) in age based on radioisotopic and magnetostratigraphic age constraints from the lower Chinle Formation of northern Arizona and New Mexico (Irmis et al., 2011; Ramezani et al., 2011, 2014; Zeigler et al., 2017; Kent et al., 2018). The lower part of the Monitor Butte Member interfingers with the Shinarump Member in the Circle Cliffs area, including just east of the fossil site (Fig. 3; Stewart, 1957; Stewart et al., 1972; Martz et al., 2017: Fig. 16D; RBI, personal observation). Locally, the lower Monitor Butte can also form channel-fill deposits scoured into the sandstones and conglomerates of the Shinarump Member (e.g., Stewart et al., 1972: Fig. 7, p. 27; Dubiel, 1987: p. 37). Lateral equivalents of the Shinarump Member (i.e., Mesa Redondo Member) have been radioisotopically dated to between 225 and 227 Ma in northern Arizona (Ramezani et al., 2011; Atchley et al., 2013); however, the *Poposaurus* specimen comes from high in the Monitor Butte Member, and it is unclear exactly how this stratigraphic level correlates to dated Chinle Formation units (e.g., Blue Mesa and Sonsela members) further south in Arizona (*cf*. Blakey and Gubitosa, 1983: Fig. 3C). *Poposaurus gracilis* specimens in Arizona have been found in the middle Blue Mesa Member through lowermost Sonsela Member (Parker and Nesbitt, 2013: Fig. 2), an interval dated to between ~223 and 218 Ma (Ramezani et al., 2011; Atchley et al., 2013), though occurrences from Texas and Wyoming are likely older.

The fossiliferous horizon itself (Fig. 3B) comprises a ~1.3 m thick moderate reddish-brown (10R 4/6) micaceous siltstone with rare greenish gray (5GY 6/1) small mottles, containing thin (1–2 cm) lenses of greenish-gray (5GY 6/1) very fine- to fine-grained sandstone whose abundance increases up-section. The sediment surrounding the bones (laterally up to 2 m away from the skeletons) contains abundant spherical carbonate concretions (5–10 mm diameter) that are so dense right around the skeleton they sometimes form a solid concretionary layer (e.g., Figs. 2B, 17–19). These concretions comprise radial calcite spar crystals with minor detrital siliciclastic grains

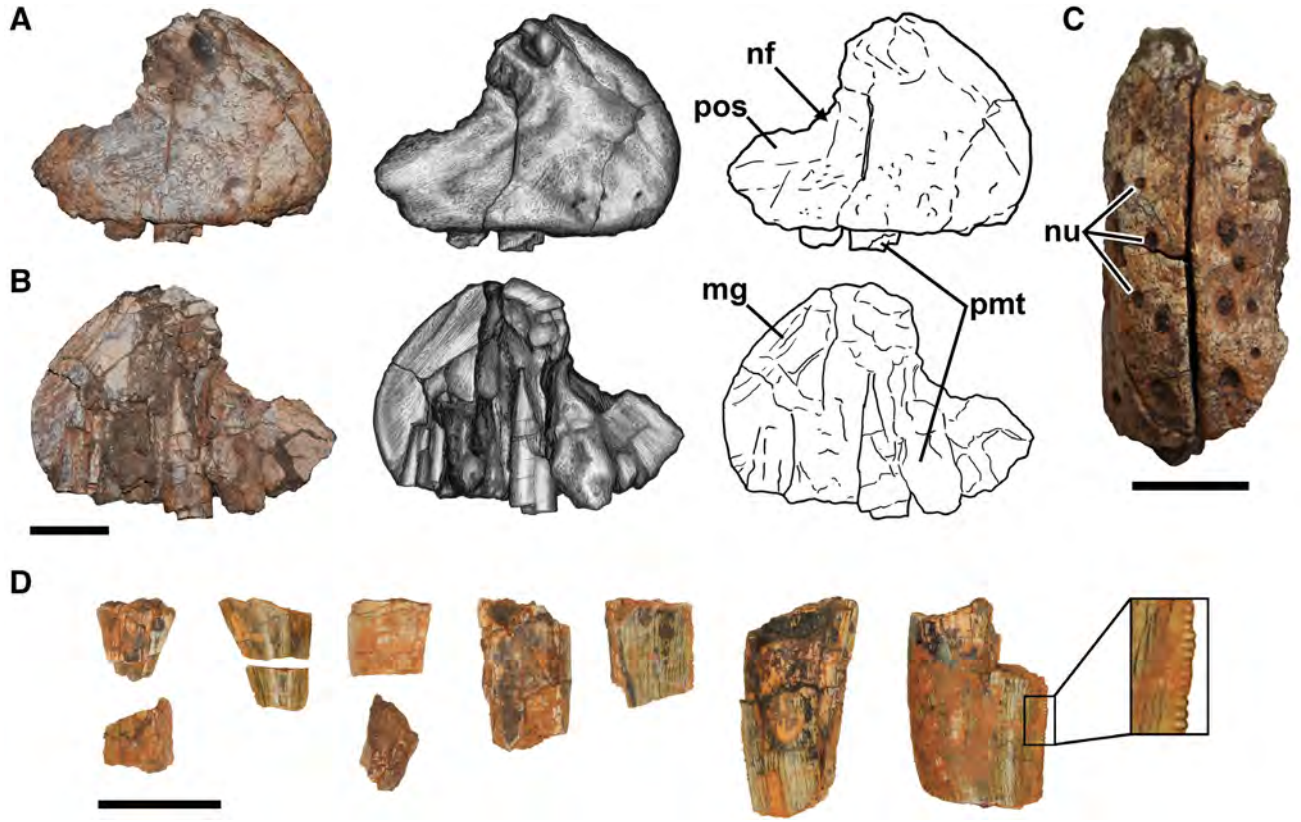

Fig. 4. Right premaxilla of YPM 57100. A photograph (left), line image (middle), and illustration (right) in lateral (**A**) and medial (**B**) views. (**C**) Articulated left and right premaxillae in rostral view. (**D**) Fragments of teeth found associated with the specimen. Abbreviations: mg, medial grooves; nf, narial fossa; nu, nutrient foramina; pmt, premaxillary teeth; pos, caudal process. Scale bars = 1 cm.

(i.e., quartz and clay) and are interpreted to represent an early diagenetic phase, possibly related to the decomposition of organic matter (e.g., Benoit and Yarborough Fitzgerald, 2004; Smith, 2012). The fossiliferous unit is capped by a 10–20 cm thick pale greenish-yellow (10Y 8/2) ripple-laminated, horizontally bedded fine-grained sandstone. This sequence likely represents distal splay overbank deposits (*cf*. Bown and Kraus, 1987; Kraus and Bown, 1988; Dubiel and Hasiotis, 2011; Howell and Blakey, 2013; Hartley and Evenstar, 2018) with weak pedogenic development. It thus seems likely that the two pseudosuchian archosaur carcasses (i.e., *Poposaurus* and a crocodylomorph) were perhaps transported and buried by floodwaters that broke through the channel levee and spread across the floodplain. The nearly completely articulated nature of both specimens (including the very distal small elements) indicates that any transport of the skeletons must have taken place before advanced decay occurred so that the soft tissues kept the specimen intact. Additionally, the specimens were likely not exposed for any prolonged amount of time after death given the well-preserved condition of the bone surfaces (*cf*. Behrensmeyer, 1978).

DESCRIPTION

Skull

The skeleton weathered out of the matrix head-first, thus most of the skull was lost to erosion prior to discovery. The remaining cranial material collected from the surface consists of partial right and left premaxillae, 12 tooth fragments, a large unidentified fragment likely pertaining to the back portion of the skull, and various fragments. The left premaxilla (Fig. 4) is fragmentary but can be articulated at the midline with the right to reconstruct a narrow rostral portion of the skull (Fig. 4C). The right premaxilla has a broken nasal (=rostrodorsal) process, but the caudal (=caudodorsal, maxillary) process is nearly complete. The lateral surface is gently rounded and the narial fossa has gently sloping margins with no distinct ventral or rostral margins. The body of the premaxilla is about twice as long craniocaudally as it is tall, similar to *Batrachotomus* (Gower, 1999), *Fasolasuchus* (Bonaparte, 1981), and the other poposauroids *Xilousuchus*, *Effigia*, and *Shuvosaurus* (despite the lack of teeth in the latter two taxa) (Nesbitt, 2007; Nesbitt et al., 2011). However, the body of the premaxilla is not nearly as elongated as in *Qianosuchus* (Li et al., 2006), and it is different from the relatively short premaxillae in *Saurosuchus* (Alcober, 2000) and rauisuchids (e.g., Sulej, 2005; Weinbaum, 2011). The caudal process is short like that of *Effigia* (Nesbitt and Norell, 2006; Nesbitt, 2007) and *Qianosuchus* (Li et al., 2006). This is in contrast to the long process present in *Lotosaurus* (SJN, *pers. obs*.). Here, the premaxilla overlaps the maxilla laterally, with a simple flat articulation. Considering the short length of the process, it is likely that the maxilla contributed to

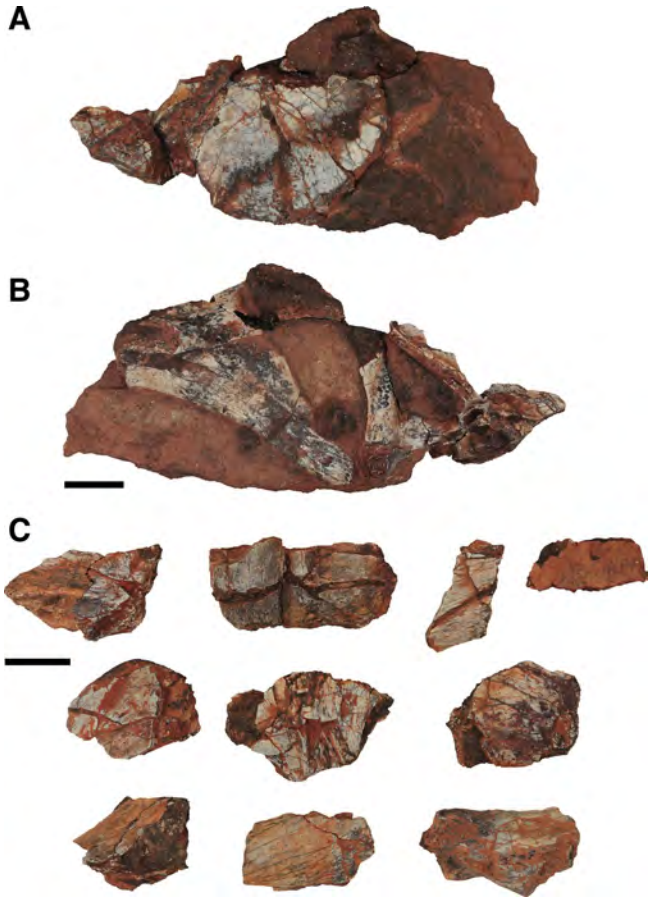

Fig. 5. Unidentified possible cranial fragments of YPM 57100. Large fragment in two views (**A**, **B**). Small fragments (**C**). Scale bars = 1 cm.

the external naris as in other poposauroids (Nesbitt, 2011), and this is consistent with the maxilla assigned to the taxon (Parker and Nesbitt, 2013). There are multiple nutrient foramina along the rostral and ventral surfaces of both premaxillae (Fig. 4C).

Medially, small but distinct ridges and grooves on a flat surface mark the midline suture (Fig. 4B). The right premaxilla preserves the alveoli and roots of five premaxillary teeth, which are oval in cross-section, but none of the crowns is preserved. The number of premaxillary teeth is highly variable in poposauroids ranging from none in the beaked shuvosaurids, to five in *Xilousuchus* (Nesbitt et al., 2011), to nine in *Qianosuchus* (Li et al., 2006).

There are 12 isolated tooth fragments associated with YPM 57100 (Fig. 4D). They are strongly laterally compressed and recurved with distinct fine serrations (approximately 3.4 per millimeter) consistent with the dental morphology described by Parker and Nesbitt (2013) for a *Poposaurus* specimen from Petrified Forest National Park, Arizona (PEFO 34865) that preserves the only other known cranial material of the taxon. There are other small cranial fragments (Fig. 5) with some containing alveoli; however, a more specific identification could not be determined.

Cervical Vertebrae

Four cervical vertebrae are preserved with YPM 57100 (Fig. 6), representing the middle and caudal portion of the cervical column. The position of each cervical vertebra was determined based on the position of the parapophysis and comparisons with other archosaurs (e.g., *Qianosuchus*, Li et al., 2006). The vertebrae are moderately well preserved; however, the majority of the processes are broken off because the vertebrae were found on or near the weathering surface. All of the cervical vertebrae have a laterally constricted spool-shaped centrum (Fig. 6C,F,I,L) with parapophyses that contact the caudolateral margin of the adjacent vertebra. The centrodiapophyseal laminae are well developed and more prominent than in *Xilousuchus* (Nesbitt et al., 2011). The middle cervical centra are shorter in height and length relative to *Qianosuchus*, and those preserved for *Xilousuchus*, *Arizonasaurus*, and *Effigia* (Nesbitt, 2005; Li et al., 2006; Nesbitt, 2007, 2011; Nesbitt et al., 2011), but not as short as those of *Poposaurus langstoni* (Stefanic and Nesbitt, 2018). The articular facets of the centra are round in the cranialmost preserved cervical vertebrae (Fig. 6C), becoming more craniocaudally ellipsoid (height > width) toward the caudal part of the cervical column (Fig. 6L). In the middle cervicals, there are marked fossae without rims on the lateral surfaces of the centra just ventral to the neurocentral suture. These fossae become shallower and less distinct in the caudalmost cervical vertebrae. The surface of the centrum is smooth ventrally in most of the preserved cervicals, whereas the cranial part of the ventral surface of C6 is slightly flattened and this surface on C7 preserves a slight ridge. The parapophyses (Fig. 6A,D,G,J) appears divided similar to other specimens of *Poposaurus* (Weinbaum and Hungerbühler, 2007) and other poposauroids (Nesbitt, 2005, 2011).

Trunk (Thoracic) Vertebrae

Twelve reasonably well-preserved trunk (T) vertebrae remained in articulation with the sacrum (Figs. 7–14). The transverse processes are broken off in all but two of the vertebrae, but they are otherwise complete. In the first three trunk vertebrae, the parapophysis projects from the neural arch, just dorsal to the neurocentral suture (Figs. 7 and 8). The parapophysis moves dorsally in T4, becoming slightly raised off of the neural arch by a short, laterally projecting pedicle. In the first three trunk vertebrae, the prezygaparapophyseal, paradiapophyseal, and centrodiapophyseal laminae are distinct with the latter two forming well-developed sharp lateral expansions with deep fossae between them (Figs. 8 and 11). The neurocentral sutures are clearly interdigitated and without any sign of closure (Figs. 7 and 8; *sensu* Brochu, 1996). In the dorsal view, when the neural arch is missing or removed, there are deep ventral depressions within the neural canals. These depressions reach their maximum depth in the midcentrum.

In general, the cranial trunk vertebrae are more transversely compressed and become more laterally expanded caudally in the column more toward the sacrum (Fig. 10); this also occurs in the poposauroid *Arizonasaurus* (Nesbitt, 2005) and the rauisuchid *Postosuchus* (Weinbaum, 2013). Caudal to the first three trunk vertebrae, the cranial articular surface of the centra

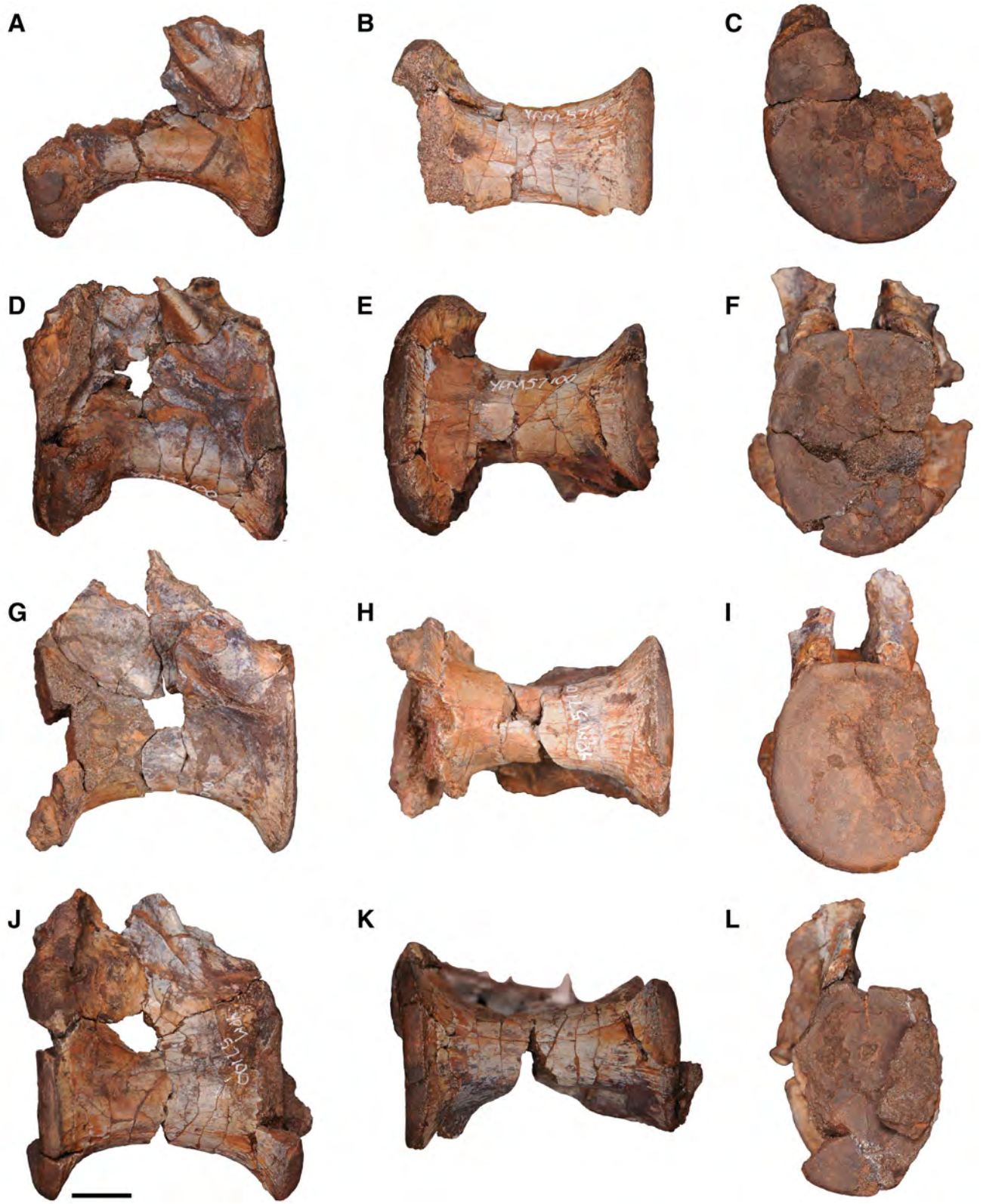

Fig. 6. The four caudalmost cervical vertebrae of YPM 57100, in left lateral view (**A**, **D**, **G**, **J**), ventral view (**B**, **E**, **H**, **K**), and cranial view (**C**, **F**, **I**, **L**), with the cranialmost cervical vertebra at the top (A) and the caudalmost cervical at the bottom (J). Scale bar = 1 cm.

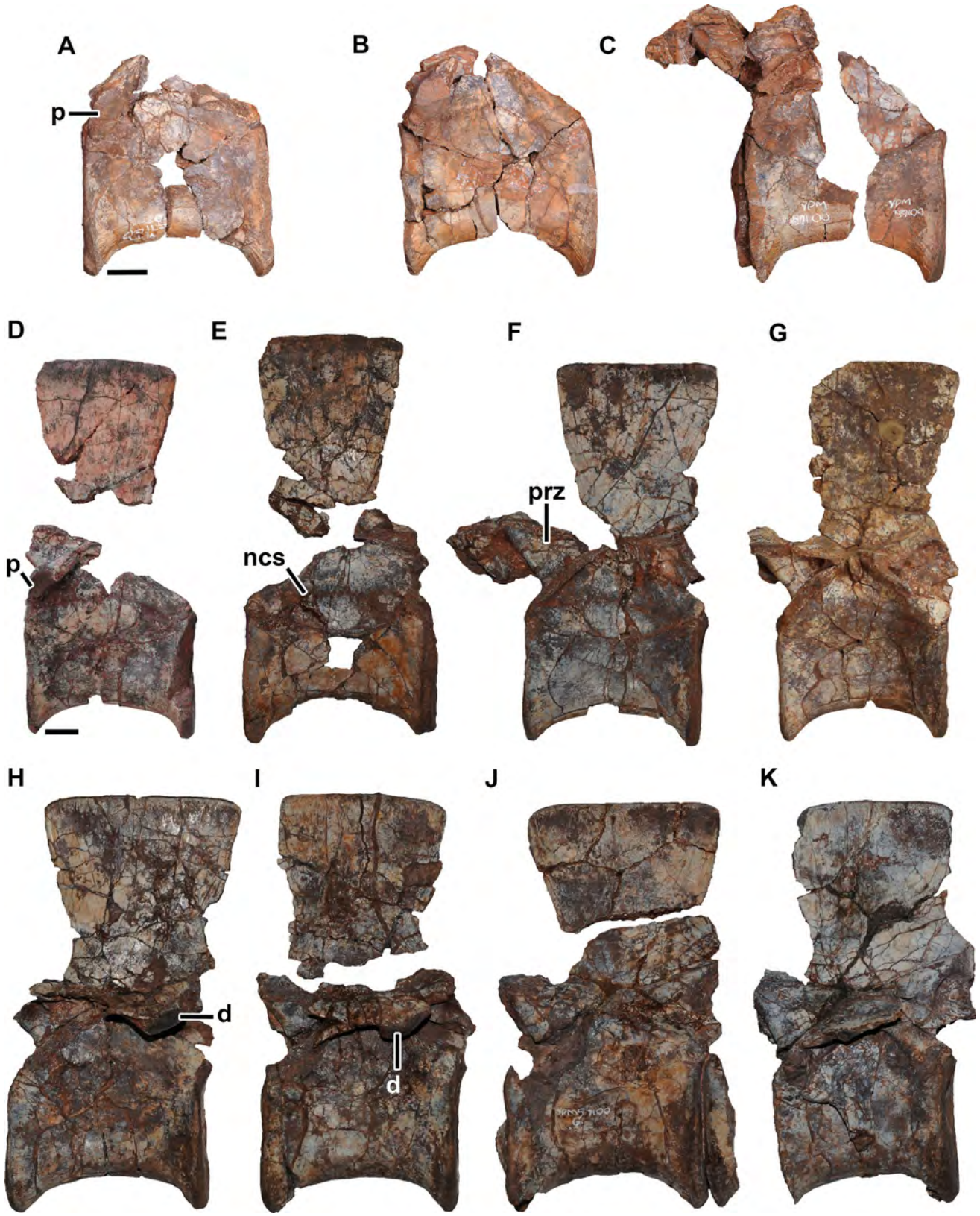

Fig. 7. Thoracic vertebrae 1–11 of YPM 57100 in left lateral view (**A**–**K**). Abbreviations: d, diapophysis; ncs, neurocentral suture; p, parapophysis; prz, prezygapophysis. Scale bars = 1 cm.

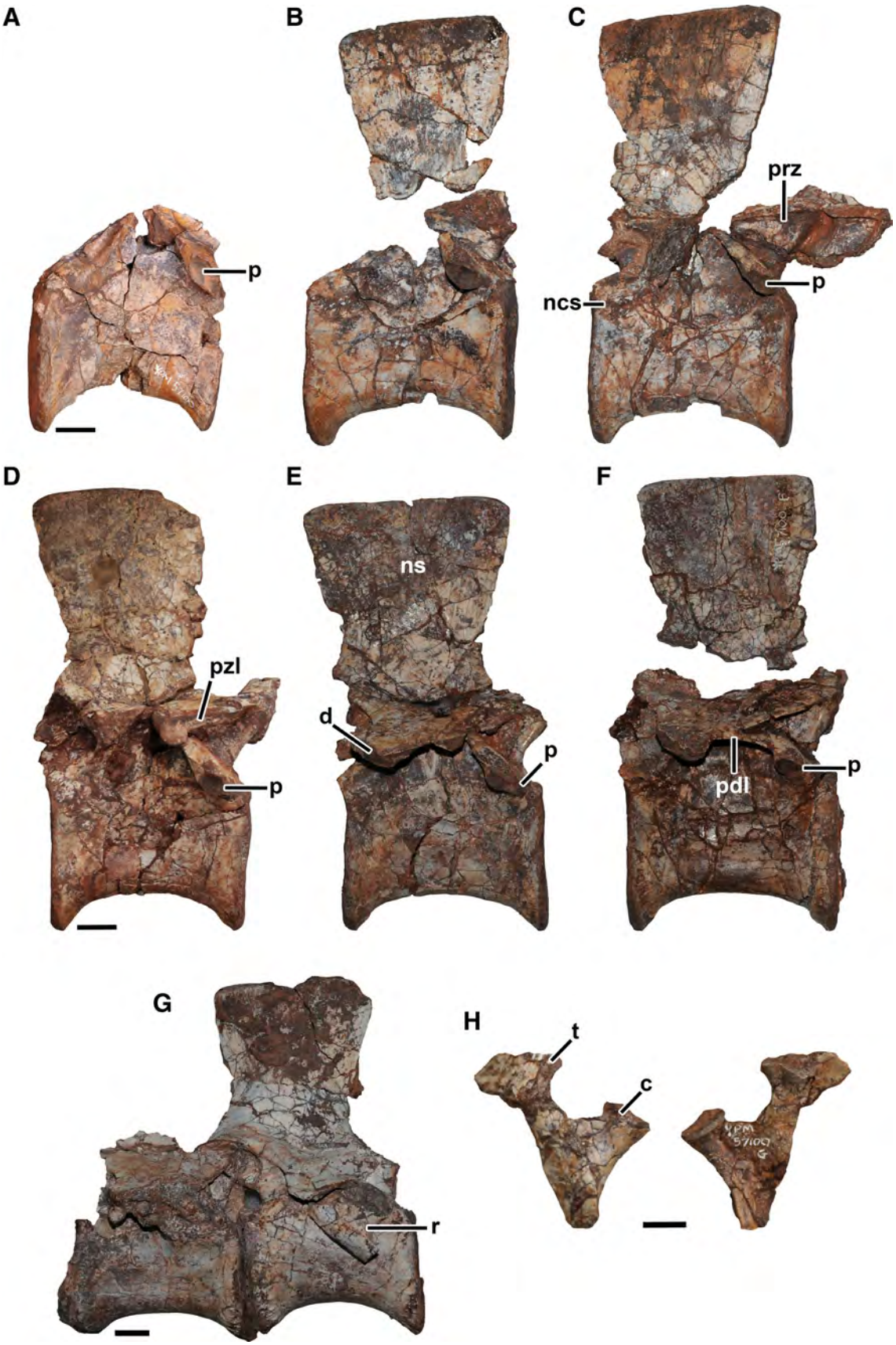

Fig. 8. Legend on next page.

(Fig. 9C–F) are oval (with a longer dorsoventral axis), amphicoelous, and similar to those of *Arizonasaurus* (Nesbitt, 2005) and the isolated Waldhaus material from the Middle Triassic of southern Germany (Butler et al., 2011). In lateral view, the centra are more deeply "waisted" (i.e., the ventral surface of the centrum arches dorsally and in ventral view, the lateral sides of centra converge toward the midline) in the middle of the centrum in the cranial half of the column whereas caudally, the vertebrae become proportionately less waisted toward the sacrum (Figs. 7 and 10). The ratio of the cranial articular faces cross-sectional area to midcentral cross-section area: T4 = 4.9137, T9 = 4.707, and T12 = 3.302. This configuration is the opposite of the trunk central morphology found in *Effigia* and *Shuvosaurus* in which the centra are wider than tall throughout much of the thoracic column.

Additionally, there are pronounced fine radiating ridges emanating from the margin of the central faces and extending craniocaudally, as in most poposauroids (Nesbitt, 2007), some rauisuchids (e.g., *Postosuchus*; Weinbaum, 2013), and dinosaurs (Nesbitt et al., 2013). There is clear intervertebral ligament marginal endplate corrugation. Very shallow depressions are present on the lateral surfaces of the centra, apneumatic fossae (O'Connor, 2006), much like *Arizonasaurus*, *Ctenosauriscus*, and *Hypselorhachis* (Nesbitt, 2005; Butler et al., 2009; Butler et al., 2011) and other pseudosuchians, but less deep than the fossae present in *Effigia*, *Shuvosaurus*, and *Sillosuchus* (PVSJ 85; Nesbitt, 2007). The articular facets of the centra become less ovate (i.e., more circular) and larger proportionally closer to the sacrum (Fig. 9).

The neural spines increase in height and craniocaudal width caudally and have a flat dorsal margin with no lateral expansion at the dorsal surface (=spine table of some; see (Nesbitt, 2011) (Figs. 7–9). Nonetheless, the neural spines are not particularly long, similar to shuvosaurids (Nesbitt, 2007) and loricatans such as *Batrachotomus* and *Postosuchus* (Gower and Schoch, 2009; Weinbaum, 2013), and unlike the long sail-forming neural spines in the early poposauroids *Xilousuchus*, *Arizonasaurus*, *Ctenosauriscus*, *Hypselorhachis*, *Lotosaurus*, and the Waldhaus taxon (Zhang, 1975; Nesbitt, 2005; Butler et al., 2009; Butler et al., 2011; Nesbitt et al., 2011). Additionally, the neural arches project dorsally only, and there is no cranial or caudal arching as in the sail-backed forms (Nesbitt, 2005). Throughout the thoracic column, the neural arches expand slightly cranially and caudally in the lateral view. The length of the neural spines of *P. gracilis* is also proportionally shorter than the purported sister taxon *Poposaurus langstoni* (Long and Murry, 1995; Stefanic and Nesbitt, 2018). The transverse processes are only preserved in three of the caudal thoracic vertebrae (T8, T9, and T11), and are dorsoventrally flattened and project caudolaterally (Figs. 7H–I and 8E–F). The diapophysis is oval (i.e., elongated craniocaudally) in lateral view and the articular surface is flattened. The parapophyses are slightly expanded laterally near the base of the neural arch throughout the vertebral column. The diapophysis is only slightly dorsal to the parapophysis but remains separate and distinct throughout the entire thoracic series (Figs. 8E–G); they do not merge as in *Effigia* (Nesbitt, 2007) and *Arizonasaurus* (Nesbitt, 2005). Very shallow fossae on the lateral surface of the base of the neural spine constrict spine thickness; these fossae are bound ventrally by the prezygadiapophyseal and postzygadiapophyseal laminae.

In the first three trunk vertebrae, the prezygaparapophyseal, paradiapophyseal, and centrodiapophyseal laminae are distinct, with the latter two forming well-developed sharp laminae, as in other poposauroids (Nesbitt, 2007; Butler et al., 2009; Butler et al., 2011). More caudally, the paradiapophyseal, prezygadiapophyseal, postzygadiapophyseal, and caudal centrodiapophyseal laminae are very well developed and all form sharp crests. These laminae are bound by three deep and distinct fossae: the centrodiapophyseal fossa, prezygadiapophyseal-paradiapophyseal fossa, and postdiapophyseal-centrodiapophyseal fossa (*sensu* Wilson et al., 2011). Hyposphene-hypantrum articulations are clearly present in thoracic vertebrae 7–12, and the cranial portion of the first sacral bears a hypantrum (Fig. 13). The cranial surface of T5 is broken and missing, and the cranial and caudal surfaces of T4 are broken and missing, but these vertebrae also likely had hyposphene-hypantrum articulations based on the preserved morphology. The articular processes on the more cranial trunk vertebrae are not well-enough preserved to determine if they are present or not. The morphology of the hyposphene structures are similar to that of other specimens of *P. gracilis and Poposaurus langstoni* (Weinbaum and Hungerbühler, 2007; Stefanic and Nesbitt, 2018), as well as other paracrocodylomophs (e.g., Weinbaum and Hungerbühler, 2007) in that they slightly expand laterally in the ventral direction. The hypantra are just simple gaps between the prezygapophyses, as in *Poposaurus langstoni* (Stefanic and Nesbitt, 2018).

Sacral Vertebrae

There are five total sacral vertebrae (Figs. 14 and 15) whereas in other specimens of *Poposaurus*, there are only four preserved (Weinbaum and Hungerbühler, 2007). It appears that sacrals 2–5 of YPM 57100 are the same as those labeled sacrals 1–4 of TMM 43683-1 in Weinbaum and Hungerbühler (2007). To clarify the homologous identity of the five sacral vertebrae of YPM 57100, we deploy the methods of Nesbitt et al. (2011) by identifying the sacral vertebrae based on their sacral rib morphology and where they attach to the ilium. From these criteria, we identify the first sacral as homologous with the last trunk vertebra of other reptiles (i.e., a dorsosacral), the second sacral of *Poposaurus* as the first primordial sacral of reptiles with only two sacral vertebra (e.g., Crocodylomorpha), the third as an insertion between the primordial sacrals (*sensu* Nesbitt, 2011), the fourth as the second primordial, and last as a caudosacral. The caudosacral possesses a broad but thin (i.e., dorsoventrally compressed) transverse

Fig. 8. Thoracic vertebrae two (**A**), four (**B**), six–nine (**C–F**), 12, and the first sacral vertebra (**G**) of YPM 57100, all in right lateral view. (**H**) Seventh thoracic rib in dorsal (left) and ventral (right) views. Abbreviations: c, capitulum; d, diapophysis; ncs, neurocentral suture; ns, neural spine; p, parapophysis; pdl, paradiapophyseal lamina; prz, prezygapophysis; pzl, prezygaparapophyseal lamina; r, rib; t, tuberculum. Scale bars = 1 cm.

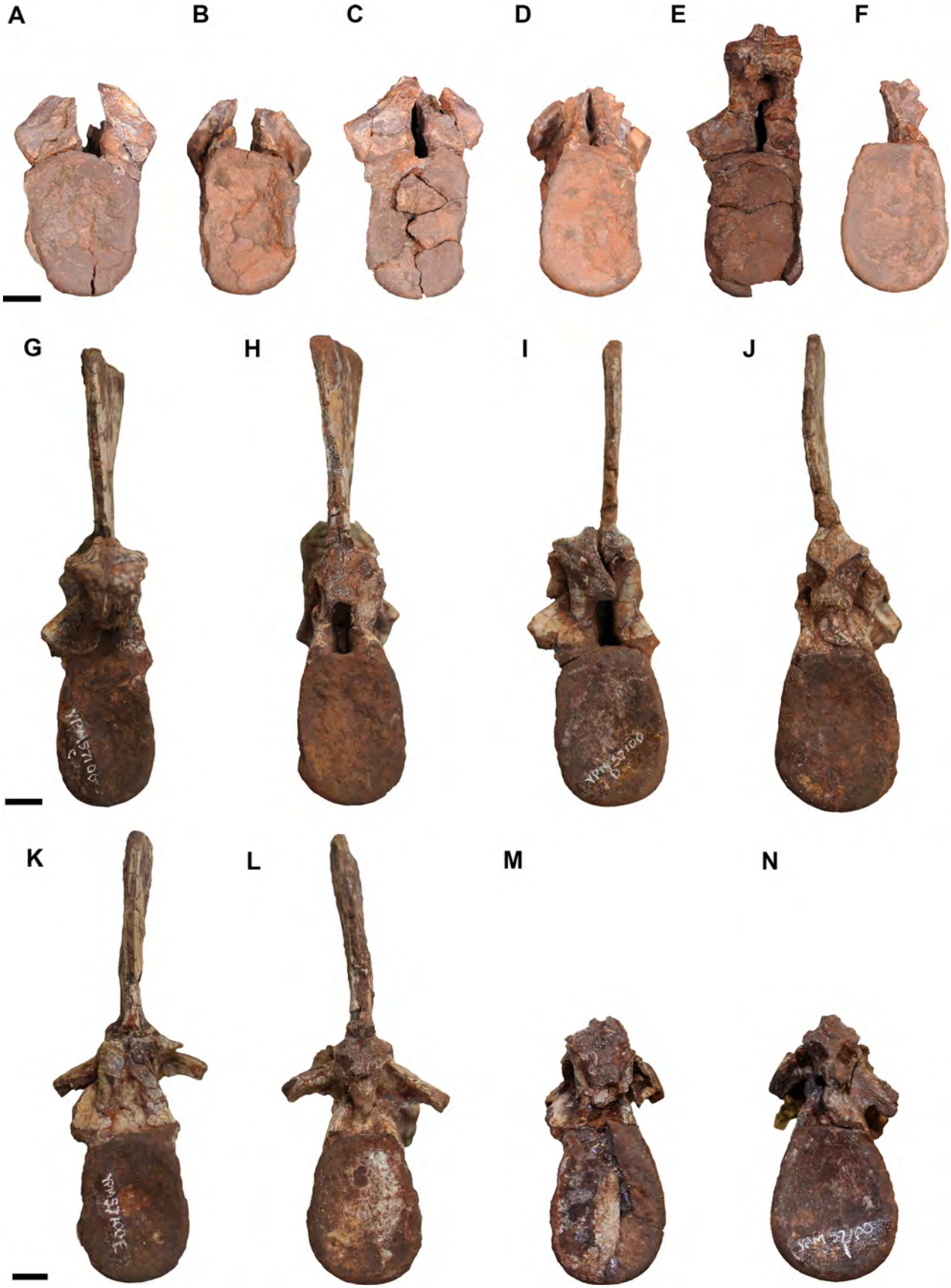

Fig. 9. Legend on next page.

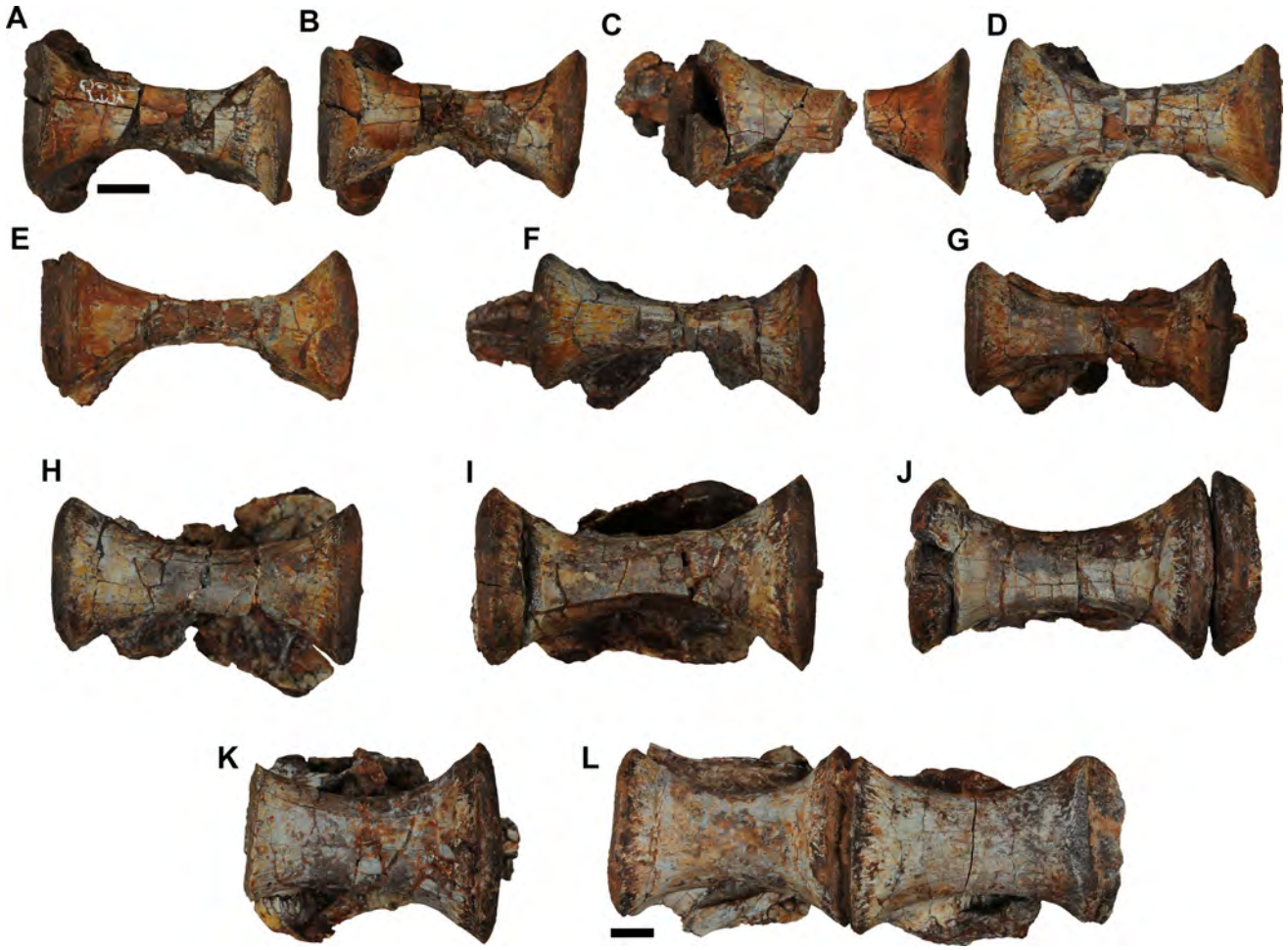

Fig. 10. Thoracic vertebrae 1–12, and the first sacral vertebra of YPM 57100 in ventral view (from left to right: **A**–**L**). Scale bars = 1 cm.

process that barely touches the caudal part of the iliac blade. The configuration of the sacral vertebrae is nearly identical to that of other specimens of *P. gracilis* (Weinbaum and Hungerbühler, 2007), but it is clear that the thin transverse process of the last sacral may easily be broken if not well preserved. Compared to other poposauroids, the first three sacral vertebrae (first primordial, insertion, and second primordial) are identical to that of *Arizonasaurus* (Nesbitt, 2005) and similar to that of shuvosaurids with the addition of one or more caudosacrals (e.g., *Sillosuchus*; Alcober and Parrish, 1997).

The sacral centra of *P. gracilis* are more dorsoventrally flattened than the trunk vertebrae and caudally, the centra have a more equant shape and a flatter ventral surface in the more caudal vertebrae, with the exception of the last caudosacral (Fig. 15). Unlike most other specimens of *Poposaurus*, in which the sacrals are partially or completely coossified (including the bases of the neural spines; see Long and Murry, 1995; Weinbaum and Hungerbühler, 2007), the sacral centra are not coossified, but the first and second sacral, and second and third sacral, are very closely appressed to each other with only a slight gap between the rims. The fourth sacral centrum (=second primordial) is the largest, as in *Effigia* and *Shuvosaurus* (Nesbitt, 2007; Nesbitt et al., 2011). Sacrals 1–4 have a moderately deep fossa on the lateral surface of centrum just ventral to the attachment locations of the sacral ribs. As in the trunk vertebrae, the edges of the articular facets of the centra have radiating fine ridges. The neurocentral and alar/transverse process sutures are highly interdigitated and narrow without closure (Fig. 14). The articular facets of the sacral centra are roughly circular to minimally dorsoventrally compressed, with a height to width ratio of 0.806 at the cranial face of S2. There is minimal wasting

Fig. 9. Thoracic vertebrae of YPM 57100. First thoracic vertebra in cranial (**A**) and caudal (**B**) views. Second thoracic vertebra in cranial (**C**) and caudal (**D**) views. Third thoracic in cranial (**E**) and caudal (**F**) views. Sixth thoracic vertebra in cranial (**G**) and caudal (**H**) views. Seventh thoracic vertebra in cranial (**I**) and caudal (**J**) views. Eighth thoracic vertebra in cranial (**K**) and caudal (**L**) views. Ninth thoracic vertebra in cranial (**M**) and caudal (**N**) views, (neural spine not pictured). Scale bars = 1 cm.

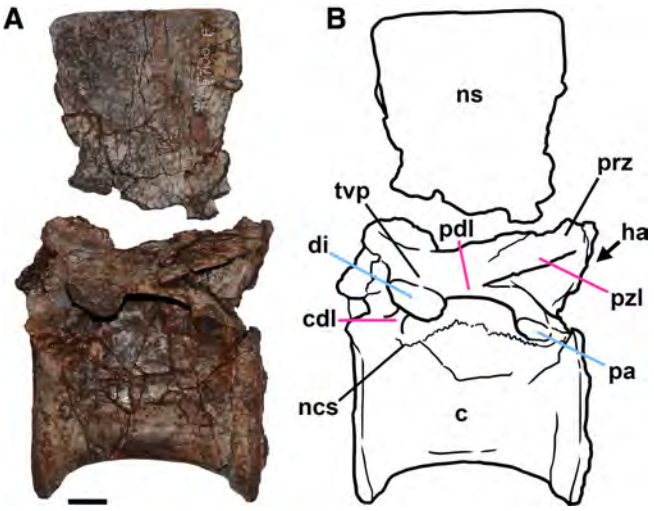

Fig. 11. Photograph (**A**) and diagrammatic illustration (**B**) of thoracic vertebra nine of YPM 57100 in right lateral views. Pink lines indicate lamina and blue lines indicate articulation with the ribs. Abbreviations: c, centrum; cdl, centrodiapophyseal lamina; di, diapophysis; ha, hypantrum; ncs, neurocentral suture; ns, neural spine; pa, parapophysis; pdl, paradiapophyseal lamina; prz, prezygapophysis; pzl, prezygaparapophyseal lamina, tvp, transverse process. Scale bar = 1 cm.

at the mid centrum with a cranial intervertebral articular face cross-sectional area to midcentral cross-sectional area ratio of 1.18 at S2. There are deep ventral depressions of the spinal canal floor similar to that described for the trunk vertebrae (see above). On sacrals 1–3, the strut of the neural arch between the dorsal edge of the centrum leading to the postzygapophysis is thin and has a large concave embayment directed cranioventrally just above the neurocentral suture. Structures that would be the equivalent of the prezyga- and postzyga-diapophyseal laminae of dinosaurs are well developed as thin horizontal crests in all sacral vertebrae. The neural spines of the first two sacrals are very similar in height to that of the trunk vertebrae but are broader at the dorsal apex in lateral view. The neural spine of the third sacral vertebra broadens to the apex like sacrals one and two but also has a slight caudodorsal inclination. The fourth and fifth neural spines (the caudosacrals) are much narrower craniocaudally in lateral view and also possess a distinct caudodorsal inclination.

The sacral ribs are paired with their respective vertebrae (Fig. 15B,C), and are not shared between centra, unlike *Effigia* and *Sillosuchus* (see Nesbitt, 2007) where sacral ribs attach on the centrum rims. The sacral ribs are broken across the vertebrae and the ilium and have been slightly compressed. All of the sacral ribs are restricted to the dorsal part of the centrum and do not expand ventrally (Fig. 15B,C). The attachment point of the sacral rib to the vertebra is cranially placed relative to the origin on sacral one (=first primordial), and the other sacral ribs are progressively more caudally placed through the sacral column. Sacral rib one attaches mostly to the preacetabular process and nearly contacts the cranial tip; the caudal margin of the first sacral rib is on the medial side of the pubic peduncle. The sacral rib of the second sacral vertebra is horizontally oriented and attaches to just dorsal to the acetabulum on the medial surface. The sacral rib of the third sacral (=second primordial) attaches to the caudal portion of the iliac blade, is dorsoventrally expanded cranially, and it barely reaches the medial surface of the base of the ischial peduncle. The rib of the fourth sacral attaches to the caudal aspect of the caudal iliac blade. The attachment site of the sacral rib of the fifth sacral barely touches the caudal tip of the caudal iliac blade and slightly overlaps the caudal margin of the sacral rib of sacral four dorsally.

Caudal Vertebrae

All of the caudal vertebrae appear to be present (Figs. 16–20); however, a short series of middle caudals (likely five individual vertebrae) after caudal vertebra 14 was still buried in the matrix at the time of analysis. Therefore, we estimate that there are a total of approximately 56 caudal vertebrae. The number of caudal vertebrae exceeds estimates of other poposauroids with partially preserved tails (e.g., *Qianosuchus*, 50 vertebrae, (Li et al., 2006). It is similar to the estimation of 55 caudal vertebrae for the pseudosuchian archosaur, *Ticinosuchus ferox* (Krebs, 1965). The number of caudal vertebrae in *Poposaurus* also exceeds that in neotheropod dinosaurs (estimated at 40 for *Coelophysis bauri*; Colbert, 1989). Neurocentral sutures are clearly open in proximal caudal vertebrae but are not visible more distally; the exact change to closed sutures is not clear because of poor surface detail in the middle portion of the column.

The caudal centra are robust with a wide centrum near the sacrum, becoming gradually more slender in lateral view and elongate craniocaudally, with a morphological transition occurring at caudal vertebra 13, in which they are at least twice as long as they are tall. The proximal caudal centra are amphicoelous, whereas the mid and distal caudal centra are platycoelous. In the proximal caudal vertebrae, there is a shallow fossa on the lateral surface of the centra ventral to the boundary between the centrum and the neural arch; craniocaudal length of this depression is approximately one-third of the length of the centrum. Starting on the second caudal vertebra, (Figs. 2 and 16) distinct chevron facets are present on the ventrolateral margin of the caudal articular surfaces of the centra. In the middle caudal vertebrae, paramedian ridges on the ventral surface of the centrum extend cranially from the chevron facets, bounding a shallow, ventrally open fossa on the midline.

The prezygapophyses of the middle and distal caudal vertebrae are elongated, extending cranially to overlap with one-fifth of the length of the preceding vertebra (Figs. 19 and 20). The cranial third of each prezygapophysis extends beyond the articulation with the corresponding postzygapophysis. This is also present in shuvosaurids (Nesbitt and Norell, 2006; Nesbitt, 2007) but is absent in the poposauroid *Qianosuchus* (Li et al., 2006). The postzygapophyses extend caudal to the cranial rim of the subsequent vertebra. The neural spines of the first eight caudal vertebrae are compressed, craniocaudally wide in lateral view, project caudodorsally, and gradually widen craniocaudally toward the dorsal margin (Figs. 17 and 18). More distal caudal vertebrae display a marked decrease in height distally; however, the exact transition of this

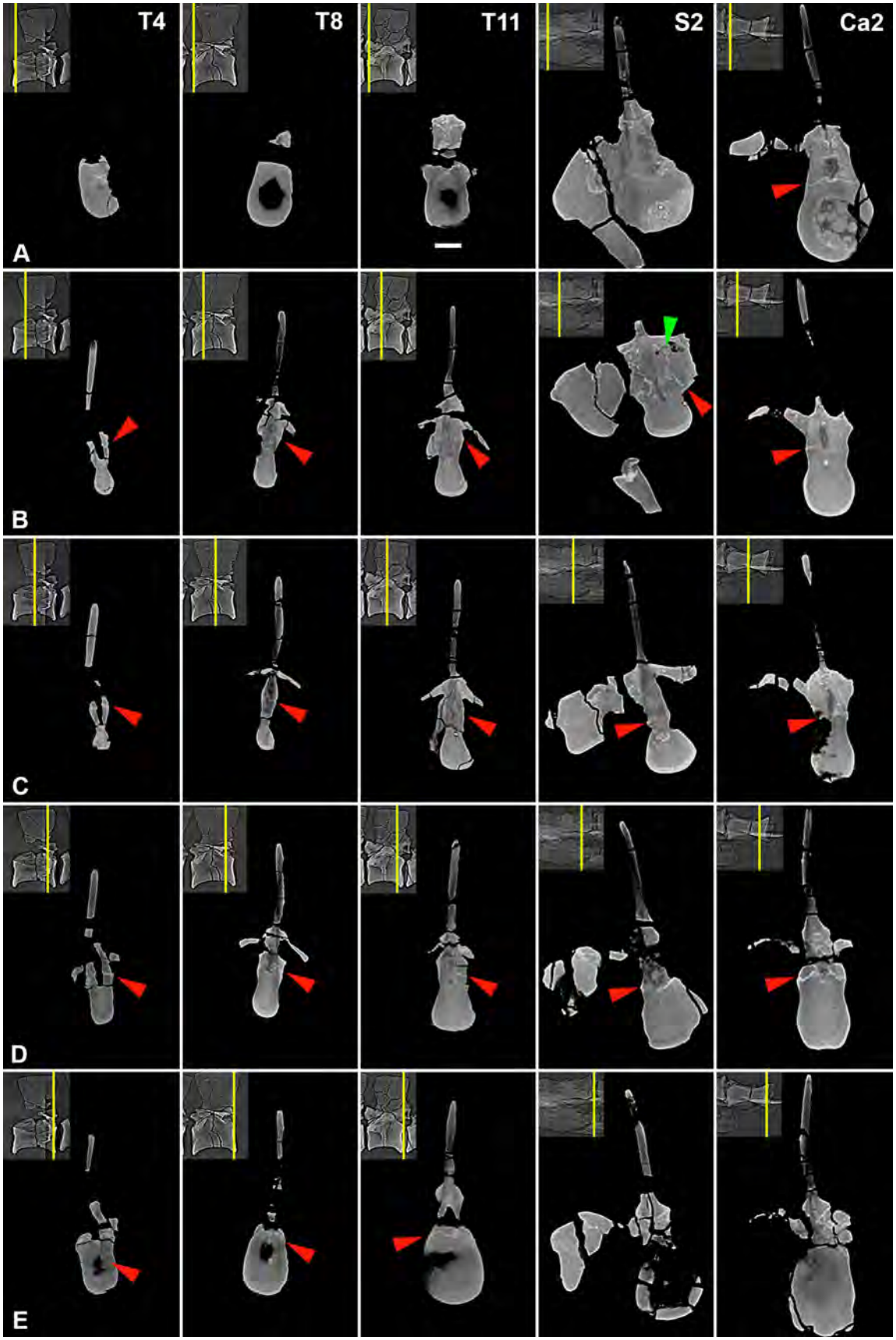

Fig. 12. Legend on next page.

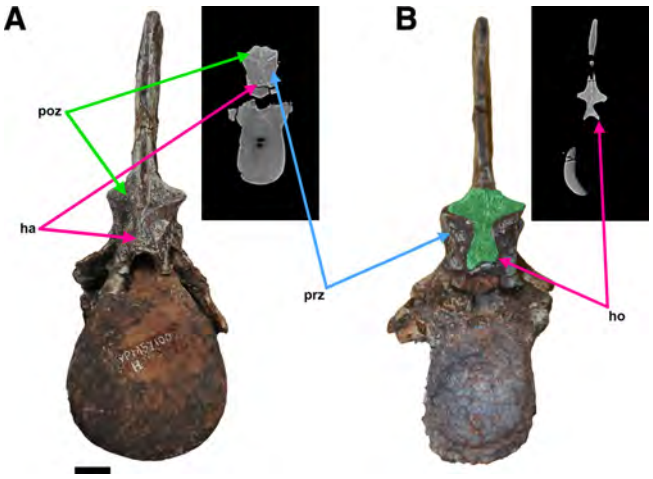

Fig. 13. Interlocked hyposphene-hypantrum: cranial view of T11 of YPM 57100 with axial CT image inserts—cranial surface in (**A**), and caudal surface in (**B**), showing the CT scan image correlation between the appearance of the articulated zygapophyseal joints and hyposphene-hypantra in (A). The postzygapophysis and hyposphene are indicated by the green arrow in (A), and highlighted green in (B). The blue arrows indicate the prezygapophyses. The pink arrows in (A) correlate with the disarticulated hypantrum in the associated CT image; the pink arrows in (B) correlate with the disarticulated hyposphene on the CT image of the caudal side of T11. Abbreviations: ha, hypantrum; ho, hyposphene; poz, postzygapophysis; pre, prezygapophysis. Scale bar = 1 cm.

morphological change is not clear given that the change occurs in the section of the tail that is still buried in the matrix (Figs. 2, 17, and 18). The transverse processes of the proximal caudal vertebrae are dorsoventrally flattened and angled caudolaterally. Like the transition in the neural spines, the transverse processes diminish distal to the 12th vertebra, but the exact vertebral position where the transverse processes disappears remains covered in matrix. No vertebral laminae are present on the neural arches of the caudal vertebrae.

Ribs and Chevrons

The cranial and mid-thoracic rib heads have distinct capitula and tubercula separated by a thin lamina of bone (Fig. 8H), as in most archosaurs. The capitulum is larger and has a subcircular articular facet, whereas the tuberculum is smaller and has a craniocaudally oriented elliptical articular facet. The rib heads articulate in a near-horizontal plane throughout the thoracic series, with the tuberculum only slightly elevated relative to the capitulum. Proximally, the rib shaft is subtriangular in

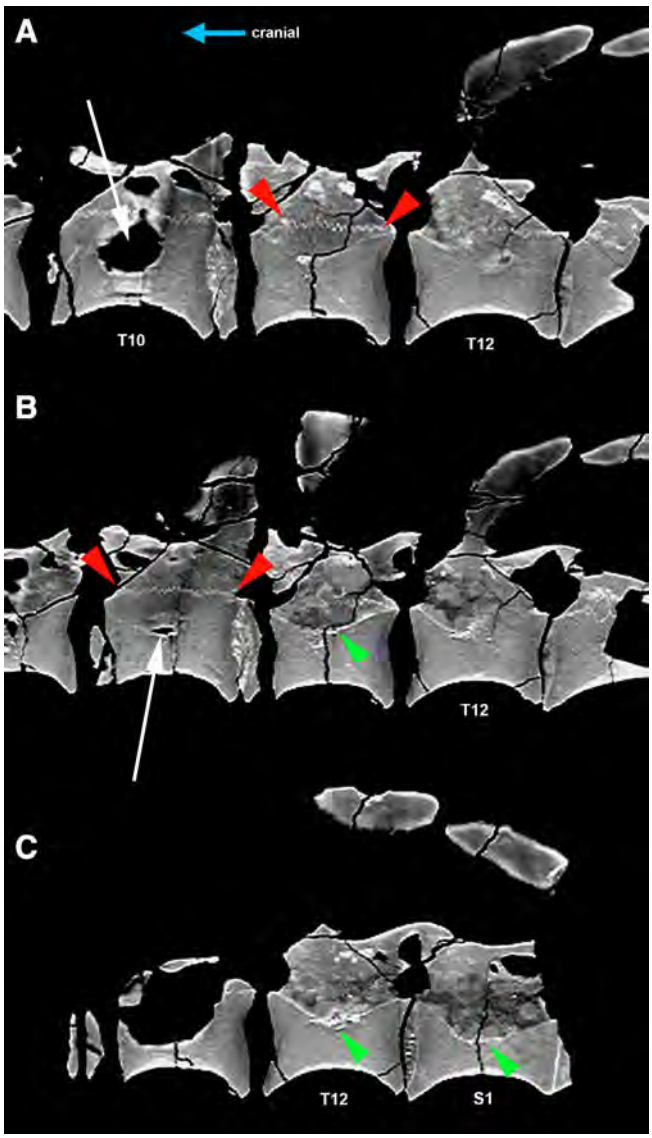

Fig. 14. Sagittal reconstruction of a CT scan of T10-S1 of YPM 57100. Rows (**A**) through (**C**) progress from lateral/superficial to medial/deep. White arrow in (A) shows apneumatic lateral fossa that terminates in vascular foramen [white arrow in (**B**)]. Note how midcentral vascular foramen approximates the deepest extent of spinal cord ventral depression indicated with green arrowheads in (B) and (C). Red arrowheads indicate neurocentral sutures. Note serrated/interdigitated morphology. Serrations are deeper and wider laterally as the sutural ridges radiate from the midcentrum. The thickness of the "white line" contact throughout the length of the sutures is similar from T10 through T12 as best shown in (A). There is no effacement/remodeling to indicate fusion and all appear similar in maturity.

Fig. 12. Serial transverse CT images comparing the morphologies of vertebrae T4, T8, T11, S2, Ca2 (columns) of YPM 57100. Rows (**A**–**E**) are axial slice images obtained at the same relative locations spaced at 25% increments of the vertebral lengths (localizer images with slice locations are provided in the upper left corner). The middle row (C) is midcentral. The increase in size and transition from transversely compressed to more circular cross-sectional shape is evident form T4 through Ca2. Comparison between the end rows (A) and (E) to the midcentral row (C) illustrates the degree of midcentral waisting or tapering of the centra. Red arrowheads indicate the neurocentral sutures. Green arrowhead in (S2/B) shows the alar/transverse process suture. All images are to scale. Scale bar = 1 cm.

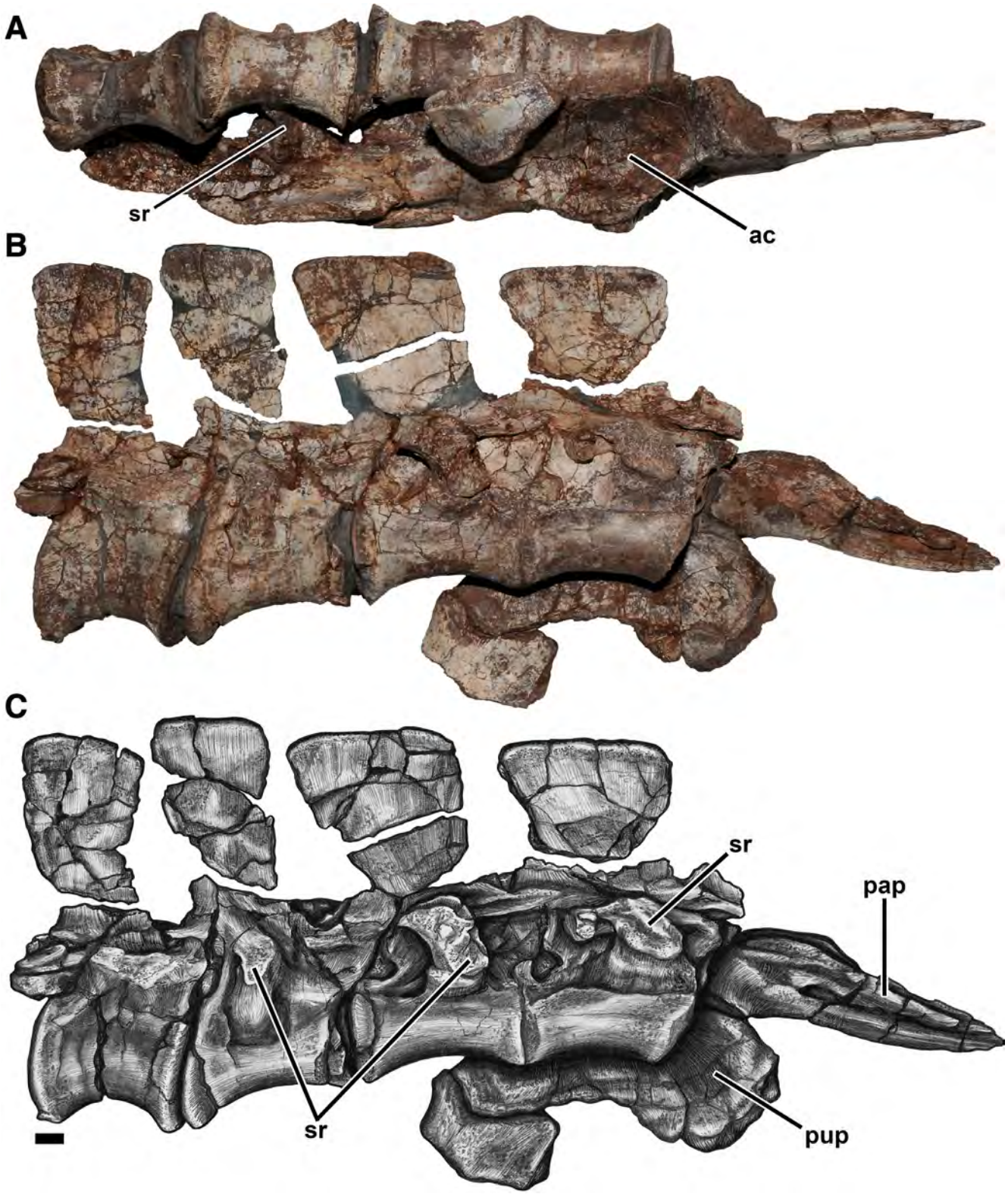

Fig. 15. Sacral vertebrae with attached right ilium of YPM 57100 in ventral (**A**) and right lateral views (**B**, **C**). Abbreviations: ac, acetabulum; pap, preacetabular process; pup, pubic process; sr, sacral ribs. Scale bar = 1 cm.

Fig. 16. Proximal caudal vertebrae of YPM 57100 in left lateral view. Scale bar = 1 cm.

cross-section with a distinct flange on the lateral edge; about halfway down the shaft, the flange disappears and the cross-section becomes slightly more oval in shape. The rib heads never converge in the caudal thoracic vertebrae like that of extant crocodilians (Schachner et al., 2011a), but in the caudalmost trunk vertebrae of *P. gracilis*, the capitulum and tuberculum are separated only by a narrow ridge.

The chevrons associated with the proximal caudal vertebrae are long (approximately 2.5× the length of the proximal caudal centra), laterally compressed, oriented caudoventrally, and slightly expand distally in lateral view into a rounded spatulate tip (Figs. 17 and 18). The proximal chevrons are long, and about equal in length to the overall height of its corresponding vertebra (Fig. 18). The chevrons reduce in length distally at caudal vertebra 20, where they are approximately equal to the craniocaudal length of the corresponding centrum, and eventually the chevrons disappear at approximately two-third the length of the tail (Fig. 19). The chevrons in the middle portion of the tail are more caudally directed than the proximal ones.

Fig. 17. The caudal vertebrae (minus the three most proximal caudals) of YPM 57100 in the original field jackets. Scale bars = 10 cm.

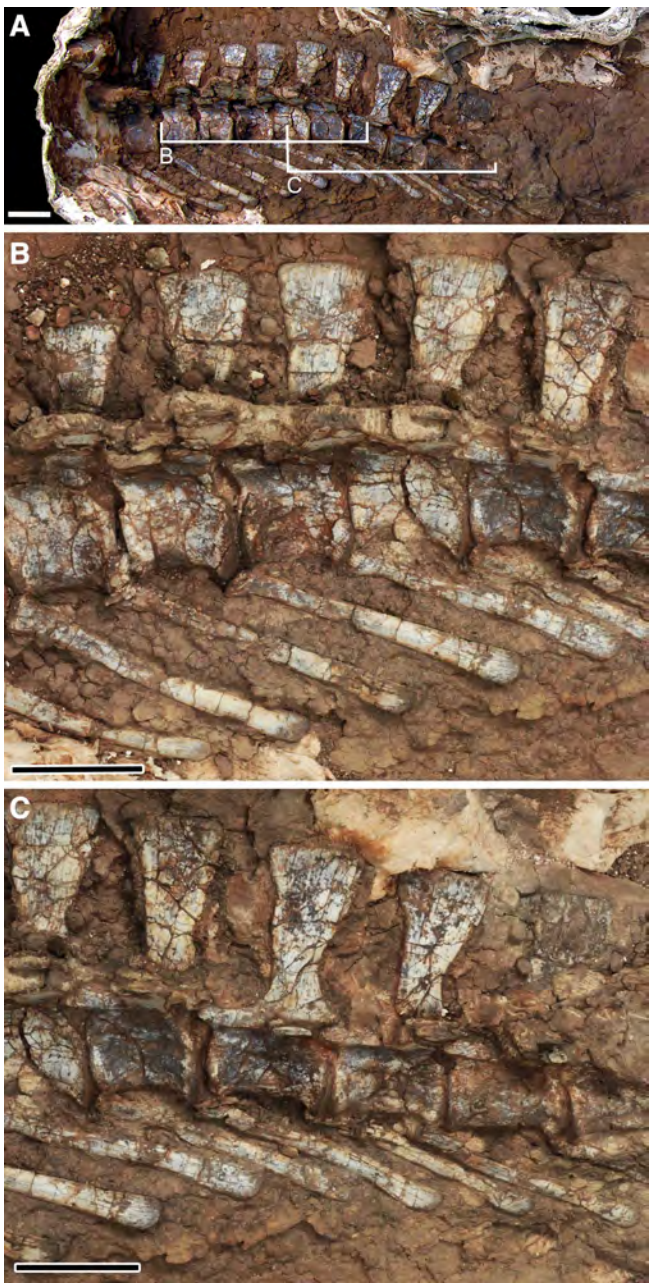

Fig. 18. (**A**) Detailed view of the proximal third of the caudal vertebrae of YPM 57100 in the original field jacket, in left lateral view. Regions identified in (A) are represented at a higher resolution in (**B**) and (**C**). Scale bars = 5 cm.

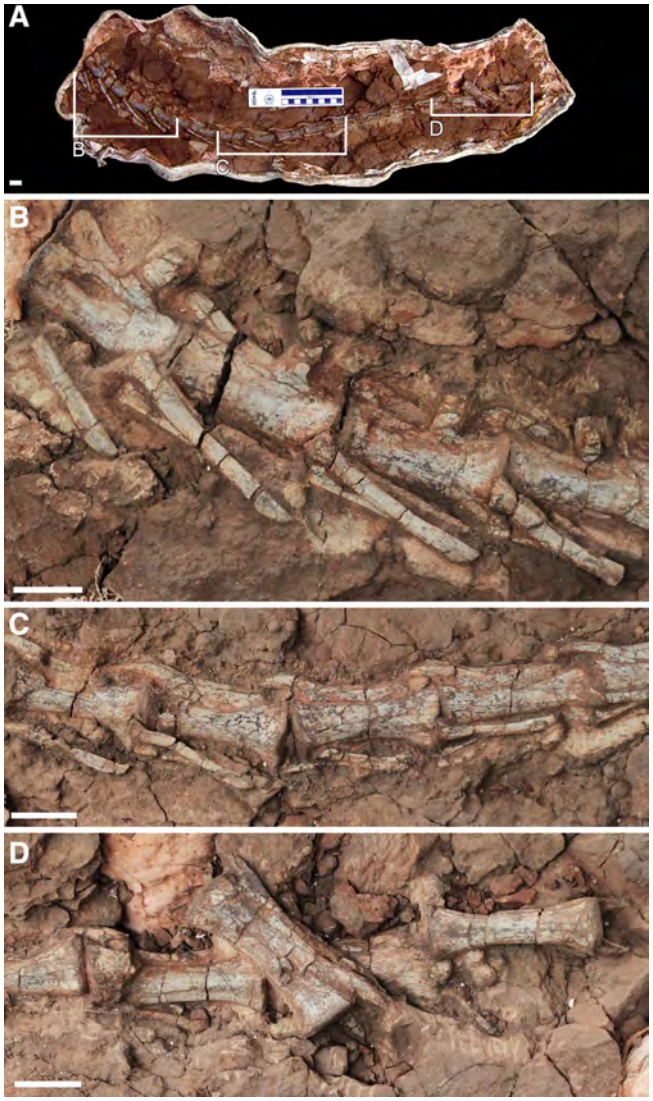

Fig. 19. (**A**) Detailed view of the middle third of the caudal vertebrae of YPM 57100 in the original field jacket, in left lateral view. Regions identified in (A) are represented at a higher resolution in (**B**–**D**). Scale bars = 2 cm.

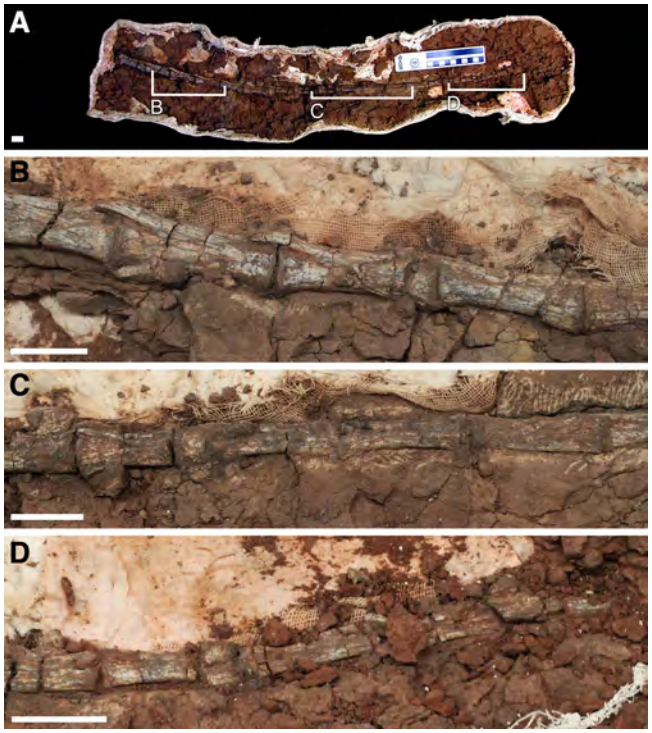

Fig. 20. (**A**) Detailed view of the distal third of the caudal vertebrae of YPM 57100 in the original field jacket, in left lateral view. Regions identified in (A) are represented at a higher resolution in (**B**–**D**). Scale bars = 2 cm.

Scapula

Both scapulae are present. The much more complete left scapula is missing the craniodorsal margin, whereas the right is missing most of the scapular blade except the distal end (Fig. 21A–D). The scapulae possess a narrow, constricted shaft with proximal and distal expansions. They are more similar in form to the scapulae of the poposauroids *Arizonasaurus* (Nesbitt, 2005) and *Lotosaurus* (IVPP unnumbered), and other pseudosuchians (e.g., aetosaurs and loricatans), than they are to the craniocaudally wide, but mediolaterally thin-bladed scapula of *Effigia*, *Shuvosaurus*, and possibly *Sillosuchus* (Nesbitt, 2007) or the short craniocaudally wide scapula of *Qianosuchus* (Li et al., 2006). The scapular portion of the glenoid fossa of *P. gracilis* is completely oriented caudoventrally, with no lateral component. This orientation is present in other poposauroids (e.g., *Effigia*; Nesbitt, 2007), and other loricatans such as *Batrachotomus* (Gower and Schoch, 2009), rauisuchids (*Postosuchus kirkpatricki*; Weinbaum, 2013), and crocodylomorphs (Clark et al., 2004). Additionally, this glenoid orientation is also present in ornithodirans that hold their forelimbs in a more ventrally oriented position (e.g., Langer and Benton, 2006; Nesbitt, 2011). In proximal view, the proximal end of the scapula is subtriangular in outline and this surface articulates with the coracoid. Unlike *Arizonasaurus* (Nesbitt, 2005), the scapular shaft of *Poposaurus* lacks a distinct groove on the caudolateral surface, although there is a small but distinct obliquely oriented raised muscle scar on the ventral surface (Fig. 21), approximately one-third of the distance from the proximal end. This scar would likely be an attachment site for m. scapulohumeralis posterior (Dilkes, 1999), based on comparisons with living crocodylians (Brochu, 1992; Meers, 2003). There is a very shallow but distinct groove on the caudomedial surface that leads from this muscle scar distally along the shaft. This could either be a continuation of the attachment site for m. scapulohumeralis, or an origin site for *m. serratus* superficialis based on the reconstruction for *Maiasaura* (Dilkes, 1999), and extant crocodylians (Brochu, 1992; Meers, 2003). The preserved portion of the craniodorsal margin is mediolaterally thin and distinctly convex in lateral view. Because the complete craniodorsal margin is missing on both scapulae, it is unclear if the scapula of *Poposaurus* shares the unusual axe-shaped anatomy of

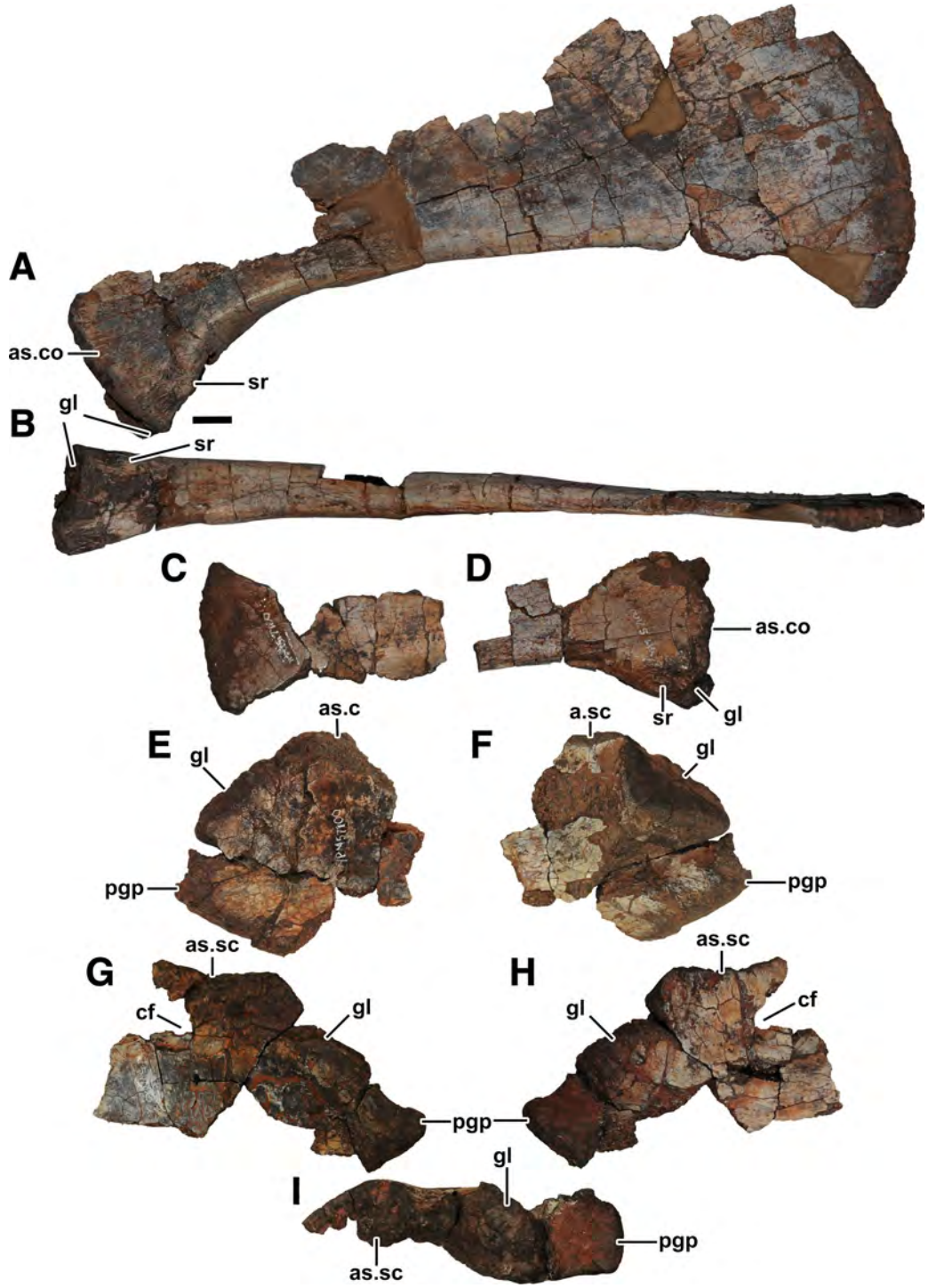

Fig. 21. Left scapula of YPM 57100 in lateral view (**A**) and ventral view (**B**). Distal portion of the right scapula (**C**) and proximal portion of the right scapula (**D**) in lateral views. Left coracoid in medial (**E**) and lateral (**F**) views. Right coracoid in medial (**G**), lateral (**H**), and articular (**I**) views. Abbreviation: as., articulates with; *cf*, coracoid foramen; co, coracoid; gl, glenoid; pgp, postglenoid process; sc, scapula; sr, scar. Scale bar = 1 cm.

the distal portion of the scapula in *Qianosuchus* (Li et al., 2006). Nonetheless, it is clear that the distal margin is convex and markedly flared (Fig. 21A), similar to the scapula of *Arizonasaurus*.

Coracoid and Clavicle

Only the proximal portions of the coracoids are preserved (Fig. 21E–I) because they were found weathered and fragmented. The surface that articulates with the

Fig. 22. Clavicular fragments of YPM 57100. Scale bar = 1 cm.

scapula is rugose, and in contrast to the scapula, the glenoid is oriented caudally with a slight lateral component. The caudoventral edge is thickened relative to the preserved cranial portion and is rugose as in *Arizonasaurus* (Nesbitt, 2005), and other suchians and dinosauromorphs (Nesbitt, 2011). A short, but mediolaterally thick postglenoid process is present, and this expansion is similar to *Arizonasaurus* (Nesbitt, 2005), *Qianosuchus* (Li et al., 2006; Nesbitt, 2007), *Batrachotomus* (Gower and Schoch, 2009), and rauisuchids (*Postosuchus kirkpatricki*; Weinbaum, 2013). In contrast, the shuvosaurids have much longer postglenoid processes (Nesbitt, 2007, 2011). A coracoid foramen is present; however, the exact shape of the foramen is not clear because the cranial margin is broken (Fig. 21).

Flat pieces of bone recovered on the surface are interpreted to be the remains of the clavicle and possibly the interclavicle (Fig. 22). The fragments possess a flattened ellipsoid shape in cross-section, and there are faint longitudinal striations on both of the surfaces. Similar fragments were interpreted as clavicle pieces in *Arizonasaurus* (Nesbitt, 2005) and the pseudosuchian *Nundasuchus* (Nesbitt et al., 2014).

Humerus

The left humerus is mostly complete (Fig. 23A–G), but only the proximal end of the right humerus is preserved (Fig. 23H-J). Overall, the humerus of *P. gracilis* has a more gracile morphology when compared to pseudosuchians with greatly expanded proximal and distal ends, for example, *Prestosuchus* (von Huene, 1938) and aetosaurs (Long and Murry, 1995), but it is more similar in proportions to that of the rauisuchid *Postosuchus* (Chatterjee, 1985; Weinbaum, 2013). Among poposauroids, the proportions of the proximal and distal ends relative to shaft of *P. gracilis* are similar to *Qianosuchus* (Li et al., 2006), less robust than *Lotosaurus* (Zhang, 1975), but more expanded relative to shuvosaurids (Nesbitt, 2007). The proximal expansion is slightly greater than the distal expansion, but only slightly.

In proximal view (Fig. 23F,J), the articular surface is morphologically similar to *Postosuchus alisonae*; however, the articular surfaces and deltopectoral crest are slightly more gracile (i.e., less developed). The humeral head is distinct but not hemispherically shaped as in *Effigia* and *Shuvosaurus* (Long and Murry, 1995; Nesbitt, 2007). There is a slight craniocaudal expansion of the proximal articular surface just medial to the deltopectoral crest. The deltopectoral crest (Fig. 23A,B) is mediolaterally narrow with a rounded margin in medial view. Its crest is contiguous with the proximal articular surface. The apex of the crest is located approximately one-sixth of the length of the humerus, distal from the proximal surface, and the base of the crest is located approximately one-quarter of the length of the humerus. The length of the entire crest is longer than in *Shuvosaurus* (Long and Murry, 1995) but is similar to that of *Lotosaurus* (Zhang, 1975). The deltopectoral crest in *Poposaurus* projects more cranially than in *Effigia* (Nesbitt, 2007) or *Shuvosaurus* (Long and Murry, 1995) but is not as robust or distinct as in the loricatans *Postosuchus alisonae* and *Batrachotomus* (Nesbitt, 2011). The lateral margin of the humeral shaft is largely straight, whereas the medial margin is distinctly concave in the proximal third.

Despite a slight oblique mediolateral distortion of the left humerus, a modest flaring of the distal condyles is evident (Fig. 23D). Both condyles are equally expanded. The cranial margin of the ectepicondyle is flat, whereas it is rounded on the entepicondyle, a condition also present in *Effigia* and *Shuvosaurus* (Long and Murry, 1995; Nesbitt, 2007). Both condyles have a caudal margin that forms a rounded ridge that extends proximally onto the shaft of the humerus and these ridges bound a triangular fossa between the condyles. There is a distinct groove on the caudolateral surface of the shaft, just proximal to the ectepicondyle (an ectepicondylar groove) (Fig. 23B). This condition is present in phytosaurs, aetosaurs, and most loricatans, but absent in *Effigia* and *Shuvosaurus* and other poposauroids, most early archosauriforms, and crocodylomorphs (Nesbitt, 2011). On the cranial surface just proximal to the distal condyles, there is an ovoid fossa (Fig. 23D).

Ulna

The complete left ulna is present but the proximal half is crushed (Fig. 24A,B). It is equal in length to the humerus. Despite the damage, the ulna is clearly gracile overall, with a constricted shaft and poorly expanded proximal and distal ends. The olecranon process is short but distinct (Fig. 24A,B), and small relative to other early archosaurs (Nesbitt, 2011). In the proximal view, the articular surface is triangular with rounded edges (Fig. 24E), whereas it is teardrop-shaped in *Effigia*. The lateral (=radial) tuber is distinct and tapered in proximal view, and both this process, as well as the olecranon process, are distinct as in most pseudosuchians (e.g., Peyer et al., 2008; Gower and Schoch, 2009; Nesbitt, 2011; Weinbaum, 2013), unlike the gently rounded surface of the proximal ulna in *Effigia* (Nesbitt, 2007). The medial surface of the proximal quarter of the ulna is slightly concave, as in *Batrachotomus* (Gower and Schoch, 2009) and *Postosuchus alisonae* (Peyer et al., 2008), but unlike the convex surface in *Effigia* and *Fasolasuchus* (Nesbitt, 2011). This proximal articular surface is convex caudally and concave cranially, differing from the completely convex surface in *Effigia* (Nesbitt, 2007).

The distal end of the ulna is mediolaterally compressed and flares craniocaudally (Fig. 24F), similar to the condition in other archosauriforms (*Proterosuchus*, *Vancleavea*, and phytosaurs) as well as some early pseudosuchians,

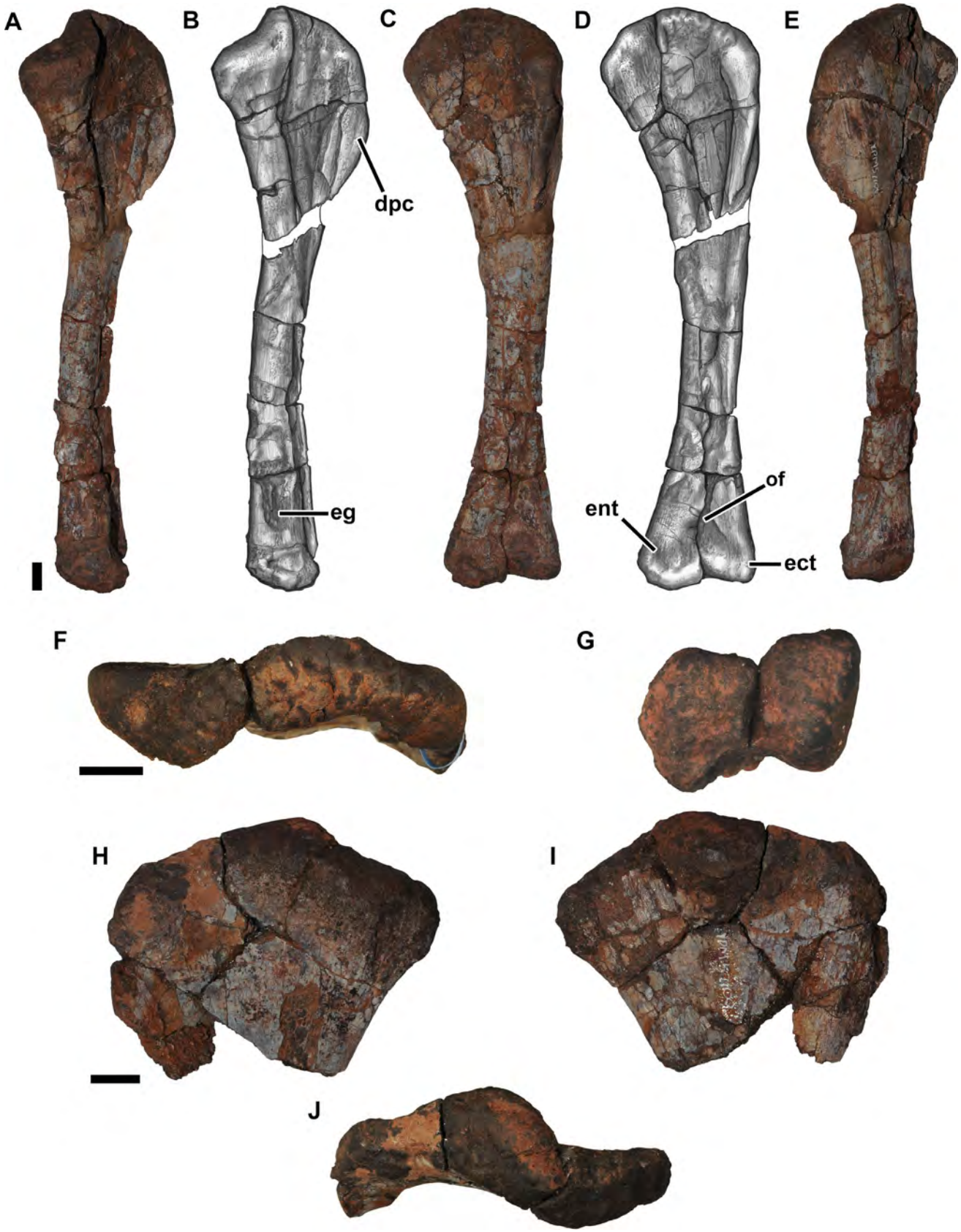

Fig. 23. Photographs and illustrations of the left humerus of YPM 57100 in medial (**A**, **B**), caudal (**C**, **D**), lateral (**E**), and proximal (**F**) and distal (**G**) articular views. Proximal articular surface and head of the right humerus in cranial (**H**), caudal (**I**), and proximal articular views. Abbreviations: dpc, deltopectoral crest; ect, ectepicondyle; eg, ectepicondylar groove; ent, entepicondyle; of, ovoid fossa. Scale bars = 1 cm.

Fig. 24. The left ulna of YPM 57100 in (**A**) lateral (**B**) medial, (**C**) cranial and, (**D**) caudal views. Proximal (**E**) and distal (**F**) articular surfaces of the left ulna. The left radius in lateral (**G**), medial (**H**), cranial (**I**), and caudal (**J**) views. Proximal (**K**) and distal (**L**) articular surfaces of the left radius. Abbreviations: ol, olecranon process; rg, radial groove. Scale bars = 1 cm.

including aetosaurs (Nesbitt, 2011). This flaring is distinct relative to *Effigia*, in which the distal articular surface is gently convex and craniocaudally elliptical in the ventral view.

Radius

The left radius is well preserved and does not exhibit any of the crushing observed in the ulna (Fig. 24C,D). The radius is subequal in length relative to both the ulna and humerus. A small portion is missing from the caudal half of the proximal articular surface of the radius, but the overall bean-shaped outline of the surface remains clear, distinct from the ellipsoid shape and less flared proximal articular surface of *Effigia* (Nesbitt, 2007). The proximal head is not as expanded as much as that of aetosaurs (Long and Murry, 1995) or *Hesperosuchus agilis* (Colbert et al., 1952) but is much more subtle like that of *Postosuchus alisonae* (Peyer et al., 2008), *Batrachotomus* (Gower and Schoch, 2009), and *Lotosaurus* (Zhang, 1975). The proximal articular surface is slightly saddle-shaped in lateral view (Fig. 24G,H,K). The proximal head fits into the craniolateral concavity on the proximal portion of the ulnar shaft. The radial shaft constricts immediately distal to the proximal end maintaining a subcircular cross-sectional shape throughout its length. There are slight grooves that are located all around the shaft that are likely associated with the interosseous membrane, and the origin of the digital flexors and extensors (Meers, 2003). Distally, the radius

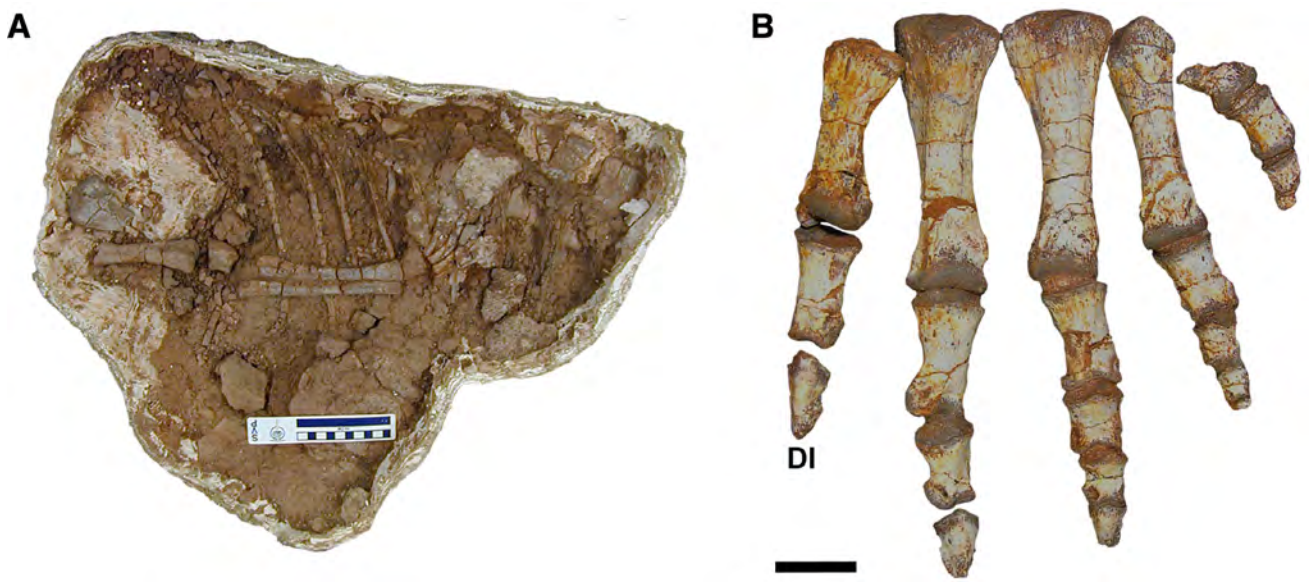

Fig. 25. (**A**) The original field jacket containing the thoracic and forelimb elements of YPM 57100; (**B**) the left manus after removal and articulation Abbreviation: DI, digit I. Scale bar for A = 10 cm; for B = 1 cm.

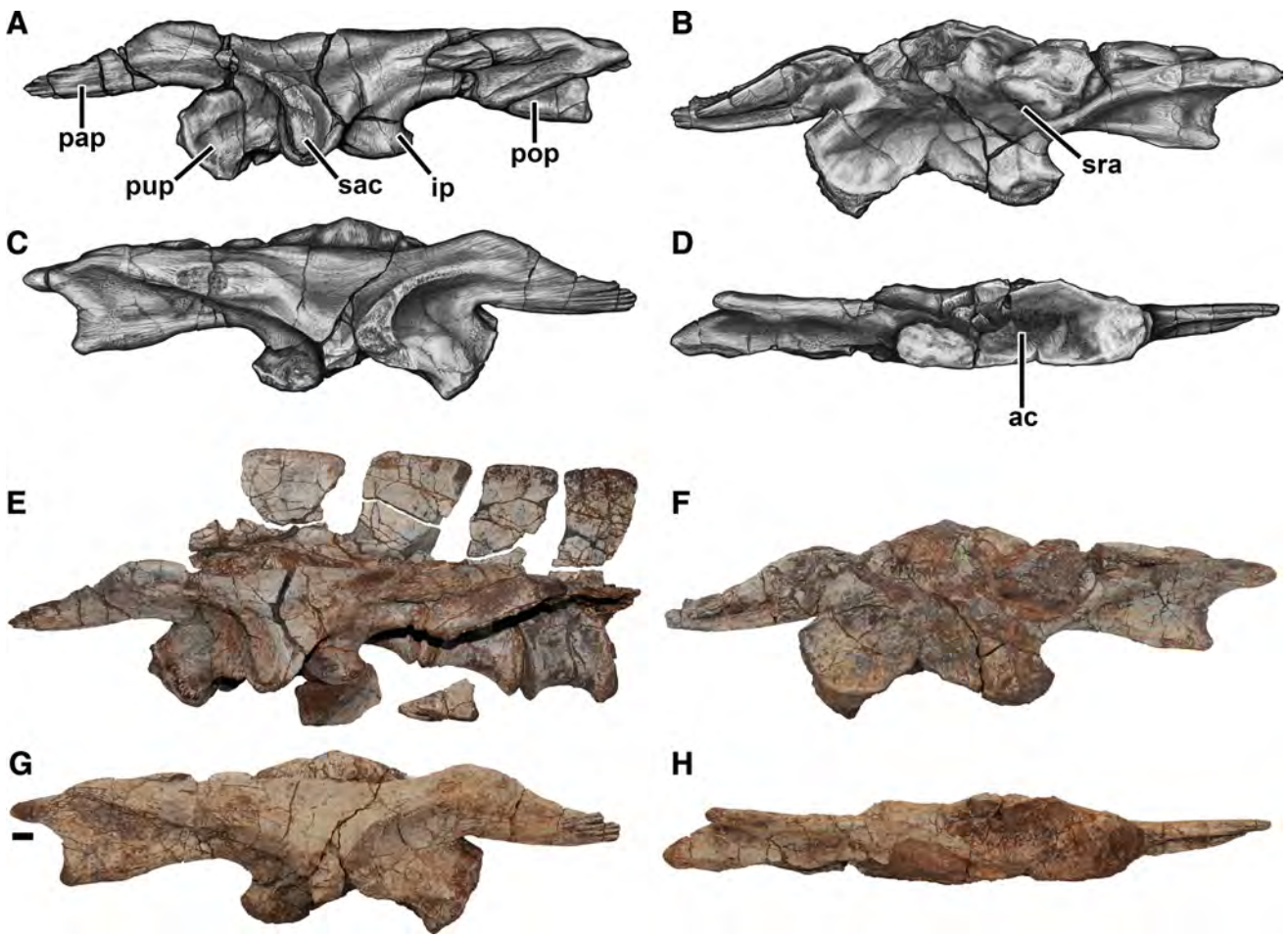

Fig. 26. The left ilium YPM 57100 in lateral view, without (**A**) and with (**E**) sacral vertebrae 2–5 attached. The right ilium of YPM 57100 in medial (**B**, **F**), lateral (**C**, **G**), and ventral (**D**, **H**) views. The ventral portion of the postacetabular process is pictured separately in (E). Abbreviations: ac, acetabulum; pap, preacetabular process; pop, postacetabular process; sac, supraacetabular crest; sra, sacral rib articulation. Scale bar = 1 cm.

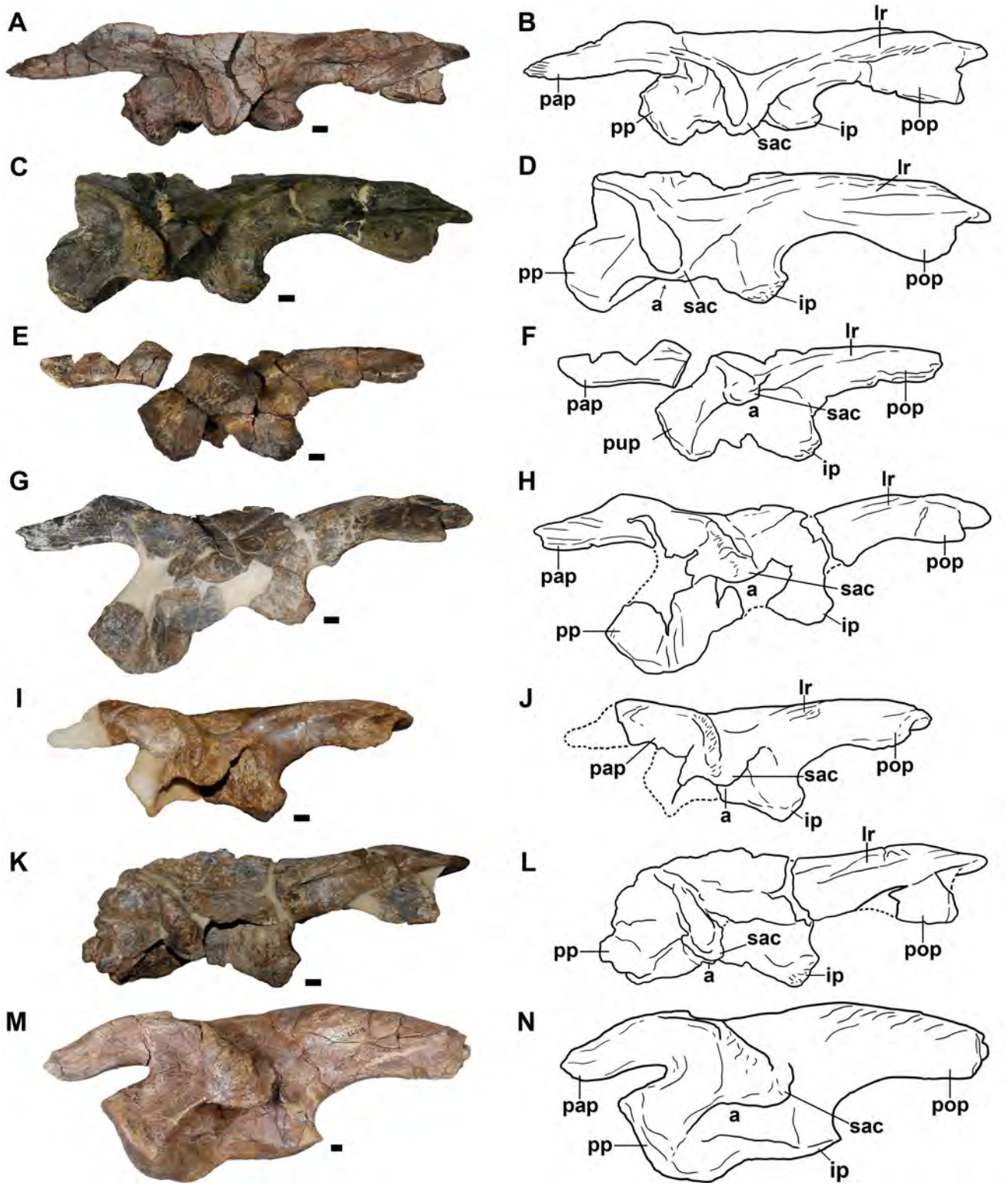

Fig. 27. The left ilia of various specimens of *Poposaurus* in lateral view (with two exceptions). (**A**, **B**) Photograph and illustration of the Yale specimen (YPM VP 57100). (**C**, **D**) Photograph and illustration of the ilium of the holotype of *P. gracilis* (FMNH UR 357). (**E**, **F**) Photograph and illustration of the ilium of *P. gracilis* (TMM 4368). (**G**, **H**) Photograph and illustration of the right ilium in lateral view of *P. gracilis* (TTU-P 11203); ilium has been flipped horizontally to visually match the others. (**I**, **J**) Photograph and illustration of the ilium of *P. gracilis* (TTU-P 9243). (**K**, **L**) Photograph and illustration of *P. gracilis* (TTU-P 11203). (**M**, **N**) Photograph and illustration of the right ilium of *P. langstoni* (TMM 31025-12) in lateral view; ilium has been flipped horizontally to visually match the others. Abbreviations: a, acetabulum; ip, ischial process; lr, lateral ridge; pp, pubic process; pap, preacetabular process; pop, postacetabular process; sac, supraacetabular crest. Image modified from Gauthier et al. (2011). Scale bars = 1 cm.

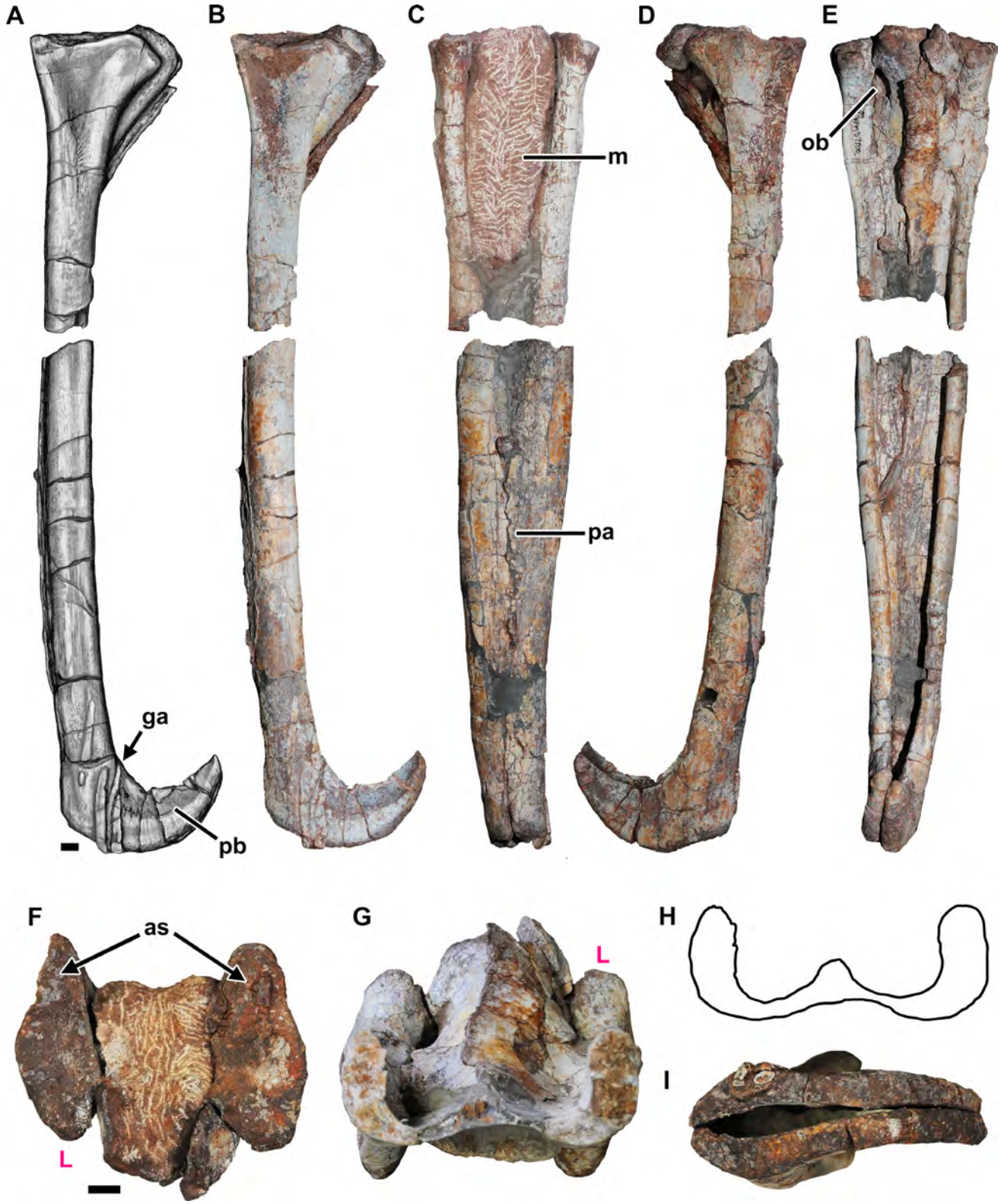

Fig. 28. The right and left pubes of YPM 57100 in left lateral (**A**, **B**), cranial (**C**), right lateral (**D**), caudal (**E**), proximal (**F**), and distal (**I**) views. (**G**) Cross-section of pubes at a natural midshaft break. (**H**) Diagrammatic illustration of the cross-section. Abbreviations: as, articular surface; ga, gastralia; m, matrix; ob, obturator foramen; pa, pubic apron. Red "L" indicates the left pubis to assist with orientation. Scale bars = 1 cm.

TABLE 1. Length measurements of the left pelvic girdle and hindlimb elements in *Poposaurus gracilis* YPM57100

Limb element	Measurement (mm)
Ilium (anteroposterior length)	286*
Pubis	510*
Ischium	327*
Femur	356
Tibia	300
Fibula	283
Metatarsal (MT) I	100
MT II	131
MT III	151
MT IV	132
MT V	83
Third digit, phalanx I	56
Third digit, phalanx II	39
Third digit, phalanx III	31

Measures indicated by an asterisk were acquired from photographs.

flares modestly laterally and slightly medially, terminating in a subcircular distal articular end and the overall morphology of the distal end is strikingly similar to that of *Postosuchus alisonae* (Peyer et al., 2008). This surface is relatively flat but more convex medially and flat laterally. There is a shallow longitudinal groove on the caudal side of the distal end (Fig. 24J), as in *Postosuchus alisonae* (Peyer et al., 2008), *Hesperosuchus agilis* (Colbert et al., 1952), and *Revueltosaurus callenderi* (Nesbitt, 2011).

Manus

The left manus of YPM 57100 is complete and as a result, is one of the most complete examples of any early pseudosuchian manus found thus far (Fig. 25). The small size of the manus of *P. gracilis* is perhaps its most remarkable feature; the maximum length, at digit III, is subequal to metatarsal I alone, and less than 30% the maximum length of the pes. Although most early archosaur taxa have a smaller manus relative to the pes compared to early archosauriforms (Nesbitt, 2011: char. 245), in both early archosauriforms and early archosaurs, the manus is generally 40%–50% the size of the pes (e.g., Padian et al., 2009). In contrast, the length of MC III is approximately 30% the length of MT III in *P. gracilis* and *Postosuchus* (Peyer et al., 2008; Weinbaum, 2013), and even smaller (~20%) in the shuvosaurid *Effigia* (Nesbitt, 2007). The complete manus of *P. gracilis* demonstrates and confirms that the manus of poposauroids are highly reduced relative to most of their pseudosuchian cousins.

No carpals are preserved and it appears that none was ossified at death. There are five digits, with a phalangeal formula of 2–3-4-?4–3 (Fig. 25). Metacarpal I is approximately two-thirds the length of metacarpals II and III, and about 80% the length of metacarpal IV. It is dorsoventrally flattened relative to the other metacarpals. Metacarpals II and III are the longest, are subequal in length, and are less than a quarter of the length of the radius and ulna. Metacarpal III is flared proximally, unlike the asymmetrical shape of this element identified in *Effigia* (Nesbitt, 2007). Metacarpal IV is approximately 80% the length of metacarpal III. The proximal articular surfaces of metacarpals III and IV are much more rounded than the blocky articular surfaces of *Effigia* (Nesbitt, 2007). Metacarpal V is present but not well exposed; both the medial and lateral surfaces are obscured by matrix; however, it can be determined that metacarpal V is the smallest of the series. A similar element found with the manus of *Effigia*, originally identified as potentially metacarpal I may, in fact, be metacarpal V; thus, it is possible that the partially articulated manus of *Effigia* identified as digits III–IV of the right manus may pertain to digits I–III or the left manus.

All of the metacarpals of *P. gracilis* are expanded both proximally and distally, with convexly rounded proximal articular surfaces. They are more gracile (longer with waisted midshafts) than in early archosauriforms, *Revueltosaurus*, aetosaurs, and *Postosuchus*, but similar to those of phytosaurs (Nesbitt, 2011: Fig. 32). Metacarpals I–IV have clear well-developed extensor pits, and the lateral ligament pits are well developed.

All of the phalanges are shorter than the shortest metacarpal, longer than wide, and have well-developed ligament pits at the distal ends. Phalanx 1 of digits II and III has more developed extensor pits in comparison with the other phalanges. Distal phalanges may be missing for digits IV and V. We suspect only the ungual is missing for digit IV because of the size of the last preserved phalanx; however, other pseudosuchian specimens lack preserved unguals here (SJN, *pers. obs.*) so this cannot be determined with any certainty. The unguals are shorter than their articulating phalanx and taper distally. Unlike other pseudosuchians with a recurved ungual, like the first digit in *Postosuchus alisonae* (Peyer et al., 2008), the unguals of *P. gracilis* are flattened ventrally into hooflike elements. This morphology is consistent with the unguals of the pes (Figs. 35 and 36; see below).

Ilium

Both ilia, found in articulation with the sacral vertebrae, are well preserved with little distortion (Fig. 26). The ilium of YPM 57100 is near identical to that of the holotype and the other referred ilia to *P. gracilis* (Fig. 27), but there are a few minor differences noted below. The preacetabular process is elongated, prong-like, mediolaterally compressed, and it extends cranially to the pubic process. A nearly identical process is present in *Poposaurus langstoni* (Long and Murry, 1995; Weinbaum and Hungerbühler, 2007). In contrast, the process is mediolaterally thinner and longer than that of *Arizonasaurus*, *Bromsgroveia*, *Lotosaurus*, the Waldhaus taxon, and *Qianosuchus* (Galton, 1985; Galton and Walker, 1996; Nesbitt, 2005; Li et al., 2006; Butler et al., 2011), in which the preacetabular process does not extend beyond the pubic peduncle. The lateral side of the cranial tip of the preacetabular process is covered in long, deep, striated muscle scars and these scars have been reconstructed as being associated with the origin of m. iliotibialis and m puboischiofemoralis internus 1 (Schachner et al., 2011b). In *P. gracilis*, the cranial process narrows just caudal to a dorsally enlarged ridge that is reconstructed as the origin site for m. iliotibialis 1 (Schachner et al., 2011b), unlike the dorsally expanded

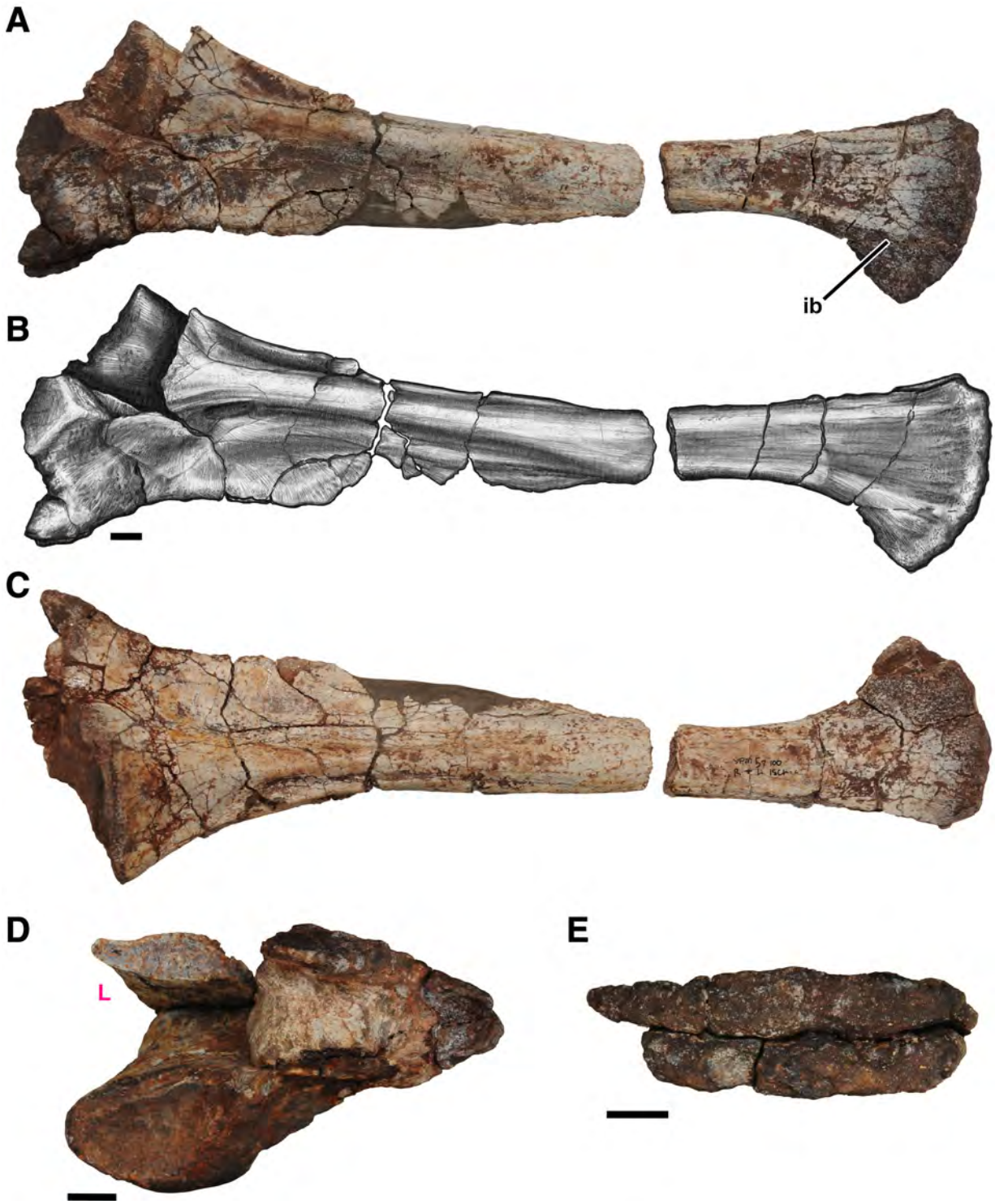

Fig. 29. The right and left appressed ischia of YPM 57100 in left lateral (**A**, **B**), right lateral (**B**), proximal/articular (**D**), and distal (**E**) views. Abbreviation: ib, ischial boot. Red "L" indicates the left ischium to assist with orientation. Scale bars = 1 cm.

and broad cranial process of shuvosaurids (Long and Murry, 1995; Alcober and Parrish, 1997; Nesbitt, 2007).

The iliac blade dorsal to the acetabulum is low with a straight dorsal margin in lateral view, similar to most early archosauriforms and pseudosuchians (Nesbitt, 2011), but unlike the tall convex blade of shuvosaurids (Nesbitt, 2007, 2011; see Fig. 11B Martz et al., 2013). A sharp raised ridge originates just ventral to the origin for

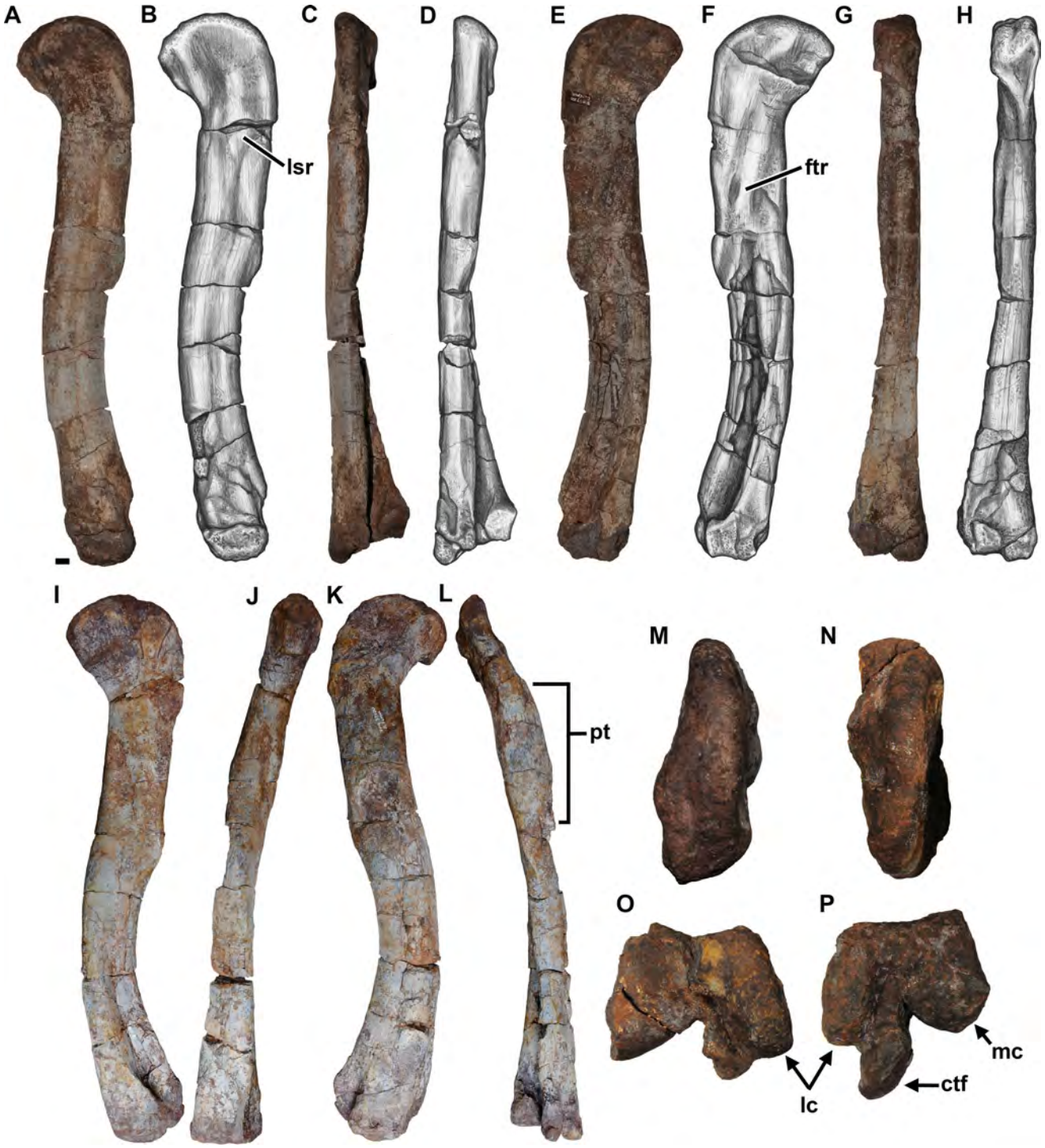

Fig. 30. Photographs and illustrations of left femur of YPM 57100 in lateral (**A**, **B**), caudal (**C**, **D**), medial (**E**, **F**), and cranial (**G**, **H**) views. The right femur of YPM 57100 in lateral (**I**), cranial (**J**), medial (**K**), and caudal (**L**) views. The proximal articular surfaces of the left (**M**) and right (**N**) femora. The distal articular surfaces of the left (**O**) and right (**P**) femora. Abbreviations: ctf, crista tibiofibularis; ftr, fourth trochanter; lc, lateral condyle; lsr, lancelet-shaped rugosity; pt, pathological thickening; mc, medial condyle. Scale bar = 1 cm.

m. iliotibialis 1 on the preacetabular process and extends caudoventrally, terminating at the dorsal margin in the craniocaudal center of the supraacetabular crest. This ridge divides the cranial and caudal origin of the m. iliofemoralis (Schachner et al., 2011b), and is present in most paracrocodylomorphs (Nesbitt, 2011: char. 265), but its length and craniodorsal-caudoventral inclination in *P. gracilis* is shared only with *Lotosaurus* and

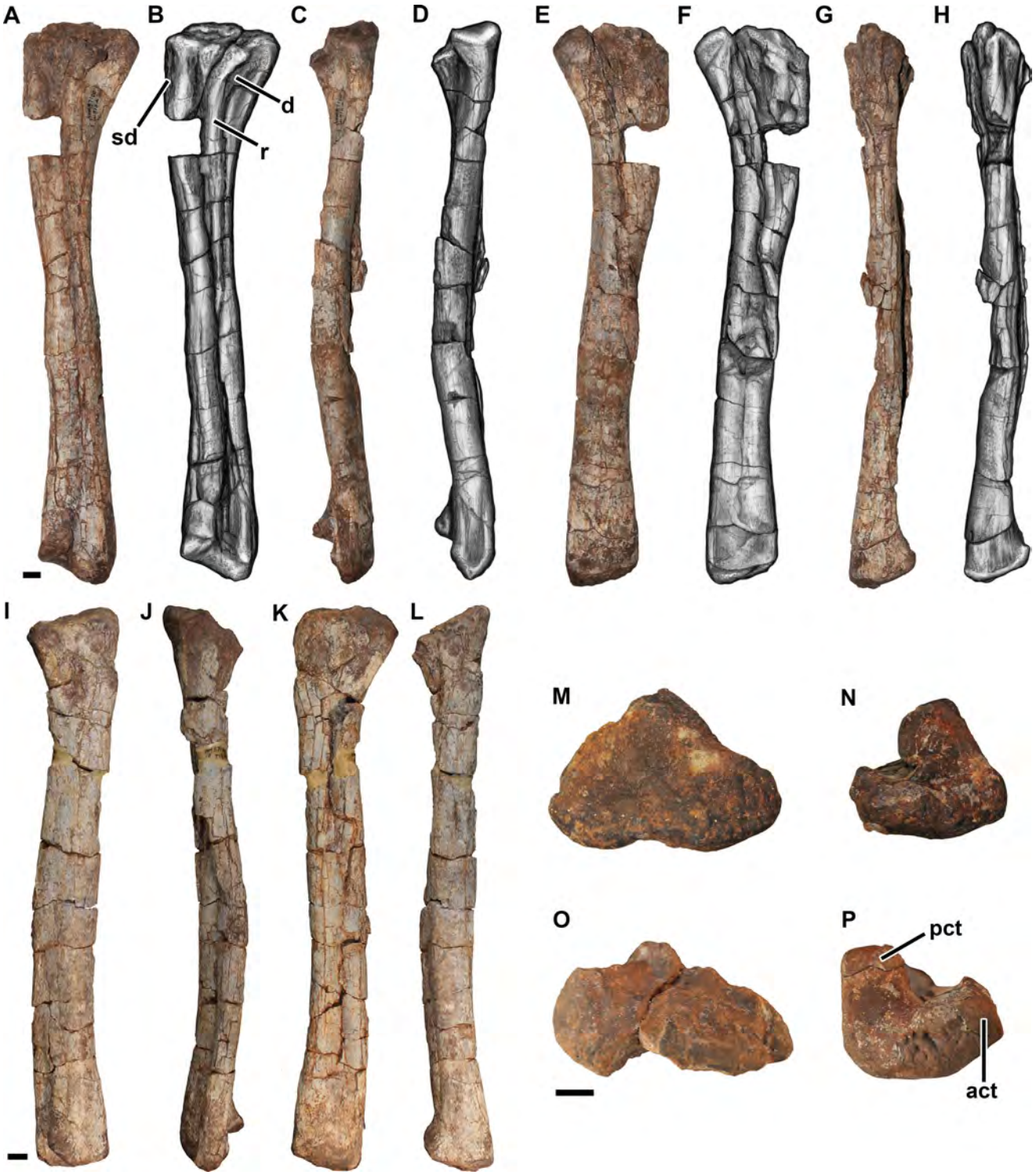

Fig. 31. Photographs and illustrations of the left tibia of YPM 57100 in lateral (**A**, **B**), caudal (**C**, **D**), medial (**E**, **F**), and cranial (**G**, **H**) views. The right tibia of YPM 57100 in lateral (**I**), caudal (**J**), medial (**K**), and cranial (**L**) views. The proximal (**M**, **O**), and distal (**N**, **P**) articular surfaces of both tibiae. Abbreviations: act, cranial condyle of the tibia; d, depression; pct, caudal condyle of the tibia; r, ridge; sd, slight depression. Scale bars = 1 cm.

shuvosaurids (Nesbitt, 2011: char. 266). As in all poposauroids, the supraacetabular crest of *P. gracilis* is well developed and extends cranially onto the lateral surface of the preacetabular process, forming the margin of a deep acetabulum (Fig. 26A). The lateral and ventral edges of the crest are sharper, and project further

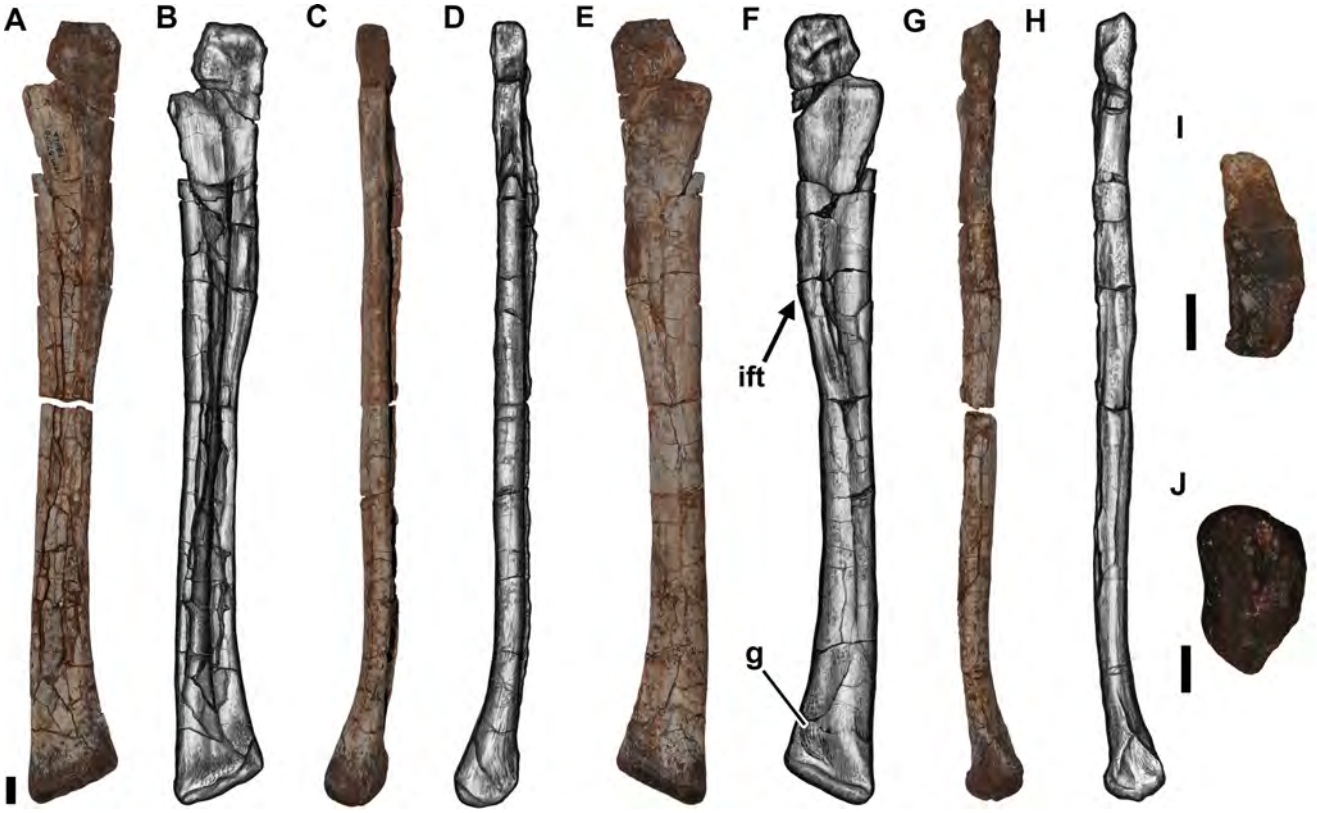

Fig. 32. Photographs and illustrations of the left fibula of YPM 57100 in medial (**A**, **B**), cranial (**C**, **D**), lateral (**E**, **F**), caudal (**G**, **H**), proximal (**I**), and distal (**J**) views. Abbreviations: g, groove; ift, iliofibularis trochanter. Scale bars = 1 cm.

ventrolaterally than in *Arizonasaurus*, *Bromsgroveia*, the Waldhaus taxon, and *Qianosuchus* (Galton, 1985; Nesbitt, 2005; Li et al., 2006; Butler et al., 2011), and is more similar to that of shuvosaurids (Nesbitt, 2007, 2011), although it is not as hood-like (i.e., highly curved dorsally with a large lateral extension overhanging the acetabulum) as in shuvosaurids *Effigia*, *Sillosuchus*, and *Shuvosaurus* (Long and Murry, 1995; Alcober and Parrish, 1997; Nesbitt, 2007). The ventral border of the acetabulum is concave in lateral view, and it is clear that the acetabulum was open when in articulation with the pubes and ischia. This open acetabular morphology is similar to shuvosaurids (Nesbitt, 2007, 2011), but is in contrast to the more plesiomorphic convex right angle ventral margins of the ilia of *Arizonasaurus*, *Bromsgroveia*, the Waldhaus taxon, *Qianosuchus*, and most early archosauriforms and archosaurs (Galton, 1985; Galton and Walker, 1996; Nesbitt, 2005; Li et al., 2006; Butler et al., 2011; Nesbitt, 2011). The medial surface is relatively flat, with clear rugose articular surfaces for the sacral vertebrae. Like other *P. gracilis* (Gauthier et al., 2011) specimens (Fig. 27), the pubic peduncle is short and stout, though not as relatively elongate as in some specimens (TTU-P 10419), and relatively smaller than the peduncle in *Poposaurus langstoni* (TMM 31025-12). The articular surface of the pubic peduncle is rugose and is triangular in the ventral view. The ischial peduncle is much smaller than the pubic peduncle, and is rugose with a rounded edge in lateral view and teardrop shape in the ventral view. The convex surface of the ischial peduncle fits a complementary concave surface of the ischium, a diagnostic character of *Poposaurus* (Weinbaum and Hungerbühler, 2007; Parker and Nesbitt, 2013). This size discrepancy between the two pelvic peduncles is also present in *Effigia*, *Sillosuchus*, and *Shuvosaurus* (Long and Murry, 1995; Alcober and Parrish, 1997; Nesbitt, 2007), but not in *Arizonasaurus*, *Bromsgroveia*, the Waldhaus material, or *Qianosuchus* (Galton, 1985; Galton and Walker, 1996; Nesbitt, 2005; Li et al., 2006; Butler et al., 2011; Nesbitt, 2011) where the peduncles are much more similar in size.

The postacetabular process is subtriangular with a concave ventral margin in the lateral view. Unlike other specimens of *P. gracilis* (e.g., FMNH UR 357, TTUP 9243, and TTUP 11203; Fig. 27C,D,G–L), the postacetabular process of YPM 57100 is laterally compressed, with a much smaller brevis shelf than in other poposauroids (Fig. 27A,B), and thus a smaller origin site for m. caudofemoralis brevis. The small brevis shelf in this specimen (YPM 57100; Fig. 27A,B) is likely anatomical and does not appear to be due to diagenetic or taphonomic distortion. On the lateral surface of the postacetabular process, there is a discernible rugosity on the postacetabular ridge, which is reconstructed as the origin site of m. iliofibularis (Schachner et al., 2011b). This is present on the majority of the length of the postacetabular process, merging cranially with the rim of the acetabulum. This distinct ridge is present in all specimens of

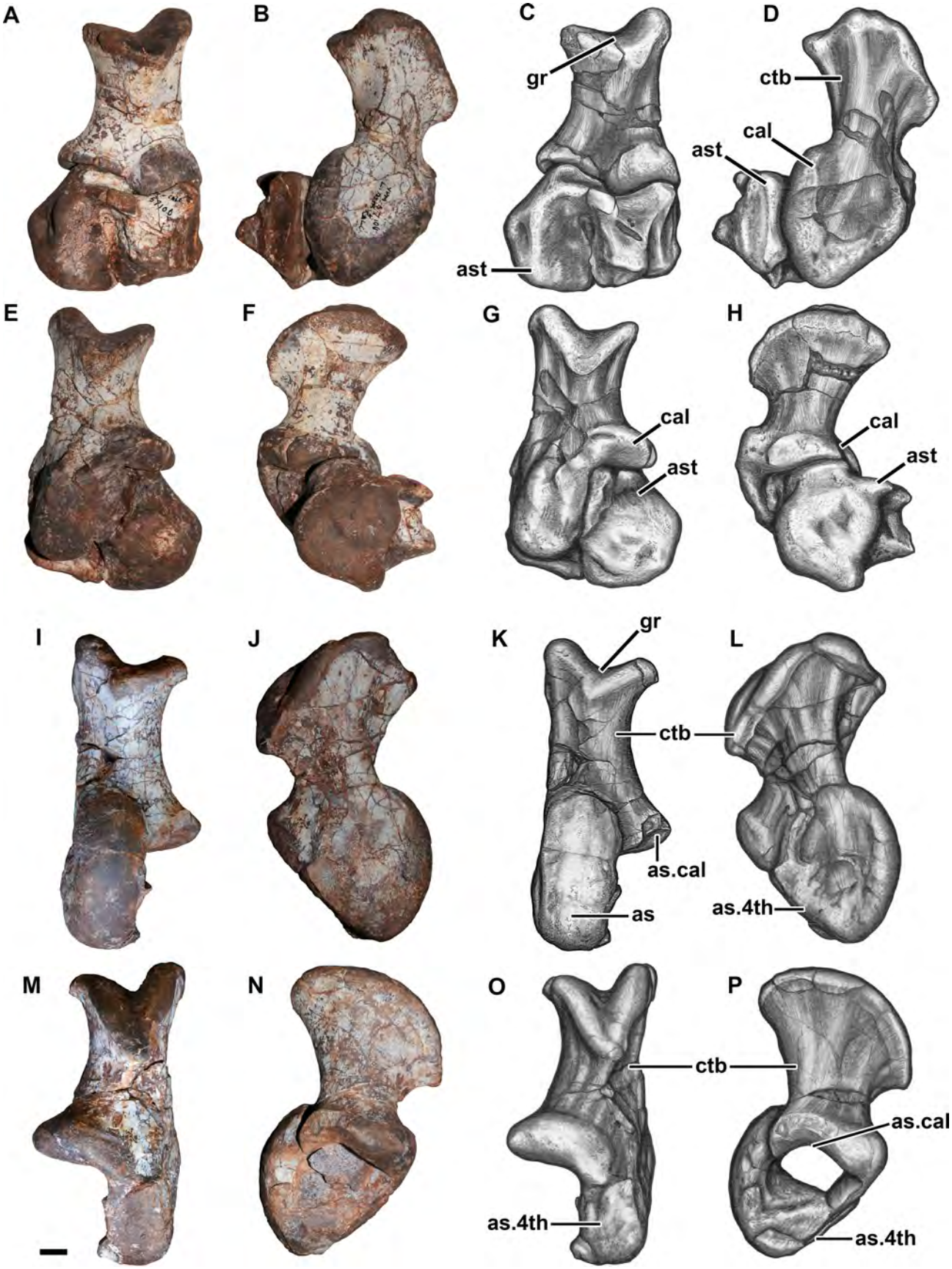

Fig. 33. Legend on next page.

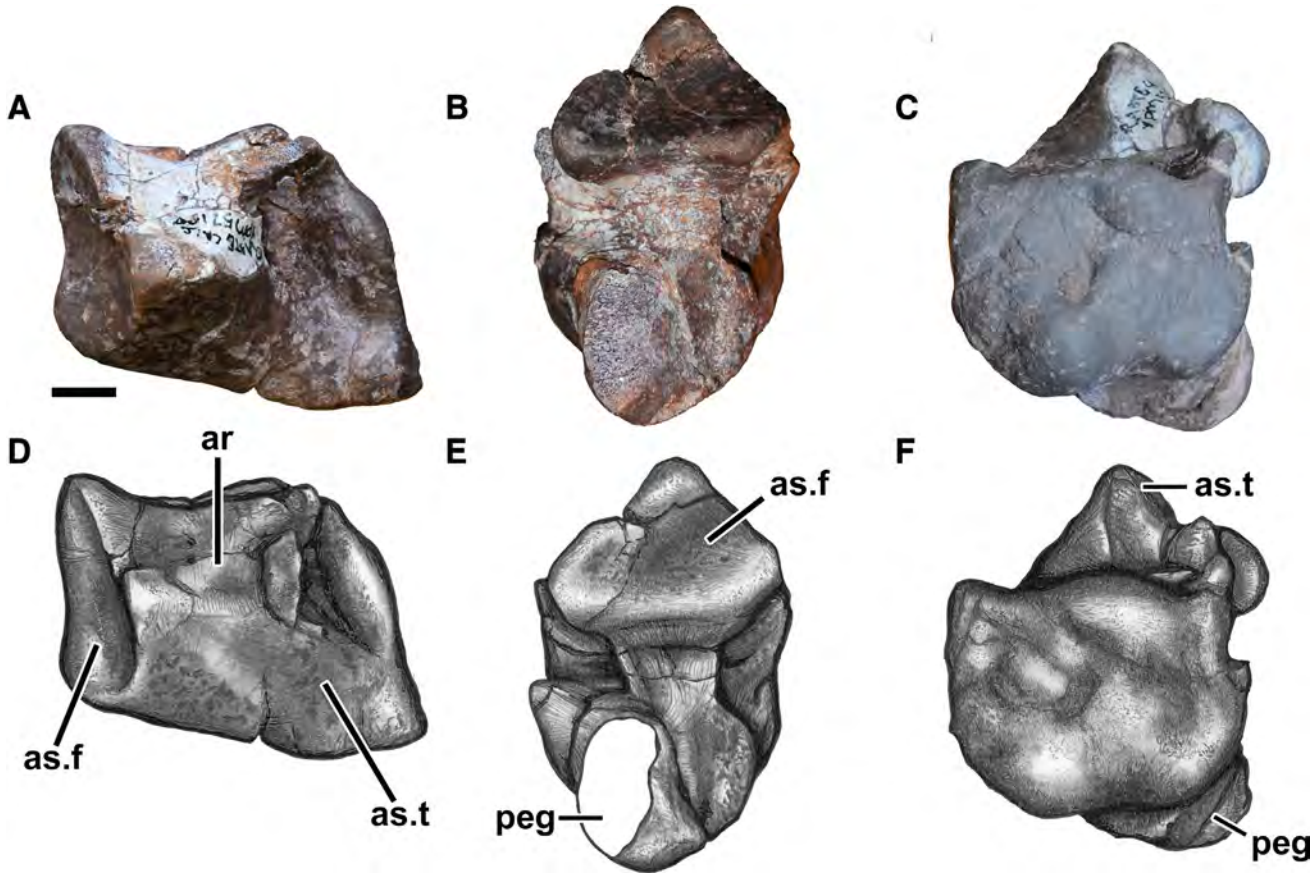

Fig. 34. The right astragalus of YPM 57100 in proximal (**A**, **D**), lateral (**B**, **E**), and medial (**C**, **F**) views. Abbreviations: ar, astragalar ridge; as.f, articulates with the fibula; as.t, articulates with the tibia. Scale bar = 1 cm.

Poposaurus and appears diagnostic of the clade (Weinbaum and Hungerbühler, 2007).

Pubis

The left and right pubes remain articulated with little distortion (Fig. 28), but there is some slight displacement in the proximal third of the shaft with the right medial apron overlapping the left. The articulation between the left and right pubes extends along the entire length, forming a complete apron, which narrows distally (Fig. 28C). The obturator foramen is elliptical and oriented caudolaterally as with other reptiles. There is a distinct subtriangular depression on the lateral surface of each pubis just distal to the proximal articular surface demarcating the reconstructed site for the origin of m. ambiens (Schachner et al., 2011b). In cross-section, the pubic shaft is subelliptical with a craniocaudally oriented long axis; the pubic apron is craniocaudally thin and cranially flat in the distal two-third of the shaft. The apron has an I-beam-like cross-section proximally (Fig. 28H) and becomes more rounded distally to form a half-circle in cross-section (Fig. 28I). The connection of the pubic apron to the shaft is along the ventral margin of the shaft proximally and the dorsal margin distally, generating a deep recess between the two pubes proximodorsally.

The pubes are 154 mm longer than the femora, 196 mm longer than the ischia, and significantly longer (224 mm) than the craniocaudal length of the ilium (Table 1). There is a hook-shaped caudal expansion of the distal end (=pubic boot) with a minor cranial expansion (Fig. 28A,B, D). The caudal expansion is not as long craniocaudally as that of *Shuvosaurus* or *Effigia* (Nesbitt, 2007) but is much longer than the caudal expansion of the poposauroids *Arizonasaurus* and *Qianosuchus* and other suchians (Nesbitt, 2011). The ventral margins of the expansions contact each other at the cranialmost and caudal aspects, resulting in a lateral bowing of the boot and a lancelet-shaped gap between the two sides. This caudal contact is not typical for other poposauroids and is reminiscent of that of loricatans with large distal expansions such as *Postosuchus alisonae*, (Peyer et al., 2008) and *Postosuchus kirkpatricki*, for which there are several complete pubes (see Weinbaum, 2013), as well as coelurosaurian theropod dinosaurs (e.g., *Tyrannosaurus rex*, Brochu, 2003). The origin site of m. puboischiofemoralis externus 2 is clear

Fig. 33. The left articulated calcaneum and astragalus of YPM 57100 in proximal (**A**, **C**), lateral (proximal is to the left) (**B**, **D**), distal (**E**, **G**), and medial (**F**, **H**) views. The right calcaneum in proximal/extensor (**I**, **K**), lateral (**J**, **L**), distal/flexor (**M**, **O**), and medial (**N**, **P**) views. Abbreviations: as, articular surface; as., articulates with; ast, astragalus; 4th, fourth tarsal; cal, calcaneum; ctb, calcaneal tuber; gr, groove. Scale bar = 1 cm.

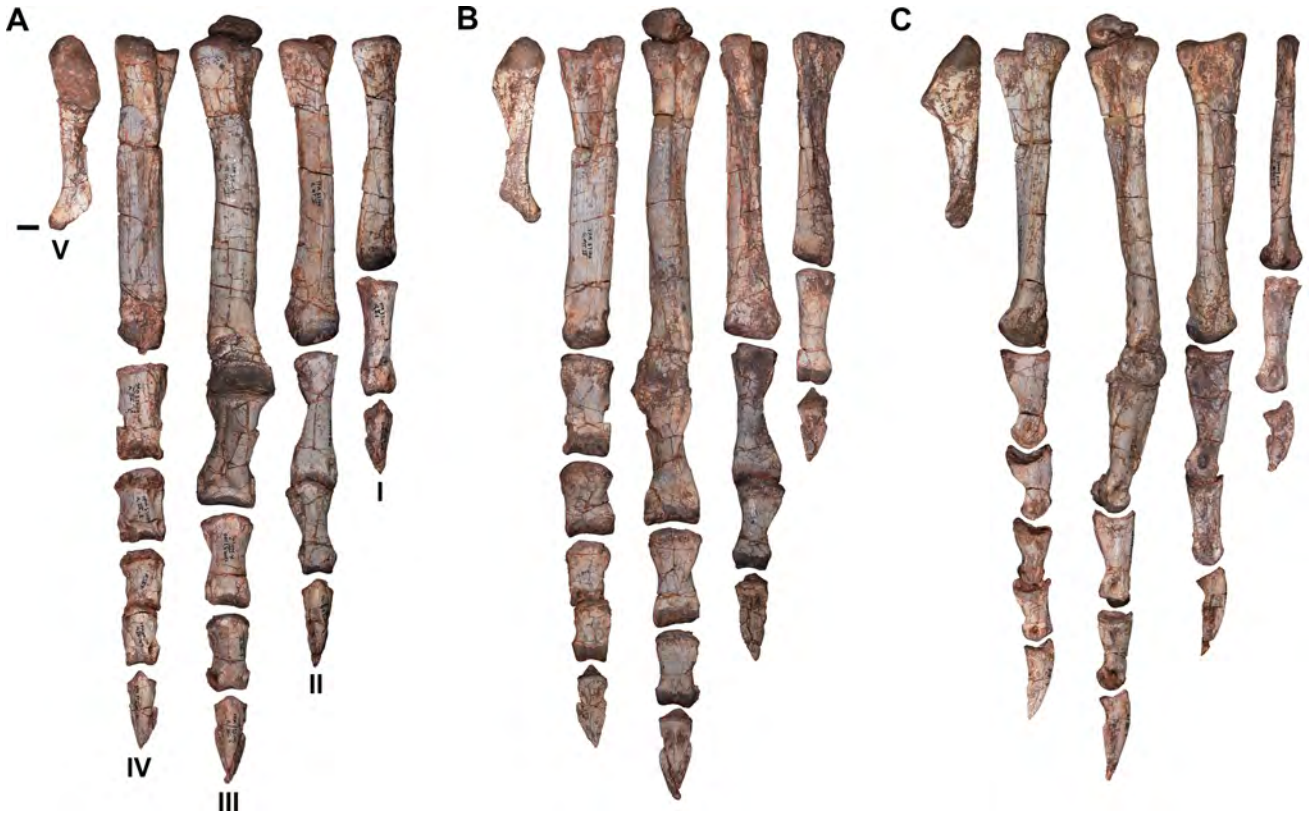

Fig. 35. Right pes of YPM 57100 with one associated tarsal attached to metatarsal III in dorsal/extensor (**A**), plantar/flexor (**B**), and lateral (**C**) views. Scale bar = 1 cm.

(Schachner et al., 2011b) and bounded ventrally by a slight groove. There are three individual gastralia that were diagenetically fused onto the left lateral surface of the pubic boot (Fig. 28A,B), and one to the inside surface of the apron. This demonstrates that the gastralia were likely continuous with the pubis.

Ischium

Like all poposauroids and some loricatans, the ischia (Fig. 29) are closely appressed along their entire length; however, they are not fused as in shuvosaurids (Nesbitt, 2007, 2011). The proximal portion forms a V in cross-section (Fig. 29D), with a narrow gap at the dorsal margin. The articular surface that contacts the ilium is concave and ellipsoid (craniocaudally oriented long axis) (Fig. 29D). The shaft of the ischia is semicircular in cross-section proximally, becoming more oval distally, eventually flattening out into a dorsal and ventral expansion (=ischial boot), similar to that of *Qianosuchus* and *Arizonasaurus*, but different from shuvosaurids, where the shaft is dorsoventrally flattened (Nesbitt, 2007). The shaft is craniocaudally constricted and more gracile than *Qianosuchus* (Li et al., 2006). Proximoventrally, there is a mediolaterally flattened ischial lamina that is present for approximately half the length of the ischium and gradually merges with the shaft. This lamina serves as the origin site for the m. puboischiotibialis proximally and the m. adductor 1 distally (Schachner et al., 2011b). Fine striations on the proximolateral surface of the ischial shaft indicate the origin site of m. ischiotrochantericus (Schachner et al., 2011b). Along the dorsolateral surface of the proximal half of the shaft, there is a distinct groove reconstructed as being associated with the origin of m. flexor tibialis internus and m. adductor 2 (Schachner et al., 2011b). The distal end of the ischium of *P. gracilis* flares into a laterally compressed boot that expands in both directions, but predominantly cranioventrally and has a convex ventral margin (Fig. 29E). The holotype of *P. gracilis* (FMNH UR 357) also has this expansion, but it was originally interpreted as the distal portion of the pubis (Mehl, 1915; Colbert, 1961). Unlike the pubic boot, there is no gap between the left and right ischia (Fig. 29E). The flattened lateral surface of the ischial boot serves as the likely origin site of m. puboischiofemoralis externus 3 (Schachner et al., 2011b).

Femur

The femora of YPM 57100 are both present, mostly complete (Fig. 30), but compressed postmortem. The left and right femora possess peculiar differences. For example, the left femur (Fig. 30A–H) is straighter and more robust than the right (Fig. 30I–J). The right femur has a thickened portion approximately one-third of the way down the shaft, and an overall medially oriented bowing of the proximal half of shaft, both of which may have been pathological (Fig. 30I–L).

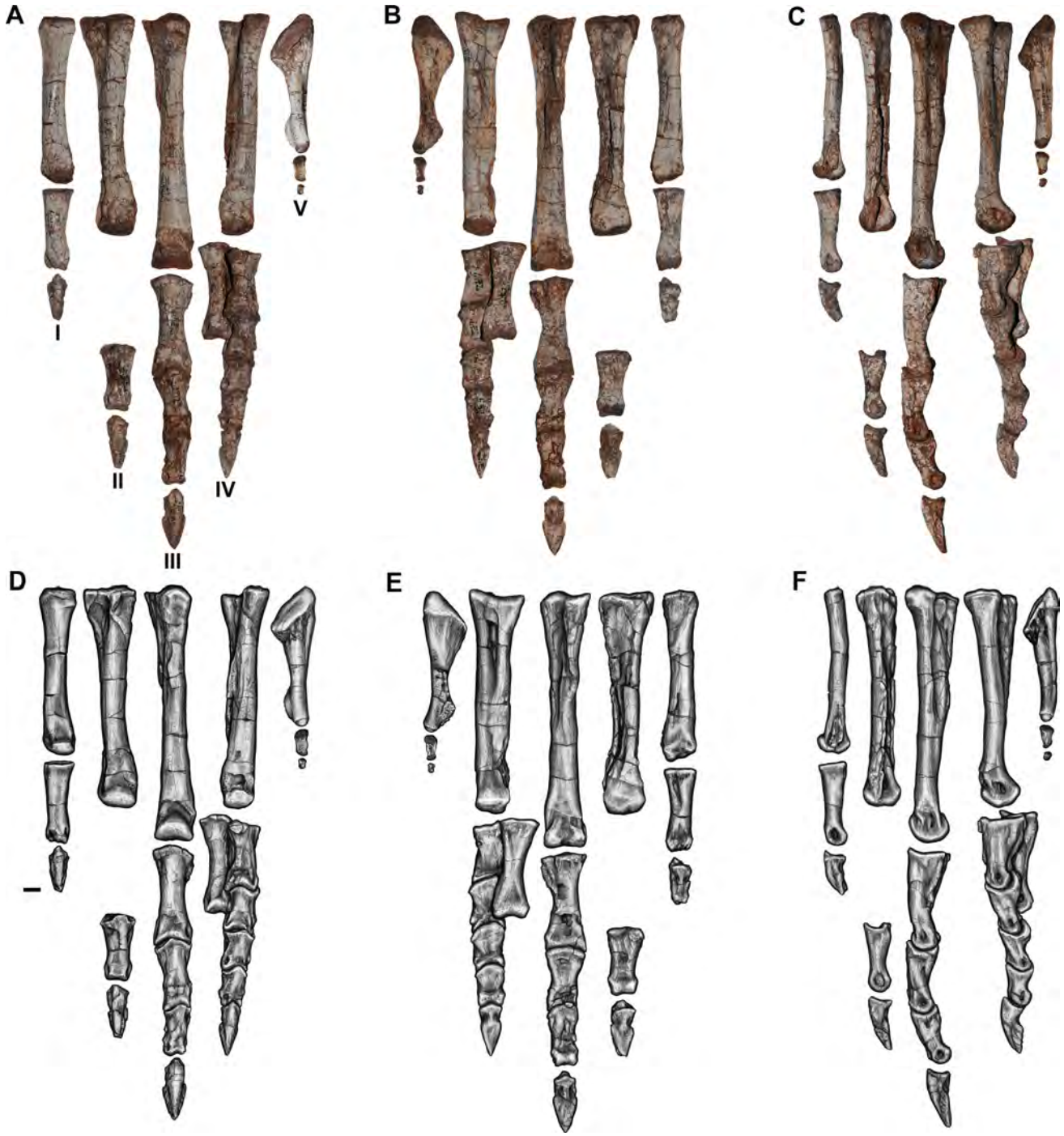

Fig. 36. Left pes of YPM 57100 in dorsal/extensor (**A**, **D**), plantar/flexor (**B**, **E**), and lateral (**C**, **F**) views. Scale bar = 1 cm.

The long axis of the proximal articular head is oriented mostly craniocaudally, and articulates with the acetabulum in pillar-erect manner found in pseudosuchians (Bonaparte, 1984). When in articulation, the large ventrally projecting supraacetabular crest of the ilium would have precluded extensive abduction of the femur, limiting the range of motion largely to the sagittal plane. The proximal surface of the femoral head (Fig. 30M,N) is rugose with a shallow median groove as with other poposauroids (Nesbitt, 2005, 2007, 2011) and identical to that described for the proximal femur of TTUP-10419 (Weinbaum and Hungerbühler, 2007) and UCMP A269/28359 (Long and Murry, 1995). The dorsal margin is convex and semicircular in craniolateral view with a distinct craniomedial projection of the femoral head that is angled cranioventrally. All three proximal tubera are

present and are about equal in size and expansion. Like most pseudosuchians, the craniolateral tuber is prominent on the craniolateral surface and forms the cranial margin of a large and well-developed insertion site for the m. puboischiofemoralis internus 1 and 2 (Schachner et al., 2011b). In addition, like most other pseudosuchians, both the craniomedial and caudomedial tubera are well developed, but the craniomedial tuber is not nearly as hook shaped as in *Effigia* and *Shuvosaurus* (Nesbitt, 2007). The ventral margin of the craniomedial tuber is distinctly faceted. There is a lancelet-shaped rugosity on the lateral surface of the femur (Fig. 30A,B) and this expansion is also present in close relatives of shuvosaurids (Nesbitt, 2005) and shuvosaurids (Nesbitt, 2007) but not typically in other pseudosuchians (Nesbitt, 2011). This rugosity is just distal to the femoral head and may be associated with the insertion site of m. iliofemoralis. On the medial surface and slightly more distal to the lancelet-shaped rugosity (approximately a third of the way down the shaft), there are two clear depressions separated by a small ridge (=fourth trochanter; Fig. 30E,F) associated with the insertion of the m. caudofemoralis longus tendon and m. caudofemoralis brevis (Schachner et al., 2011b) as in all poposauroids. At midshaft on the caudal side, there is a short raised and rugose tuberosity that is associated with the insertion of m. adductor 1 (Schachner et al., 2011b). Just distal to the tuberosity, the caudal surface of the femur exhibits a low but sharp ridge that is present on the distal third of the femoral shaft, indicating the boundary of the insertion of m. adductor 2 (Schachner et al., 2011b). There is a shallow depression on the cranial surface of the femur representing the distal aspect of the origin of the m. femorotibialis (Schachner et al., 2011b). As a result, the cranial margin of the distal portion of the femur is concave in the distal view, which differs from *Arizonasaurus*, but is similar to shuvosaurids (Nesbitt, 2005, 2011).

The distal femoral condyles are slightly crushed in both elements, mediolaterally in the right femur and craniocaudally in the left (Fig. 30O,P). There is a large lateral condyle, which ends distally in a large crest-like crista tibiofibularis (Fig. 30P). This process is expanded caudally to a much greater extent than the lateral and medial condyles, unlike the condition observed in *Arizonasaurus*; however, in both *Poposaurus* and shuvosaurids, there is a distinct shelf separating the crista tibiofibularis from the lateral condyle. The medial and lateral condyles are subequal in size. In the distal view, a slight depression is present between the lateral condyle and the crista tibiofibularis (Fig. 30O,P) as in shuvosaurids (Nesbitt, 2007). Like *Effigia*, other poposauroids, and *Postosuchus*, the femora are hollow and thin walled (Nesbitt, 2007).

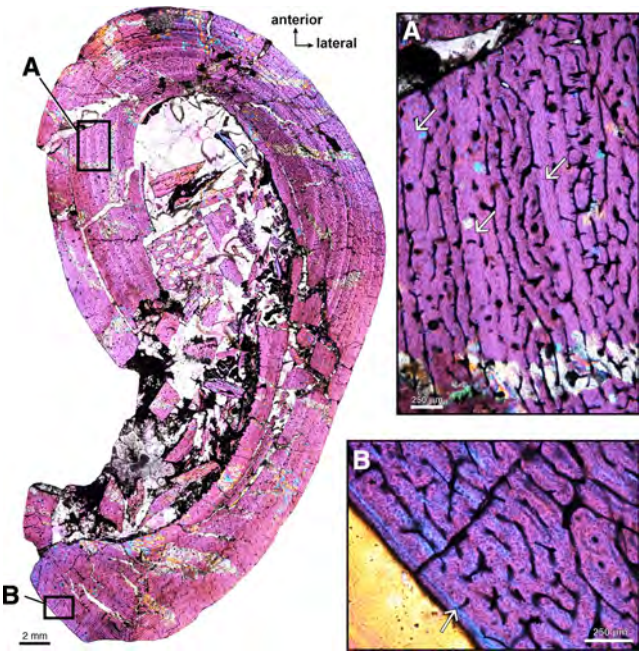

Fig. 37. Photomicrograph of mid-diaphyseal thin-section through the left femur of YPM 57100 (viewed under polarized light with quarter-wave retardation plate). (**A**) Close-up of craniomedial femoral cortex showing reticular fibrolamellar bone punctuated by several lines of arrested growth (arrows). (**B**) Close-up of outermost cortex in caudal region showing a thin (~50 μm) outer layer of parallel-fibered bone associated with a single outer growth mark, suggesting that the individual likely died during an unfavorable growth season.

Tibia

The tibiae are mostly complete and well preserved, with some minor crushing along the shaft of both right and left elements (Fig. 31). The tibia is more robust and slightly longer than the fibula, craniocaudally elliptical in cross-section and thin walled like that of the femur. The proximal end (Fig. 31M,O) expands caudally and laterally like other suchians (Nesbitt, 2011), and the proximal surface is rugose. The cranial margin of the proximal end is more pointed than the more rounded margin in *Effigia*. Like most suchians, there is a well-developed depression on the lateral condyle of the proximal surface. On the caudolateral surface (Fig. 31A,B,E,F,I,J), there is a distinct depression associated with the insertion of m. puboischiotibialis, m. flexor tibialis internus, and m. flexor tibialis externus (Schachner et al., 2011b) (Fig. 31A,B). Cranially to the ridge (Fig. 31B), there is a slight depression associated with the insertion site of m. triceps femoris (=m. iliotibialis, m. femorotibialis, and m. ambiens) (Schachner et al., 2011b). In *Effigia*, there is a sharp ridge on the lateral surface of the tibia distinct to this taxon and *Shuvosaurus*; in *Poposaurus*, there is a rounded convex area with no indication of a ridge.

The distal end of the tibia expands slightly relative to the midshaft and has two facets for articulation with the astragalus (Fig. 31N,P). The cranial condyle, which forms the main facet for articulation with the astragalus, is expanded and subrectangular in distal view, whereas this articular facet is relatively smaller in shuvosaurids. The caudal condyle is smaller but forms a distinct narrow ridge in *Poposaurus*, whereas conversely, in shuvosaurids, it is a broad feature (Nesbitt, 2007). Both condyles of *Poposaurus* project laterally, and appear to be very slightly oriented proximally, more so than in *Shuvosaurus*, *Postosuchus*, *Effigia*, crocodylomorphs, and stagonolepidids (Nesbitt, 2007). There is a distinct proximodistally oriented ridge on the caudomedial surface of the distal tibia bounded on either side by two

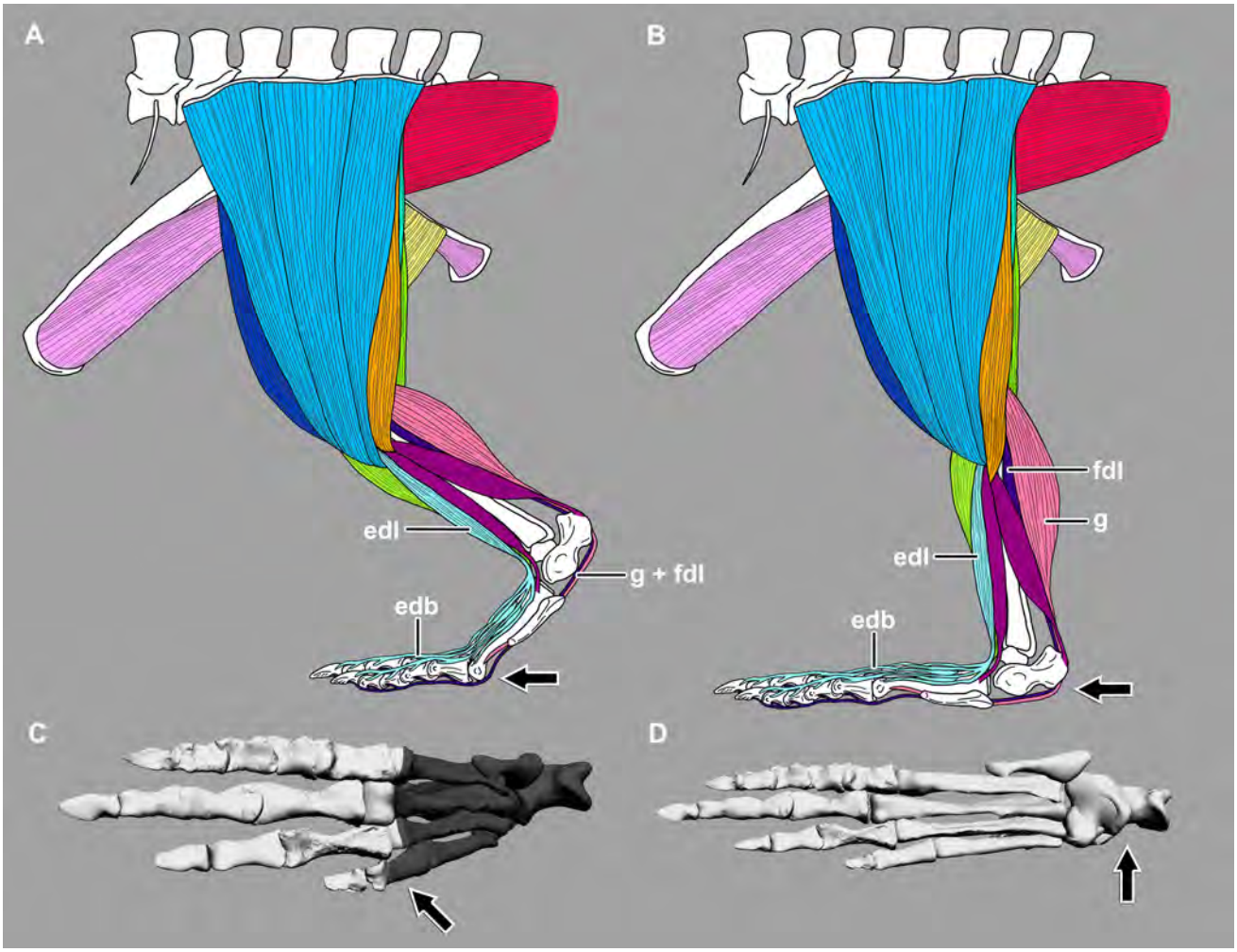

Fig. 38. (**A**) Diagrammatic reconstruction of the pelvic and hindlimb musculature of *Poposaurus* in left lateral view, modified into digitigrade (A) and plantigrade (**B**) pedal postures from Schachner et al. (2011b); muscle size and fiber lengths are speculative. (**C**) Ventral view of a digital reconstruction of the pes of *P. gracilis* articulated in a digitigrade posture with the non-weight bearing elements shaded in gray. (**D**) Ventral view of a digital reconstruction of the pes of *P. gracilis* articulated in a plantigrade posture showing the weight-bearing aspect of the pes. Arrows indicate the "heel" of each respective posture in the four different views. Abbreviations: edb, m. extensor digitorum brevis; edl, m. extensor digitorum longus; fdl, m. flexor digitorum longus; g, m. gastrocnemius.

shallow depressions. The distal articular surface is L-shaped, rugose caudally, and smooth cranially.

Fibula

The fibulae are both mostly complete with a small piece missing from the proximocranial surface of the right fibula and the proximocaudal surface of the left fibula (Fig. 32). Both are slightly crushed along the shaft, however, the overall shape is preserved. They are long, slender, and mediolaterally compressed over their entire length and semicircular in cross-section with the more convex side being the lateral surface. The proximal end is more mediolaterally compressed than the distal end, which is rounded in a cranial view (Fig. 32I). There is a rugose swelling approximately one-third of the way down the shaft from the proximal head associated with the poorly developed but clear insertion site of m. iliofibularis (=the "iliofibularis" trochanter) (Fig. 32F), similar to that of other archosauriforms (Nesbitt, 2007). Just distal to this rugose surface, the shaft becomes more constricted, and then flares out at the distal articular surface (Fig. 32J). The proximal articular surface is rugose (Fig. 32I), whereas the distal surface is smooth (Fig. 32J). Just proximal to the distal surface, there is a shallow groove on the caudal portion of the lateral surface that angles caudodorsally that serves as the origin site for m. extensor hallucis longus (Schachner et al., 2011b). The distal end is asymmetrical in the lateral view, whereas the cranial portion is much more proximally positioned than the caudal edge. Overall, the fibulae are very similar to those of *Effigia*; however, the depression adjacent to the insertions scar for m. iliofibularis and the groove associated with the origin of m. extensor hallucis longus (Fig. 32F) are more developed in *P. gracilis*.

Astragalus

There is some distortion in the right astragalus due to what is hypothesized to be pathology, but overall the astragali are complete and well preserved (Figs. 33 and 34). The left astragalus is diagenetically connected with, and slightly crushed into the associated calcaneum (Fig. 33A–H), which has distorted the astragular peg to a minor degree. The maximum mediolateral and proximodistal dimensions of the astragalus are subequal and the fibular facet and astragular peg are nearly the same craniocaudal length. The tibial facet occupies approximately two-thirds of the proximal surface of the astragalus whereas the fibular facet occupies the remaining third. This surface is concave caudomedially and convex cranially forming an undulating surface that is complementary to the distal end of the tibia. A rimmed fossa is present at the base of the facet, similar to extant crocodylians, *Postosuchus kirkpatricki*, and early crocodylomorphs (Nesbitt, 2011), but absent in *Effigia* (Nesbitt, 2007). The caudal margin of the tibial facet is bounded by a tall proximally projecting crest (Fig. 34A,D; ar). There is a tall proximally projecting pyramidal process that separates the tibial and fibular facets and caudal to this, there is a concave fossa with small foramina located within it. The fibular facet slopes distolaterally and articulates with the medial half of the distal articular surface of the fibula. The medial surface of the astragalus forms a rounded, but lumpy surface (Figs. 33F,H and 34C,F). The ventral aspect of this surface lies proximal to the articulation with the metatarsals, but the astragalus and the metatarsals did not contact directly here. There is a depression with small foramina on the lateral half of the ventral surface of the astragalus just cranial to the articulation with the calcaneum (=the "anterior hollow") as in other pseudosuchians including extant crocodylians (Nesbitt, 2011). The articular surface of the astragular peg is elliptical in cross-section terminating in a laterally projecting point that articulates with a socket of the calcaneum.

Calcaneum

Both of the calcanea are well preserved in YPM 57100 (Fig. 33). The calcaneal tuber is elongate, well developed with a constricted neck and a dorsoventrally flared distal surface as in other pseudosuchians and specimens referred to the taxon (Long and Murry, 1995). The tuber projects directly caudally at a right angle to the long axis formed by the articulated proximal tarsals. The caudal surface of the tuber bears a deep dorsoventrally oriented groove that contained the insertion tendons of the m. gastrocnemius and the m. flexor digitorum longus as they traveled distally to the ventral surface of the pes to insert on the metatarsals and phalanges (Schachner et al., 2011b). This groove is present in crocodylomorphs and in some loricatans (e.g., *Postosuchus*, *Fasolasuchus*, Bonaparte, 1981) but absent in other poposauroids (e.g., *Qianosuchus*, *Lotosaurus*, and *Shuvosaurus*). In lateral view (Fig. 33B,D,F,H,J,L,N,P), the tuber flares both dorsally and ventrally at its caudal extent. On the lateral margin of the caudal surface of the calcaneal tuber, there is a small raised tuberosity associated with the insertion tendon of m. peroneus brevis (Schachner et al., 2011b). There is a robust, but smooth ridge on the lateral surface of the shaft of the tuber, and another ridge running along on the ventral surface. Ventrally, compact bone separates the caudal end of the calcaneum from the distal surface that articulates with the distal tarsals.

The surface of the calcaneum that articulates with the fibula is distinctly convex in lateral view with a surface that arcs ~170 degrees and is well constricted mediolaterally. This surface is continuous cranially with the flat distal surface that articulated with the distal tarsals. The socket on the medial side of the calcaneum that accepts the astragular peg extends laterally to lie distal to the fibular facet. This articulation surface is bounded caudally by a thick medially projecting astragular process, which is D-shaped in cranial view. There is distinct bilateral asymmetry between the left and right calcanea (Fig. 33A,I), likely associated with an unidentified right hindlimb pathology.

Distal Tarsals

The two left distal tarsals were found articulated with one another and in their natural arrangement with the corresponding metatarsals (Fig. 35). Similar to other crown archosaurs, we interpret these elements as pertaining to distal tarsals III and IV. The right tarsal III was found articulated with the third metatarsal whereas the right tarsal IV is missing. The proximal surface of distal tarsal III is flat and angles laterally and distally, with a rounded prominence on the caudomedial surface. There is a small stepped process on distal tarsal III that is directed cranially. Laterally, tarsal III tapers to a rounded crest. Medially, the surface is slightly convex with a distinct distally positioned depression containing two vascular foramina separated by a ridge. Distally, there is a curved facet that corresponds to and articulates with the proximal (and articular) surface of metatarsal III.

The cranial part of the proximal aspect of left tarsal IV is flat whereas the caudal portion of this surface is convex with a process that projects caudodorsally. The distal surface of tarsal IV is subtriangular in the outline. There is an elliptically concave facet directed both distally and slightly craniolaterally. This facet articulates with metatarsal IV. The caudolateral surface is separated from this facet by a distinct ridge and is convex. The medial surface is markedly concave for articulation with distal tarsal III. The facet of distal tarsal IV that articulates with the metatarsal IV is subtriangular, grooved, and poorly defined. The caudal aspect of distal tarsal IV is not as expanded as in *Postosuchus alisonae* (Peyer et al., 2008) and tapers similar to that of *Revueltosaurus callenderi*, although the cranial portion of the tarsal in *P. gracilis* is not as expanded as *Revueltosaurus* (Nesbitt, 2011). It is similar to distal tarsal IV of *Effigia*, although the distal pyramidal-shaped portion is not as expanded or as elongated as in *Effigia* (Nesbitt, 2007).

Metatarsals

The five metatarsals in both pedes are well preserved with minimal crushing in the left metatarsals II, III, and IV and in all of the right metatarsals (Figs. 35 and 36). The overall shape of the five metatarsals is nearly identical to these elements in *Effigia*; however, distally, the

metatarsals appear to be wider relative to the shaft of each metatarsal in *Poposaurus* relative to *Effigia*. Proximally, the metatarsals articulate with one another tightly, resulting in an overall flaring of the articulated metatarsals distally in cranial view, reminiscent of early ornithodiran and theropod metatarsals (Benton, 2004; Nesbitt, 2011). The proximal aspects of metatarsals I–IV are oriented craniolaterally and caudomedially. The plantar surfaces of metatarsals I–IV (i.e., the ventrolateral shaft) all have distinct grooves, which are interpreted as the osteological correlate for the insertion of the m. gastrocnemius tendons (Schachner et al., 2011b). The depth and development of the ligament pits are asymmetrical in metatarsals I–IV, with larger pits on the lateral surface of each metatarsal. The largest asymmetry is found in the more medial metatarsals.

Metatarsal I is 100 mm long, and craniolaterally to caudomedially compressed (Figs. 35 and 36). The proximal articular surface is lenticular with a rounded surface laterally and a flat surface medially. Proximally, metatarsal I articulates tightly with a concave embayment on the craniomedial surface of metatarsal II. The distal articular surface is convex and extends onto the cranial surface of the metatarsal. In the distal view, it is approximately as wide as it is tall, with a distinct and well-developed lateral trochlea. Metatarsal I is two-thirds of the length of metatarsal III. Metatarsal I is proportionately much shorter relative to metatarsal III in *Poposaurus*, than metatarsal I is to III in *Effigia*, *Postosuchus alisonae*, and *Qianosuchus*, in which metatarsal I is over three quarters the length of metatarsal III.

Metatarsal II (Figs. 35 and 36) is 131 mm long, and slightly shorter in length than metatarsal III (approximately 87% of the length), unlike in *Effigia* in which the two elements are subequal. Proximally, the articular surface is oriented craniolaterally and caudomedially with a subrectangular shape that is concave medially for reception of metatarsal I, and flat laterally for articulation with metatarsal III. This articular surface is convex cranially and flat caudally. The cranial margin is slightly concave proximally. The shaft of metatarsal II expands gradually both proximally and distally from the midshaft and is wider than metatarsal I but slightly narrower in width to metatarsals II and IV. There is a shallow but distinct extensor pit on the cranial surface, just proximal to the articular surface. The distal articular surface is convex, wider than tall, and the lateral trochlea is more developed than the medial one, although this asymmetry is less distinct than in metatarsal I.

Metatarsal III is 151 mm, and is the longest of the metatarsals (Figs. 35 and 36), in contrast with *Effigia*, *Saurosuchus*, *Postosuchus alisonae* and some crocodylomorphs, where it is subequal in length with metatarsal II (Nesbitt, 2011). It is approximately half the length of the tibia (left tibial length: 300 mm) (Table 1). As in metatarsals I and II, the proximal articular surface is oriented craniolaterally and caudomedially; proximally, the articular surface is subrectangular, convex cranially, and slightly concave caudally. The medial margin is flat for articulation with metatarsal II, and the lateral margin is concave for articulation with metatarsal IV. The extensor pit at the distal end is deeper than that of metatarsal II, with a slightly raised ridge bounding the pit laterally. The articular surface extends proximally to the cranial surface of the distal end of the metatarsal. Unlike metatarsals I and II, the lateral and medial trochlea are subequally developed. The articular surface is wider than tall and subrectangular in shape.

Metatarsal IV is approximately 90% the length of metatarsal III (Figs. 35 and 36). The proximal articular surface is subtriangular with an expanded cranial margin and constricted caudal margin, mimicking the overall shape of distal tarsal IV. In the proximal view, the articular surface is convex cranially and concave caudally. Both the lateral and medial surfaces are concave for articulation with adjacent metatarsals. Like metatarsal III, the extensor pit is well developed, with a ridge bounding the pit laterally. The distal articular surface is taller than it is wide, convex, and the trochleae are not as extended as in metatarsals I–III. The taller than wide asymmetric distal surface is similar to the condition in *Effigia*, *Shuvosaurus*, *P. alisonae*, and dinosauriforms, whereas other early archosaurs have a wider more symmetrical shape (Nesbitt, 2011).

The fifth metatarsal is slightly less than half the length of metatarsal III, and overall quite different morphologically (Figs. 35 and 36). It has a large medially facing oval articular surface, the distal half of which is flat for articulation with metatarsal IV and the proximal half is slightly convex for articulation with distal tarsal IV. This gives the proximal half of the metatarsal a subtriangular shape in cranial and caudal views. The shaft of metatarsal V tapers to a simple rounded and convex distal articular surface that curves medially. There is a caudally projecting rugose flange on the distal half of the shaft. The proximal articular surface of metatarsal V is very similar to *Effigia* (Nesbitt, 2007). The overall morphology of this element is similar in the two taxa; however, a medially projecting flange is present in *Effigia* rather than the laterally directed flange found in *P. gracilis*.

Phalanges and Unguals

The phalangeal formula is 2-3-4-5-2 (Figs. 35 and 36). Phalanx I-1 is slightly shorter than phalanges II-1 and III-1, which are subequal in length, but longer than any of the more distal phalanges on any pedal digit. Unlike the first phalanx on digits two through four, PI-1 lacks a distinct extensor pit on its dorsal surface. This pit is very poorly developed or absent in all distal phalanges of all digits. On digits II–IV, there is a sequential reduction in length distally, and the phalanges are always longer than wide. The terminal phalanges on digit V decrease in size rapidly and the terminal phalanx is a small nub with no distinctive features. The ligament pits are well developed on both sides of all of the distal phalanges with the exception of the two small phalanges on digit V. For a detailed quantitative comparative analysis of the pedal morphology of *P. gracilis* with other archosaurs, see Farlow et al. (2014).

The unguals are well preserved with some slight oblique distortion in a few of them (Figs. 35 and 36). The proximal articular surface is subtriangular with a dorsoventrally oriented ridge present on the midline. Ventral to the lateral groove, there are paired rugose processes that flare out medially and laterally that were likely attachment sites for a keratinous sheath (e.g., Clark et al., 1999; Xu et al., 1999; Xu et al., 2000; Xu et al., 2003). These processes give the unguals an arrowhead-

like shape in dorsal and ventral view. Although the ungual is weakly recurved in medial and lateral profile, these processes form a flat hooflike ventral surface similar to that of shuvosaurids (Nesbitt, 2011). In the ventral view, proximal to the flat hooflike surface, there is a median ridge bounded by small concave depressions on either side. Although *Effigia* and *Shuvosaurus* have the laterally flared processes, the ungual in *Effigia* is more elongate and recurved along its entire length (Nesbitt, 2007). The ungual on digit I appears to be asymmetrical in dorsal view; however, it is unclear if this is the actual anatomy or if it is due to taphonomic processes. The length of the unguals on digits I–IV is similar to each other and the reduction in the size of the unguals across the pedes of loricatans (e.g., *Postosuchus alisonae*, Peyer et al., 2008; Crocodylia) is not present in *P. gracilis*.

Bone Histology and Growth

To investigate the growth patterns and ontogenetic stage of the individual, we thin-sectioned the midshaft of the left (non-pathologic) femur and describe its histologic structure here. In general, the cortex is dominated by well-vascularized fibrolamellar bone tissue interrupted by occasional zones of parallel-fibered bone containing cyclic growth marks. The growth zones, which incorporated dense primary vascular canals showing combinations of reticular and subplexiform vascular structure, resemble those found in other large-bodied archosaurs and mammalian herbivores that demonstrate cyclic growth over many seasons (Köhler et al., 2012). The bone wall is fairly thin, approximately 5–8 mm with some variation around the circumference, and shows an abrupt transition between the cortex and medullary cavity demarcated by a thin band of endosteally deposited lamellar bone.

The tissue texture of the cortex was predominately formed by a woven-fibered interosteonal matrix with globular osteocyte lacunae forming a haphazardly arranged lacunocanalicular network (Fig. 37). The vascular network consists of large but densely packed primary osteons thereby comprising a fibrolamellar tissue complex (Francillon-Vieillot et al., 1990; Huttenlocker et al., 2013; Lee et al., 2013; Stein and Prondvai, 2014). The predominant orientation of the primary osteons is reticular to subplexiform but varying circularly around the cortex. Vascular arrangements are primarily reticular in the craniolateral peripheral margins of the cortex but appear more plexiform on the caudal side of the bone. In this regard, the tissue texture of *Poposaurus* is more similar to other large-bodied, fast-growing archosaurs (e.g., dinosauriforms) than its smaller-bodied relative *Effigia*, which incorporates extensive parallel-fibered bone with simple longitudinal and reticular vascular canals, and only localized fibrolamellar bone (Nesbitt, 2007: Fig. 53). However, the vascular canal sizes and densities overlap with those reported in other fossil pseudosuchians and extant crocodylians, having a mean vascular density of 55 canals per mm^2 and an osteocyte density of 1,645 per mm^2 (Huttenlocker and Farmer, 2017) compared to 47–59/mm^2 and 697–1,000/mm^2, respectively, in extant *Crocodylus niloticus* (Cubo et al., 2012).

There are as many as seven approximately evenly spaced cyclic growth marks preserved in the cortex in the form of lines of arrested growth (or "LAGs"), including a single growth mark in the outermost cortex. The average thickness of each growth zone bounded by these LAGs is 900 μm, showing no evidence of decreased spacing toward the outer periphery of the bone. Averaged over ~385 days in a Triassic year, we estimate that radial bone deposition would have proceeded at approximately 2.3–4.6 μm/day (Woodward et al., 2013). Coupled with the individual's relatively small size compared to other *Poposaurus* specimens and the lack of an outer circumferential layer, these observations support that the individual was skeletally immature, likely a subadult, and that *Poposaurus* exhibited a strategy of multi-year growth to adult body size. A single layer of slower-growing parallel-fibered bone is punctuated by a LAG in the outermost 50 μm of the subperiosteal region (Fig. 37B), indicating that the individual likely died during the unfavorable season. The lack of histological evidence for slowed growth (i.e., LAGs becoming more closely spaced toward the periosteum or an increase in relative abundance of longitudinal vascular canals toward the periosteum, as observed in *Effigia*—see Nesbitt, 2007) is consistent with the presence of open neurocentral sutures throughout most of the vertebral column (*cf.* Brochu, 1996; Irmis, 2007). These data indicate that the individual was still actively growing at the time of death and not skeletally mature. However, the presence of at least seven LAGs also indicates that YPM 57100 was not a young juvenile.

DISCUSSION

Plantigrade versus Digitigrade

The posture of the foot and ankle in pseudosuchian archosaurs has been of interest and remained controversial for decades with many recent papers reconstructing pseudosuchians in their anatomical silhouettes as both plantigrade (e.g., Lautenschlager and Rauhut, 2015; Drymala and Zanno, 2016) and digitigrade (Nesbitt, 2007; Gower and Schoch, 2009) [for a discussion on the bipedal posture of *Poposaurus* see Gauthier et al. (2011)]. It is highly likely that there is a range of pedal postures in these taxa, with multiple possible reversals; however, the pes of *Poposaurus* exhibits a suite of adaptations and osteological correlates for soft tissue structures that support the hypothesis that *Poposaurus* was digitigrade. The enlarged calcaneal tuber demonstrates correlates for the insertion site of m. peroneus longus laterally, and a groove caudally that has been reconstructed as the path for the combined insertion tendon of the two heads of M. gastrocnemius as it travels ventrally to the flexor surfaces of metatarsals I–IV (Schachner et al., 2011b). The tight articulation between the distal articular surfaces of the tibia and fibula, and the proximal articular surface of the astragalus, along with the anatomy of the rotary joint between the astragalus and calcaneum, have been interpreted by Gauthier et al. (2011) as evidence indicating a lack of mediolateral rotation of the ankle joint. Wear facets on the flexor surfaces of the metatarsals and calcaneum indicate a large range of motion for each joint, and that the pes was capable of being positioned in either a digitigrade or plantigrade position (Gauthier et al., 2011). When the ankle joint is flexed, if in a plantigrade position with no lateral rotation, the ventral aspect of the tuber would be in direct contact with the ground, applying pressure to the tendon of the mm. gastrocnemius and flexor digitorum longus (Fig. 38). Additionally, this would put

the seemingly semi-vestigial digit V in contact with the ground, and there are no obvious discernible aspects of this digit that indicate that it was weight bearing (Figs. 35 and 36).

Farlow et al. (2014) conducted a comprehensive quantitative analysis of the pedal proportions of *P. gracilis* in comparison to a broad sampling of phylogenetically relevant digitigrade and plantigrade extant taxa, as well as other basal archosaurs, and dinosaurs. Various individual pedal elements match different archosaurian groups, but the overall phalangeal proportions are most similar to basal ornithopods, basal sauropodomorphs, various non-avian theropods, and numerous galliform birds, all digitigrade taxa (Farlow et al., 2014). Though all of these lines of evidence together provide a compelling argument that *Poposaurus* did indeed habitually possess a digitigrade posture, the unique nature of the pseudosuchian hip and ankle joint, and lack of any true extant functional analog necessitate further investigation to fully address pedal posture in poposauroids.

Cursorial Specializations

Most definitions of cursoriality are based upon distinct locomotor categories of modern mammals, with "cursors" being considered as animals that can generally run for long distances based upon their morphology (Gregory, 1912) and a parasagittally erect posture (Jenkins Jr., 1971; Biewener, 1989, 1990). Carrano (1999) found through statistical evaluation of the morphological measurements of the hindlimbs of extant mammals and both avian and non-avian dinosaurs, morphology generally provides a continuum of cursoriality. Despite this, clear trends are generally accepted within extinct taxa associated with specific traits, and some distinct features commonly associated with cursoriality are present in *Poposaurus*. The forelimb-to-hindlimb ratio is 47%, which is reduced relative to other pseudosuchians but similar to *Effigia* and theropod dinosaurs (Nesbitt, 2007) and associated with bipedality and cursoriality (Coombs Jr., 1978; Gauthier et al., 2011). Femoral length usually varies very little with respect to locomotor speed, and evaluation of cursoriality in the hindlimb is generally associated with the morphology of the distal limb (i.e., from the tibia and fibula down) (Carrano, 1999; Persons IV and Currie, 2016). Digit V of the pes is reduced to an almost semi-vestigial state, and if the pes were in a digitigrade posture, they would not come in contact with the ground at any point during the step cycle. Additionally, digit V does not possess a terminal ungual or claw (Fig. 35). The reduction of the lateral pedal digits is a largely ubiquitous trait in cursorial taxa (Coombs Jr., 1978). On digits 1–IV, the terminal unguals are highly modified and hooflike (Figs. 35 and 36), much like those of *Boverisuchus vorax*, a pristichampsine eusuchian (e.g., see Fig. 1 of Brochu, 2013) also inferred to be cursorial. Similar hooflike terminal unguals, with flanges running along the lateral surfaces, have been described for the basal ornithischian dinosaurs *Zalmoxes* (Weishampel et al., 2003), *Hypsilophodon* (Galton, 1974), and *Thescelosaurus* (Gilmore, 1915), and to a lesser degree in ornithomimid theropods (e.g., Longrich, 2008; Makovicky et al., 2010), and an allosauroid (White et al., 2013). Gauthier et al. (2011) calculated a body mass for this specimen of *Poposaurus* as approximately 60–75 kg, and the holotype as 90–100 kg following the methods of Anderson et al. (1985), which falls well within the optimal weight range identified for cursorial mammals (van Damme and Vanhooydonck, 2001).

ACKNOWLEDGEMENTS

The authors thank J. Gauthier, C. Norris, M. Fox, D. Brinkman, W. Joyce, and T. R. Lyson for access to and the invitation to study the specimens at the YPM, and the Bureau of Land Management's (BLM) Laurie Bryant, Scott Foss, and Alan Titus. Thanks also to B. Mueller and G. Gürtler for access to specimens at the TTU-P, and notes and helpful conversations regarding pseudosuchians. Thanks to S. Gilbert and CG Farmer for providing temporary storage facilities while the YPM specimen was on loan to ERS. Thanks to C. Levitt-Bussian for assistance with the casting, molding, and cutting for the histological analysis and facilitation of the housing of the specimen while on loan, and C. Layton for the illustration of the reconstructed *Poposaurus* in Fig. 1C. We also thank P. Dodson for a thorough editorial review, and the two reviewers, J. C. Weinbaum and J. W. Martz, for exceptionally detailed and insightful comments.

LITERATURE CITED

Alcober O. 2000. Redescription of the skull of *Saurosuchus galilei* (Archosauria: Rauisuchidae). J Vert Paleontol 20:302–316.

Alcober O, Parrish JM. 1997. A new poposaurid from the Upper Triassic of Argentina. J Vert Paleontol 17:548–556.

Anderson JF, Hall-Martin A, Russell DA. 1985. Long-bone circumference and weight in mammals, birds, and dinosaurs. J Zool Ser A 207:53–62.

Atchley SC, Nordt LC, Dworkin SI, Ramezani J, Parker WG, Ash SR, and Bowring SA. 2013. A linkage among Pangean tectonism, cyclic alluviation, climate change, and biologic turnover in the Late Triassic: the record From The Chinle Formation, Southwestern United States. *Journal of Sedimentary Research* 83: 1144–1161.

Bates KT, Schachner ER. 2012. Disparity and convergence in bipedal archosaur locomotion. J R Soc Interface 9:1339–1353.

Behrensmeyer AK. 1978. Taphonomic and ecologic information from bone weathering. Paleobiology 4:150–162.

Benoit M, Yarborough Fitzgerald V. 2004. Decay conditions of an Upper Triassic poposaur: Evidence from calcium carbonate nodules. J Vert Paleontol 24:38A.

Benton MJ. 2004. Origin and relationships of Dinosauria. In: Weishampel DB, Dodson P, Osmólska H, editors. *The Dinosauria*. 2nd ed. Berkeley: University of California Press. p 7–24.

Benton MJ, Forth J, Langer MC. 2014. Models for the rise of dinosaurs. Curr Biol 24:R87–R95.

Biewener AA. 1989. Scaling body support in mammals: limb posture and muscle mechanics. Science 245:45–48.

Biewener AA. 1990. Biomechanics of mammalian terrestrial locomotion. Science 250:1097–1103.

Blakey RC, Gubitosa R. 1983. Late Triassic paleogeography and depositional history of the Chinle Formation, southern Utah and northern Arizona. In: Reynolds MW, Dolly ED, editors. *Mesozoic paleogeography of West-Central United States*. Denver, CO: Society of Economic Paleontologists and Mineralogists, Rocky Mountain Section. p 57–76.

Bonaparte JF. 1981. Descripción de *Fasolasuchus tenax* y su significado en la sistemática y evolución de los Thecodontia. Rev Mus Argent Cienc Nat "Bernardino Rivadavia" 3:55–101.

Bonaparte JF. 1984. Locomotion in rauisuchid thecodonts. J Vert Paleontol 3:210–218.

Bown TM, Kraus MJ. 1987. Integration of channel and floodplain suites, I. Developmental sequence and lateral relations of alluvial paleosols. J Sediment Petrol 57:587–601.

Brochu CA. 1992. Ontogeny of the postcranium in crocodylomorph archosaurs. Unpublished MS thesis. Austin: University of Texas.
Brochu CA. 1996. Closure of neurocentral sutures during crocodilian ontogeny: implications for maturity assessment in fossil archosaurs. J Vert Paleontol 16:49–62.
Brochu CA. 2003. Osteology of *Tyrannosaurus rex*: insights from a nearly complete skeleton and high-resolution computed tomographic analysis of the skull. Soc Vert Paleontol Mem 7: 1–138.
Brochu CA. 2013. Phylogenetic relationships of Palaeogene ziphodont eusuchians and the status of *Pristichampsus* Gervais, 1853. Earth Environ Sci Trans R Soc Edinb 103:521–550.
Brusatte SL, Benton MJ, Ruta M, Lloyd GT. 2008. Superiority, competition, and opportunism in the evolutionary radiation of dinosaurs. Science 321:1485–1488.
Brusatte SL, Nesbitt SJ, Irmis RB, Butler RJ, Benton MJ, Norell MA. 2010. The origin and early radiation of dinosaurs. Earth-Sci Rev 101:68–100.
Butler RJ, Barrett PM, Abel RL, Gower DJ. 2009. A possible ctenosauriscid archosaur from the Middle Triassic Manda Beds of Tanzania. J Vert Paleontol 29:1022–1031.
Butler RJ, Brusatte SL, Reich M, Nesbitt SJ, Schoch RR, Hornung JJ. 2011. The sail-backed reptile *Ctenosauriscus* from the latest Early Triassic of Germany and the timing and biogeography of the early archosaur radiation. PLoS One 6:1–28.
Carrano MT. 1999. What, if anything, is a cursor? Categories versus continua for determining locomotor habit in mammals and dinosaurs. J Zool Soc London 247:29–42.
Chatterjee S. 1985. *Postosuchus*, a new thecodontian reptile from the Triassic of Texas and the origin of tyrannosaurs. Philos Trans R Soc Biol Sci 309:395–460.
Chinsamy A, Raath MA. 1992. Preparation of fossil bone for histological examination. Palaeontol Afr 29:39–44.
Clark JM, Norell MA, Chiappe LM. 1999. An oviraptorid skeleton from the Late Cretaceous of Ukhaa Tolgod, Mongolia, Preserved in an avianlike brooding position over an oviraptorid nest. Am Mus Novit 3265:1–36.
Clark JM, Xu X, Forster CA, Wang Y. 2004. A Middle Jurassic 'sphenosuchian' from China and the origin of the crocodylian skull. Nature 430:1021–1024.
Colbert EH. 1961. The Triassic reptile *Poposaurus*. Fieldiana Geol 14:59–78.
Colbert EH. 1989. The Triassic dinosaur *Coelophysis*. Mus North Ariz Bull 57:1–160.
Colbert EH, Brown B, Price LI, Hayden WB. 1952. A pseudosuchian reptile from Arizona. Bull Am Mus Nat Hist 99:565–592.
Coombs WP Jr. 1978. Theoretical aspects of cursorial adaptations in dinosaurs. Q Rev Biol 53:393–418.
Cope ED. 1869. Synopsis of the extinct Batrachia, Reptilia, and Aves of North America. Trans Am Philos Soc 40:1–252.
Cubo JN, Le Roy N, Martinez-Maza C, Montes L. 2012. Paleohistological estimation of bone growth rate in extinct archosaurs. Paleobiology 38:335–349.
van Damme R, Vanhooydonck B. 2001. Origins of interspecific variation in lizard sprint capacity. Funct Ecol 15:186–202.
Dilkes DW. 1999. Appendicular myology of the hadrosaurian dinosaur *Maiasaura peeblesorum* from the Late Cretaceous (Campanian) of Montana. Earth Environ Sci Trans R Soc Edinb 90:87–125.
Drymala SM, Zanno LE. 2016. Osteology of *Carnufex carolinensis* (Archosauria: Pseudosuchia) from the Pekin Formation of North Carolina and its implications for Early Crocodylomorph Evolution. PLoS One 11:1–34.
Dubiel RF. 1987. Sedimentology of the Upper Triassic Chinle Formation, southeastern Utah: Paleoclimatic implications. J Ariz-Nev Acad Sci 22:35–45.
Dubiel RF, Hasiotis ST. 2011. *Deposystems, paleosols, and climatic variability in a continental system: the Upper Triassic Chinle Formation, Colorado Plateau, USA*, Vol. 97. Tulsa, OK: SEPM Special Publication. p 393–421.
Farlow JO, Schachner ER, Sarrazin JC, Klein H, Currie PJ. 2014. Pedal proportions of *Poposaurus gracilis*: convergence and divergence in the feet of archosaurs. Anat Rec 297:1022–1046.
Francillon-Vieillot H, de Buffrénil V, Castanet J, Géraudie J, Meunier FJ, Sire JY, Zylberberg L, de Ricqlès A. 1990. Microstructure and mineralization of vertebrate skeletal tissues. In: Carter JG, editor. *Skeletal biomineralization: Patterns, processes and evolutionary trends*, Vol. I. New York: Van Nostrand Reinhold. p 471–671.
Galton PM. 1974. The ornithischian dinosaur Hypsilophodon from the Wealden of the Isle of Wight. Bull Br Mus (Nat Hist) Geol 25: 1–152.
Galton PM. 1985. The poposaurid thecodontian *Teratosaurus suevicus* v. Meyer plus referred specimens mostly based on prosauropod dinosaurs from the Middle Stubensandstein (Upper Triassic) of Nordwürttemberg. Stuttg Beitr Naturkd Ser B (Geol Palaeontol) 116:1–29.
Galton PM, Walker AD. 1996. Supposed prosauropod dinosaurs from Middle Triassic of England referred to Parasuchia and Dinosauriformes. Neues Jarhbuch Geol Paläontol Monatsh 1996: 727–738.
Gauthier J. 1986. Saurischian monophyly and the origin of birds. Mem Calif Acad Sci 8:1–55.
Gauthier J, Padian K. 1985. Phylogenetic, functional, and aerodynamic analyses of the origin of birds and their flight. In: Hecht MK, Ostrom JH, Viohl G, Wellnhofer P, editors. *The beginning of birds: Proceedings of the International* Archaeopteryx *Conference Eichstätt 1984*. Freunde des Jura Museums: Eichstätt. p 185–197.
Gauthier JA, Nesbitt SJ, Schachner ER, Bever GS, Joyce WG. 2011. The bipedal stem crocodilian *Poposaurus gracilis*: inferring function in fossils and innovation in archosaur locomotion. Bull Peabody Mus Nat Hist 52:107–126.
Gilmore CW. 1915. Osteology of *Thescelosaurus*, an ornithopodous dinosaur from the Lance Formation of Wyoming. Proc U S Natl Mus 49:591–616.
Gower DJ. 1999. The cranial and mandibular osteology of a new rauisuchian archosaur from the Middle Triassic of southern Germany. Stuttg Beitr Naturkd B 280:1–49.
Gower DJ, Schoch RR. 2009. Postcranial anatomy of the rauisuchian archosaur *Batrachotomus kupferzellensis*. J Vert Paleontol 29: 103–122.
Gregory WK. 1912. Notes on the principles of quadrupedal locomotion and on the mechanism of the limbs in hoofed animals. Ann N Y Acad Sci 22:287–294.
Hartley A, Evenstar L. 2018. Fluvial architecture in actively deforming salt basins: Chinle Formation, Paradox Basin, Utah. Basin Res 30:148–166.
Howell ER, Blakey RC. 2013. Sedimentological constraints on the evolution of the Cordilleran arc: new insights from the Sonsela Member, Upper Triassic Chinle Formation, Petrified Forest National Park (Arizona, USA). Geol Soc Am Bull 125:1349–1368.
von Huene F. 1938. Ein großer Stagonolepidide aus der jüngeren Trias Ostafrikas. Neues Jahrbuch Mineral Geol Palaöntol Beilagenband B 80:264–276.
Huttenlocker AK, Farmer CG. 2017. Bone microvasculature tracks red blood cell size diminution in Triassic mammal and dinosaur forerunners. Curr Biol 27:48–54.
Huttenlocker AK, Woodward HN, Hall BK. 2013. Biology of bone. In: Padian K, Lamm E-T, editors. *bone histology of fossil tetrapods: Issues, methods, and databases*. University of California Press, Berkeley, Los Angeles, London. p 13–34.
Irmis RB. 2007. Axial skeleton ontogeny in the Parasuchia (Archosauria: Pseudosuchia) and its implications for ontogenetic determination in archosaurs. J Vert Paleontol 27: 350–361.
Irmis RB, Mundil R, Martz JW, Parker WG. 2011. High-resolution U–Pb ages from the Upper Triassic Chinle Formation (New Mexico, USA) support a diachronous rise of dinosaurs. Earth Planet Sci Lett 309:258–267.
Jenkins FA Jr. 1971. Limb posture and locomotion in the Virginia opossum (*Didelphis marsupialis*) and in other non-cursorial mammals. J Zool Soc London 165:303–315.
Kent DV, Olsen PE, Rasmussen C, Lepre C, Mundil R, Irmis RB, Gehrels GE, Giesler D, Geissman JW, Parker WG. 2018. Empirical

evidence for stability of the 405-kiloyear Jupiter-Venus eccentricity cycle over hundreds of millions of years. Proc Natl Acad Sci 115: 6153–6158.

Köhler M, Marín-Moratalla N, Jordana X, Aanes R. 2012. Seasonal bone growth and physiology in endotherms shed light on dinosaur physiology. Nature 487:358–361.

Kraus MJ, Bown TM. 1988. Pedofacies analysis: A new approach to reconstructing ancient fluvial sequences. Geol Soc Am Spec Pap 216:143–152.

Krebs B. 1965. *Ticinosuchus ferox* n. g. n. sp. Ein neuer Pseudoschier aus der Trias des Monte San Giorgio. Schweiz Paläontol Abh 81: 1–140.

Langer MC, Benton MJ. 2006. Early dinosaurs: A phylogenetic study. J Syst Palaeontol 4:309–358.

Lautenschlager S, Rauhut OWM. 2015. Osteology of *Rauisuchus tiradentes* from the Late Triassic (Carnian) Santa Maria Formation of Brazil, and its implications for rauisuchid anatomy and phylogeny. Zool J Linn Soc 173:55–91.

Lee AH, Huttenlocker AK, Padian K, Woodward HN. 2013. Analysis of growth rates. In: Padian K, Lamm E-T, editors. *Bone histology of fossil tetrapods: Issues, methods, and databases*. University of California Press, Berkeley, Los Angeles, London. p 217–252.

Li C, Wu X-C, Cheng Y-N, Sato T, Wang L-T. 2006. An unusual archosaurian from the marine Triassic of China. Naturwissenschaften 93:200–206.

Long RA, Murry PA. 1995. Late Triassic (Carnian and Norian) tetrapods from the southwestern United States. N M Mus Nat Hist Sci Bull 4:1–254.

Longrich N. 2008. A new, large ornithomimid from the Cretaceous Dinosaur Park Formation of Alberta, Canada: implications for the study of dissociated dinosaur remains. Palaeontology 51: 983–997.

Makovicky PJ, Gao K-Q, Lewin M, Erickson GM, Norell MA. 2010. A giant ornithomimosaur from the Early Cretaceous of China. Proc R Soc B 277:191–198.

Martz JW, Mueller B, Nesbitt SJ, Stocker MR, Parker WG, Atanassov M, Nicholas F, Weinbaum J, Lehane JR. 2013. A taxonomic and biostratigraphic re-evaluation of the Post Quarry vertebrate assemblage from the Cooper Canyon Formation (Dockum Group, Upper Triassic) of southern Garza County, western Texas. Earth Environ Sci Trans R Soc Edinb 103:339–364.

Martz JW, Kirkland JI, Milner ARC, Parker WG, Santucci VL. 2017. Upper Triassic lithostratigraphy, depositional systems, and vertebrate paleontology across southern Utah. Geol Intermt West 4:99–180.

Meers MB. 2003. Crocodylian forelimb musculature and its relevance to Archosauria. Anat Rec 274:891–916.

Mehl MG. 1915. *Poposaurus gracilis*, a new reptile from the Triassic of Wyoming. J Geol 23:516–522.

Nesbitt SJ. 2005. Osteology of the Middle Triassic pseudosuchian archosaur *Arizonasaurus babbiitti*. Hist Biol 17:19–47.

Nesbitt SJ. 2007. The anatomy of *Effigia okeeffeae* (Archosauria, Suchia), theropod-like convergence, and the distribution of related taxa. Bull Am Mus Nat Hist 302:1–84.

Nesbitt SJ. 2011. The early evolution of archosaurs: Relationships and the origin of major clades. Bull Am Mus Nat Hist 352:1–292.

Nesbitt SJ, Norell MA. 2006. Extreme convergence in the body plans of an early suchian (Archosauria) and ornithomimid dinosaurs (Theropoda). Proc R Soc B Biol Sci 273:1045–1048.

Nesbitt SJ, Liu J, Li C. 2011. A sail-backed suchian from the Heshanggou Formation (Early Triassic: Olenekian) of China. Earth Environ Sci Trans R Soc Edinb 101:271–284.

Nesbitt SJ, Barrett PM, Werning S, Sidor CA, Charig A. 2013. The oldest dinosaur? A Middle Triassic dinosauriform from Tanzania. Biol Lett 9:1–5.

Nesbitt SJ, Sidor CA, Angielczyk KD, Smith RMH, Tsuji LA. 2014. A new archosaur from the Manda beds (Anisian, Middle Triassic) of southern Tanzania and its implications for character state optimizations at Archosauria and Pseudosuchia. J Vert Paleontol 34: 1357–1382.

Nopsca F. 1923. Die Familien der Reptilien. *Fortschritte der Geologie und Paläontologie*, Vol. 2. Berlin: Gebrüder Borntraeger.

O'Connor PM. 2006. Postcranial pneumaticity: an evaluation of soft-tissue influences on the postcranial skeleton and the reconstruction of pulmonary anatomy in archosaurs. J Morphol 267:1199–1226.

Padian K, Li C, Pchelnikova J. 2009. The trackmaker of *Apatopus* (Late Triassic, North America): implications for the evolution of archosaur stance and gait. Palaeontology 53:175–189.

Parker WG, Nesbitt SJ. 2013. Cranial remains of *Poposaurus gracilis* (Pseudosuchia: Poposauroidea) from the Upper Triassic, the distribution of the taxon, and its implications for poposauroid evolution. Geol Soc London Spec Publ 379:503–523.

Persons WS IV, Currie PJ. 2016. An approach to scoring cursorial limb proportions in carnivorous dinosaurs and an attempt to account for allometry. Sci Rep 6:1–12.

Peyer K, Carter JG, Sues H-D, Novak SE, Olsen PE. 2008. A new suchian archosaur from the Upper Triassic of North Carolina. J Vert Paleontol 28:363–381.

Ramezani J, Hoke GD, Fastovsky DE, Bowring SA, Therrien F, Dworkin SI, Atchley SC, Nordt LC. 2011. High-precision U-Pb zircon geochronology of the Late Triassic Chinle Formation, Petrified Forest National Park (Arizona, USA): Temporal constraints on the early evolution of dinosaurs. Geol Soc Am Bull 123:2142–2159.

Ramezani J, Fastovsky DE, Bowring SA. 2014. Revised chronostratigraphy of the lower Chinle Formation strata in Arizona and New Mexico (USA): high-precision U-Pb geochronological constraints on the Late Triassic evolution of dinosaurs. Am J Sci 314:981–1008.

Schachner ER, Farmer CG, McDonald AT, Dodson P. 2011a. Evolution of the dinosauriform respiratory apparatus: new evidence from the postcranial axial skeleton. Anat Rec 294:1532–1547.

Schachner ER, Manning PL, Dodson P. 2011b. Pelvic and hindlimb myology of the basal archosaur *Poposaurus gracilis* (Archosauria: Poposauroidea). J Morphol 272:1464–1491.

Smith A. 2012. Paleoenvironmental reconstruction of an Upper Triassic fossil site based on evidence from calcium carbonate nodules. Geol Soc Am Abstr Programs 44:91.

Stefanic CM, Nesbitt SJ. 2018. The axial skeleton of *Poposaurus langstoni* (Pseudosuchia: Poposauroidea) and its implications for accessory intervertebral articulation evolution in pseudosuchian archosaurs. PeerJ 6:1–37.

Stein K, Prondvai E. 2014. Rethinking the nature of fibrolamellar bone: An integrative biological revision of sauropod plexiform bone formation. Biol Rev 89:24–47.

Stewart JH. 1957. Proposed nomenclature of part of Upper Triassic strata in southeastern Utah. Bull Am Assoc Pet Geol 41:441–465.

Stewart JH, Poole FG, Wilson RF. 1972. Stratigraphy and origin of the Chinle Formation and related Upper Triassic strata in the Colorado Plateau region. US Geol Surv Prof Pap 690:1–336.

Sulej T. 2005. A new rauisuchian reptile (Diapsida: Archosauria) from the Late Triassic of Poland. J Vert Paleontol 25:78–86.

Weinbaum JC. 2011. The skull of *Postosuchus kirkpatricki* (Archosauria: Paracrocodyliformes) from the Upper Triassic of the United States. PaleoBios 30:18–44.

Weinbaum JC. 2013. Postcranial skeleton of *Postosuchus kirkpatricki* (Archosauria: Paracrocodylomorpha), from the Upper Triassic of the United States. Geol Soc London Spec Publ 379:525–553.

Weinbaum JC, Hungerbühler A. 2007. A revision of *Poposaurus gracilis* (Archosauria: Suchia) based on two new specimens from the Late Triassic of the southwestern U.S.A. Palaontol Z 81: 131–145.

Weishampel DB, Jianu C-M, Zoltan C, Norman DB. 2003. Osteology and phylogeny of *Zalmoxes* (N. G.), an unusual euornithopod dinosaur from the latest Cretaceous of Romania. J Syst Palaeontol 1: 65–123.

White MA, Benson RBJ, Tischler TR, Hocknull SA, Cook AG, Barnes DG, Poropat SF, Wooldridge SJ, Sloan T, Sinapius GHK, et al. 2013. New *Australovenator* hind limb elements pertaining to the holotype reveal the most complete neovenatorid leg. PLoS One 8:1–25.

Wilson JW. 1994. Histological techniques. In: Leiggi P, May P, editors. *Vertebrate paleontological techniques*. Cambridge: Cambridge University Press. p 204–234.

Wilson JW, D'Emic MD, Ikejiri T, Moacdieh EM, Whitlock JA. 2011. A nomenclature for vertebral fossae in sauropods and other saurischian dinosaurs. PLoS One 6:1–19.

Woodward H, Padian K, Lee AH. 2013. Skeletochronology. In: Padian K, Lamm E-T, editors. *Bone histology of fossil tetrapods: Advancing methods, analysis, and interpretation*. University of California Press, Berkeley, Los Angeles, London. p 195–215.

Xu X, Wang X-L, Wu X-C. 1999. A dromaeosaurid dinosaur with a filamentous integument from the Yixian Formation of China. Nature 401:262–266.

Xu X, Zhou Z, Wang X. 2000. The smallest known non-avian theropod dinosaur. Nature 408:705–708.

Xu X, Zhou Z, Wang X, Kuang X, Zhang F, Xiangke D. 2003. Four-winged dinosaurs from China. Nature 421:335–340.

Zeigler KE, Parker WG, Martz JW. 2017. The lower Chinle Formation (Late Triassic) at Petrified Forest National Park, southwestern USA: A case study in magnetostratigraphic correlations. In: Zeigler KE, Parker WG, editors. *Terrestrial depositional systems: Deciphering complexities through multiple stratigraphic methods*. Amsterdam: Elsevier. p 237–277.

Zhang FK. 1975. A new thecodont *Lotosaurus*, from the Middle Triassic of Hunan. Vertebr Palasiat 13:144–147.

Zittel KA. 1887–1890. *Handbuch der Paläontologie. Abteilung 1. Paläozoologie Band III. Vertebrata (Pisces, Amphibia, Reptilia, Aves)*. Munich and Leipzig: Oldenbourg.